FACULTÉ DES ÉTUDES SUPÉRIEURES ET POSTOCTORALES

uOttawa

L'Université canadienne
Canada's university

FACULTY OF GRADUATE AND POSDOCTORAL STUDIES

Marjan Soltanzadeh
AUTEUR DE LA THÈSE / AUTHOR OF THESIS

M.A.Sc. (Chemical Engineering)
GRADE / DEGREE

Faculty of Engineering
FACULTÉ, ÉCOLE, DÉPARTEMENT / FACULTY, SCHOOL, DEPARTMENT

Modeling Triple Phase Boundary (TPB) in Solid Oxide Fuel Cell (SOFC) Anode

TITRE DE LA THÈSE / TITLE OF THESIS

Marten Ternan
DIRECTEUR (DIRECTRICE) DE LA THÈSE / THESIS SUPERVISOR

CO-DIRECTEUR (CO-DIRECTRICE) DE LA THÈSE / THESIS CO-SUPERVISOR

David Taylor

Elena Baranova

Gary W. Slater
Le Doyen de la Faculté des études supérieures et postdoctorales / Dean of the Faculty of Graduate and Postdoctoral Studies

Modeling Triple Phase Boundary (TPB) in Solid Oxide Fuel Cell (SOFC) Anode

MARJAN SOLTANZADEH

Thesis submitted to the
Faculty of Graduate and Postgraduate Studies
In partial fulfilment of the requirements
For the degree of Master of Applied Science in Chemical Engineering

Department of Chemical Engineering
Faculty of Engineering
University of Ottawa

Library and Archives
Canada

Published Heritage
Branch

395 Wellington Street
Ottawa ON K1A 0N4
Canada

Bibliothèque et
Archives Canada

Direction du
Patrimoine de l'édition

395, rue Wellington
Ottawa ON K1A 0N4
Canada

Your file Votre référence
ISBN: 978-0-494-74176-4
Our file Notre référence
ISBN: 978-0-494-74176-4

NOTICE:

The author has granted a non-exclusive license allowing Library and Archives Canada to reproduce, publish, archive, preserve, conserve, communicate to the public by telecommunication or on the Internet, loan, distribute and sell theses worldwide, for commercial or non-commercial purposes, in microform, paper, electronic and/or any other formats.

The author retains copyright ownership and moral rights in this thesis. Neither the thesis nor substantial extracts from it may be printed or otherwise reproduced without the author's permission.

AVIS:

L'auteur a accordé une licence non exclusive permettant à la Bibliothèque et Archives Canada de reproduire, publier, archiver, sauvegarder, conserver, transmettre au public par télécommunication ou par l'Internet, prêter, distribuer et vendre des thèses partout dans le monde, à des fins commerciales ou autres, sur support microforme, papier, électronique et/ou autres formats.

L'auteur conserve la propriété du droit d'auteur et des droits moraux qui protège cette thèse. Ni la thèse ni des extraits substantiels de celle-ci ne doivent être imprimés ou autrement reproduits sans son autorisation.

In compliance with the Canadian Privacy Act some supporting forms may have been removed from this thesis.

While these forms may be included in the document page count, their removal does not represent any loss of content from the thesis.

Conformément à la loi canadienne sur la protection de la vie privée, quelques formulaires secondaires ont été enlevés de cette thèse.

Bien que ces formulaires aient inclus dans la pagination, il n'y aura aucun contenu manquant.

Canada

ABSTRACT

The idea of having the triple phase boundary (TPB) is extensively used in the fuel cell literature, especially with respect to solid oxide fuel cells (SOFC). The TPB concept indicates that the hydrogen oxidation reaction and the oxygen reduction reaction, which produce electric current, can actually occur at special sites, called ''triple phase boundaries'' where the gaseous fuel phase, ion conducting phase: electrolyte, and electron conducting phase, come into contact. Recent study shows that despite the common assumption about TPB, it is not just a point, but a zone that consists of two lines. The kinetic reaction often introduces a significant limitation to fuel cell performance. Therefore, understanding, characterizing, and optimizing the TPB content in fuel cells provides excellent opportunities for performance improvement.

Studying the kinetics of the reaction that takes place at the triple phase boundary is one aspect of this paper. It includes the study of all kinds of chemical and electrochemical reactions as well as their reaction rates, the surface species, and the electrochemical parameters, such as reaction rate constants and conductivity. A mathematical model is developed to describe a simplified anodic solid oxide fuel cell (SOFC) system, Ni/ H_2–H_2O/YSZ, and its reaction occurring in the vicinity of the triple phase boundary (TPB).

The model incorporates coupled diffusion, migration and reaction phenomena of the chemical components in the gas phase, Ni particle and zirconia solid state. The kinetic constants necessary for the simulations are estimated on the basis of literature data.

RÉSUMÉ

L'idée d'avoir la limite de coexistence des trois phases (TPB) est largement utilisée dans la littérature des piles à combustible, en particulier en ce qui concerne les piles à combustible à oxyde solide (SOFC). Le concept TPB indique que la réaction d'oxydation de l'hydrogène et la réaction de réduction de l'oxygène, qui produisent du courant électrique, peut effectivement se produire sur des sites spéciaux, appelés les "limites de coexistence des trois phases", où la phase du combustible gazeux, la phase de la conduite d'ions: électrolyte, et la phase de la conduite d'électrons, entrent en contact. Des recherches récentes montrent que, malgré la supposition prévalente sur la TPB, ce n'est pas seulement une ligne, mais il s'agit plutôt d'une zone large de plusieurs centaines d'angströms. La réaction cinétique introduit souvent une limitation importante à la performance des piles à combustible. Par conséquent, la compréhension, la caractérisation et l'optimisation du contenu de la TPB chez les piles à combustible fournit d'excellentes occasions d'améliorer la performance.

L'étude de la cinétique de la réaction qui a lieu à la limite de coexistence des trois phases est un aspect de notre recherche. Celle-ci comprend l'étude de toutes sortes de réactions chimiques et électrochimiques en plus de leur taux de réaction, les espèces de surface et les paramètres électrochimiques, tels que les constantes de vitesse de réaction et la conductivité.

Un modèle mathématique est développé pour décrire un système simplifiée de pile à oxyde solide (SOFC) anodique, Ni / H_2-H_2O/YSZ, et sa réaction qui se produit auz elentours de la limite de coexistence des trois phases (TPB). Le modèle intègre la diffusion couplée, les phénomènes de migration et de réaction des composants chimiques en phase gazeuse, particules de Ni et de zircone dans l'état solide. On a estimé les constantes cinétiques nécessaires pour les simulations en se basant sur les données de la littérature.

AKNOWLEGMENT

I cannot duly express my gratitude towards my thesis supervisor, Dr. Marten Ternan, as every single page in this thesis is a result of his continuous kind support, vast knowledge on the subject, financial assistantship and his gracious patience. I consider myself extremely lucky to have started my graduate studies under the mentorship of such a great character. For all theses and more, I thank Dr. Marten Ternan for granting me the privilege to work with him.

I would also like to express my sincere thanks to Dr. Javier Georgi and Dr. Arian Novruzi for supervising my work, providing me with invaluable feedbacks and funding my research.

Above all, however, I must thank my parents for their irreplaceable love and support, and my younger sister, Sara, without whom I would have not had the confidence and strength to leave my family.

TABLE OF CONTENTS

List of Figures

List of Tables

Chapter 1 Introduction

A fuel cell is an electricity generation device that converts chemical energy in a fuel (H_2, CH_4, natural gas, etc.) directly to electrical energy. It produces electricity, water and heat from the fuel (on the anode side of the electrolyte) and the oxidant (O_2, air, on the cathode side of the electrolyte), which react catalytically. An electrolyte separates the two electrodes. Fuel cells are typically fed with hydrogen as the fuel and air as the oxidant. The electrode structures are porous. The porous structure is used to maximize the three-phase interface between the electrode, electrolyte and the gas/liquid fuel or oxidant. The main purposes of the electrolyte are to (a) prevent the direct contact of fuel and oxidant such that no combustion takes place without generating electrical power, and (b) conduct ions formed from the reductant/oxidant to the other side of the electrolyte where it takes part in the electrochemical reaction.

Solid oxide fuel cells (SOFCs) are high temperature fuel cells, usually operating in a range of 800-1000°C (Crawley 2007). The central design of SOFCs is similar to many other fuel cell technologies. It consists of an anode, cathode, and electrolyte. In SOFCs, the electrolyte is made of ceramic and can conduct oxygen anions. The ceramic used most frequently in SOFCs, is yttria stabilized zirconia (YSZ). YSZ is a mixture of ZrO_2 zirconium-oxide and yttria, Y_2O_3. Zr^{4+} (radius = 79 pm) is a tetravalent cation. Y^{3+} (radius = 92 pm) is a dopant. In order to maintain charge neutrality oxygen ion vacancies occur in the YSZ. They allow oxygen ion migration. Furthermore the materials for the electrodes are usually a mixture of Ni and YSZ for the anode and LSM (lanthanum strontium manganite) for the cathode, as shown in Figure 1.1. These are called composite electrodes or cermet. Using a composite electrode rather than a porous packing of only electrocatalyst particles has advantages. It increases the electrode performance by spreading the reaction zone from a single electrode/electrolyte interface to a three dimensional electrode, and it allows stresses due to the difference in thermal expansion at the interface of electrode and electrolyte to be reduced. The most important, advantage of using composite electrodes is the extension of the TPB, the contact zone where three phases meet, throughout the electrode. Both the conduction of electrons and the migration of oxygen ions can occur in LSM so it is referred to as a mixed ionic electronic conductor.

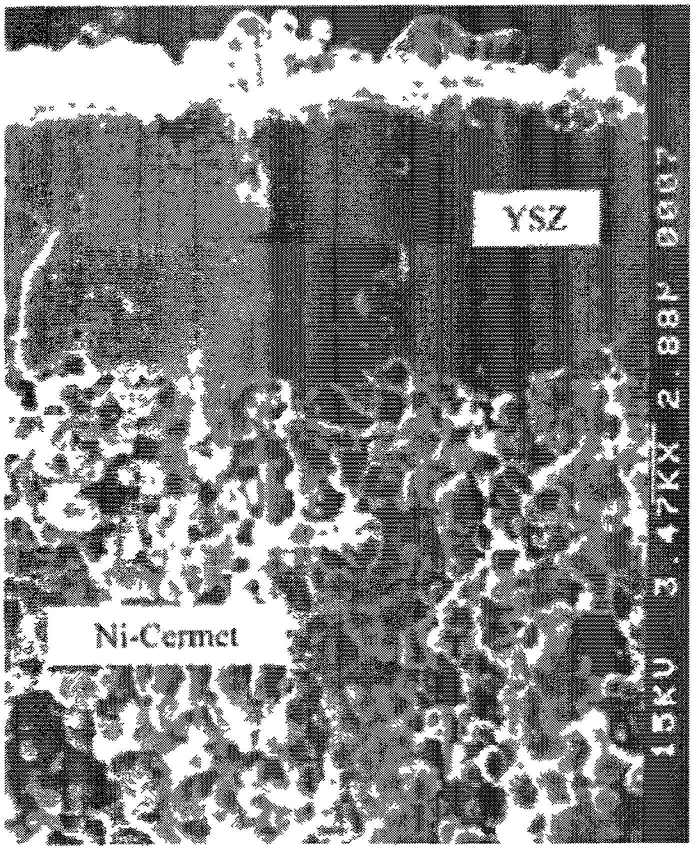

Figurel 1 SEM image of Electrolyte, and Anode of SOFC. YSZ electrolyte film is 9 m thick. NiO-YSZ was reduced in situ with H_2/H_20 at 800°C to yield final Ni/YSZ cermet structure. Souza, S D, S J Visco, and L C De Jonghe, J. Electrochem. Soc , Vol. 144, No 3, March 1997 L35. Reproduced by permission of ESC, The Electrochemical Society.

In a typical SOFC the oxygen molecules are supplied to the cathode, where they dissociate and accept electrons from the cathode to form anions (usually O^{2-}). The anions then diffuse across the electrolyte and react with the fuel at the anode, to produce the final product (usually water). An example illustrating this kind of mechanism in a SOFC that usually uses O_2 as the oxidant and H_2 as fuel is shown in Figure 1.2.

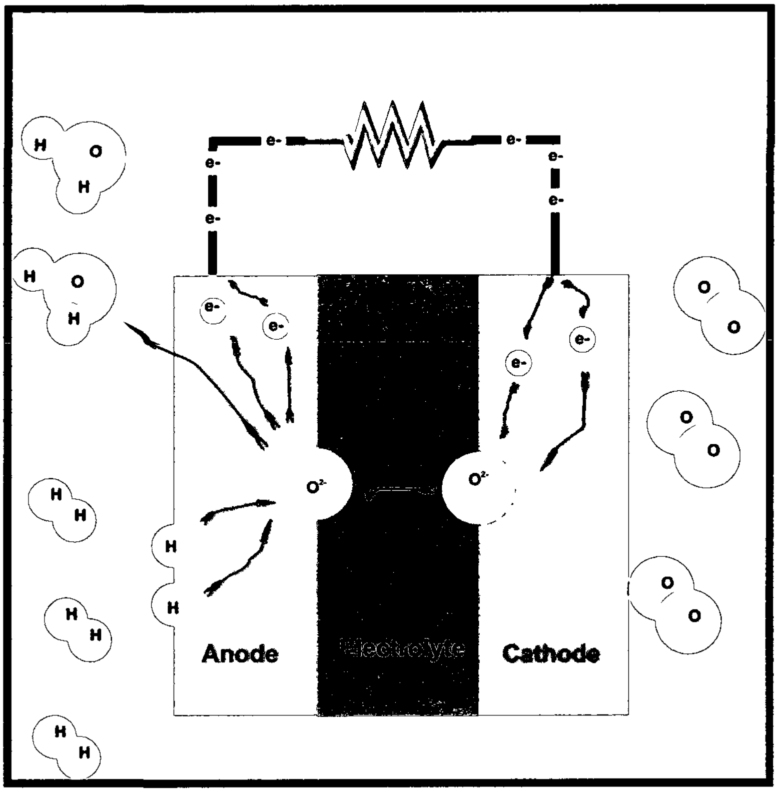

Figure1. 2 A Schematic Picture of SOFC

SOFC systems are widely considered to be promising candidates for clean stationary power. They can also be the primary or auxiliary power source for many facilities like homes, office buildings, and industrial power plants. Their attractive characteristics have provided the incentive for the development of a substantial number of numerical models for SOFC's and their components.

Modeling SOFCs continues to attract attention, since a valid mathematical model is expected to predict fuel cell performance without the need for expensive experiments. There are many papers on modeling parts of SOFCs, such as the electrolyte, the anode, and the cathode. Some of these models were reasonably successful in reproducing and simulating observed SOFC performance.

1.1 The Research Problem

The triple phase boundary (TPB) is the location where the three phases (gas, solid electrolyte, and solid electrode) intersect. It is the region where the electrochemical reaction occurs. The traditional concept of the TPB has the thickness of one reaction site. Although little has been done on TPBs, a vast range of papers exists on SOFC anodes. That work varies in terms of complexity and number of assumptions. In the past, the emphasis in a majority of the models has been either on the transport processes or on the electrochemical processes with a little attention on the TPB.

It has been shown by several electrochemical and surface science techniques that the oxidation process is not strictly limited to the TPB of the anode, as believed earlier. Instead the reaction zone extends beyond the Ni catalyst surface over several hundreds of Angstroms (Williford 2003). A valid model of The TBP would be a useful tool for guiding the design and fabrication of SOFC electrodes. Furthermore an analysis of different aspects of the TPB would optimize the performance of the cell. For SOFC fuel cell cathodes there are a few papers that develop the concept of the TPB. In contrast little work has been done on modeling the TPB at SOFC anodes.

The absence of a comprehensive model describing the processes occurring in the vicinity of an SOFC anode TPB motivated us to develop the two dimensional model described in this work. Analysing the TPB is important as this is the region, where the electron conducting phase (anode), the ion–conducting phase (electrolyte) and the gaseous phase meet (black circle in Figure 1.3). Also charge transfer reactions proceed in this region.

1.2 Objective of the Thesis

The objective of this work was to develop a two-dimensional model of the concentration distributions of species in the vicinity of the TPB (ie. the three phases: gas, nickel, and YSZ). The model should couple both mass transfer and electrochemical reaction. The numerical model was intended to be more comprehensive than the conventional definition of the TPB that considers the reaction zone of the fuel cell anode to be just a line, having the thickness of one reaction site, at the Ni/YSZ interface.

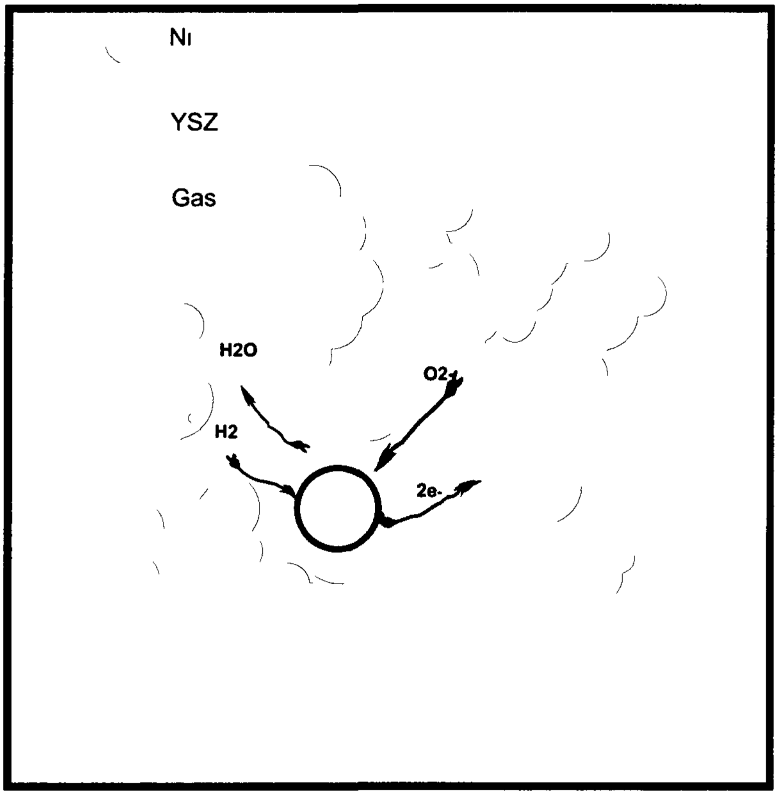

Figure1. 3 Triple Phase Boundary in SOFC

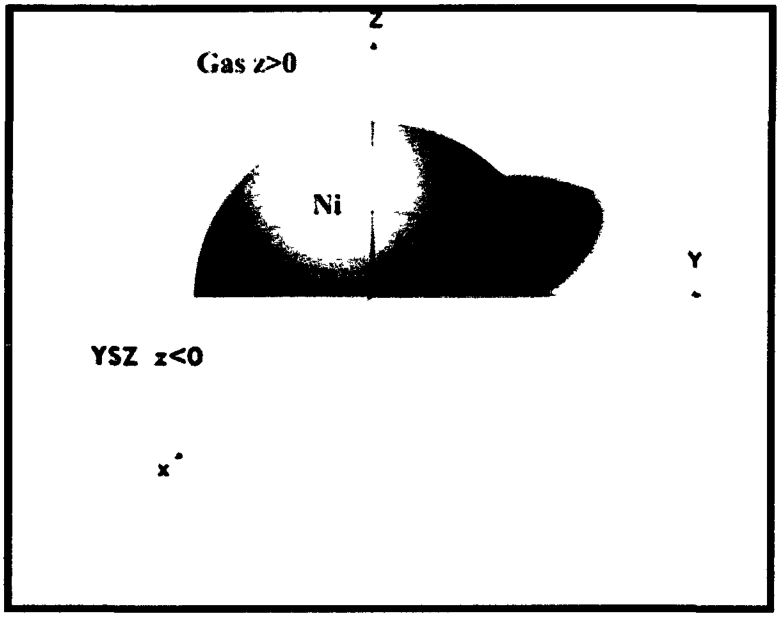

Figure1. 4 Schematic Picture of a Ni Particle in the Vicinity of YSZ and Gas of Anode Side of SOFC

A schematic diagram of the anode side of a fuel cell is shown in Figure 1.3. This schematic diagram represents the real composite anode structure shown in Figure 1.1. The triple phase region, specified by the circle in Figure 1.3, is represented in three dimensions in Figure 1.4. A hemispherical solid particle (Ni) is sitting on top of the flat electrolyte (YSZ) surface. The region above the electrolyte and outside the particle is the gas phase.

The 2D schematic diagram of the TPB shown in Fig 1.5 represents the interior of the black circle in Figure 1.3. It is the domain modeled by the work described in this thesis. In order to have a 2D picture, the 3D domain is considered as a very long, cylinder having sub-domains representing the YSZ ceramic, (Ω_{YSZ}), Ni (Ω_{Ni}), and gas (Ω_G) phases. The result is shown in Figure 1.5. Γ is the symbol used to represent the interface between different sub-domains. $\Gamma_{Bulk/G}$ is the interface between the bulk gas and Ω_G in the TPB model. $\Gamma_{Bulk/Ni}$ is the interface between the bulk nickel and the Ω_{Ni} in the TPB model. $\Gamma_{Bulk/YSZ}$ is the interface between the bulk YSZ and the Ω_{YSZ} in the TPB model.

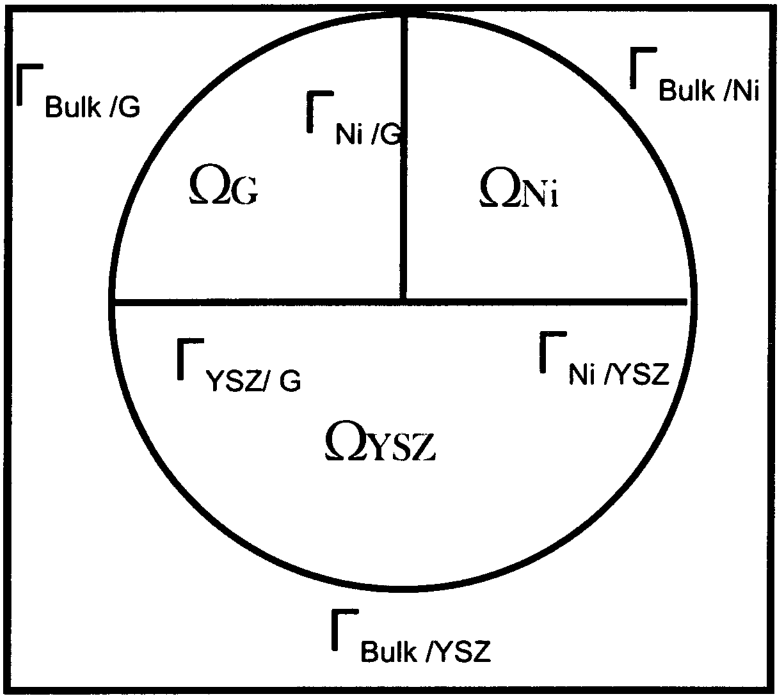

Figure1. 5 Schematic Domain for Our Problem

1.3 Organization of the Thesis

This thesis is written in 7 chapters. Chapter 2 describes the history of fuel cells, the fundamentals of their operating characteristics, the different types of fuel cells, and fuel cell applications. Chapter 3 is an overview of published research on SOFCs, with a special emphasis on modeling the anode. Chapter 4 describes the model developed in this work. Chapter 5 describes the numerical methodology used in this work. It includes some general comments on numerical methods, an overview of the finite element method, a description of the COMSOL software, and the validation of the model. The simulation data obtained from the model developed in this study are presented and discussed in Chapter 6. Comparisons with existing models are also described is this chapter. Finally Chapter 7 contains the conclusion and some suggestions for future studies.

Bibliography

COMSOL. http://www.comsol.com/ (accessed May 2009).

Fang, Q., T.suchiya, T.Yamamoto. "Finite Difference, Finite Element and Finite Volume Methods Applied to Two-Point Boundary Value Problems." Journal of Computational and Applied Mathematics 139, 2002: 9-19.

Kakaca, S, A.Pramuanjaroenkij, X.Y.Zhou. "A reviewof Numerical Modeling of Solid Oxide Fuel Cells." International Journal of Hydrogen Energy 32, 2007: 761 – 786.

Peir´o, J., S. Sherwin. "Finite Difference, Finite Element and Finite Volume Methods for Partial Differential Equations." In Handbook of Materials Modeling, 1-32. Netherlands: Springer, 2005.

Vielstich, W., A. Lamm , H.A. Gasteiger. Handbook of Fuel Cells: Fundamentals, Technology, Applications. Wiley, 2003.

Zimmerman, W.B.J. "COMSOL Multiphysics and the Basics of Numerical Analysis." In Multiphysics Modeling With Finite Element Methods. 2006.

Chapter 2 Fuel Cells

Fuel cells are a type of electrochemical device that converts the chemical energy of a reactant to electrical energy. The fuel cell concept is 160 years old (Holland 2001). They are noise pollution-free and highly effective sources of electrical energy. They are limited by the same Carnot efficiency as combustion engines. However, materials that are unable to withstand the adiabatic flame temperature limit the efficiencies of combustion engines. Electricity is produced directly in fuel cells. In contrast in combustion engines chemical energy is first converted to heat, then to mechanical energy, and eventually to electrical energy.

Batteries are the most familiar type of electrochemical device. In terms of function, fuel cells and batteries follow the same or a very similar principle (Bacon 1973). However, fuel cells use a reactant from an external source, which can be replaced continuously. This represents a thermodynamically open system. By contrast, batteries store electrical energy chemically and hence correspond to a thermodynamically closed system.

This chapter will discuss a comparison between fuel cells fuel cells fundamentals and basic features, existing fuel cell technologies, as well as their advantages and disadvantages. Solid oxide fuel cells (SOFCs) will be introduced and discussed in detail.

2.1 The History of Fuel Cells

The history of fuel cells includes two distinct periods: Some of the highlights from the first period are mentioned below. It lasted around one hundred years, and began with William Robert Grove's experiments in 1839 (Grove 1839). Grove immersed two platinum strips, surrounded by closed tubes containing hydrogen and oxygen, into dilute sulphuric acid. In 1842, Sir Grove described his invention in all detail (Grove 1842). (Fuller 2002) has attributed the first use of the term 'fuel cell' to William White Jacques in 1889. Ludwig Mond and his assistant Charles Langer developed a fuel cell using air and industrial coal gas. Mond and Langer

(Hoogers 2002) understood Grove's need for a surface of action and made significant changes in the experimental design of fuel cells. Firstly, they used a porous non-conducting diaphragm and impregnated it with dilute sulphuric acid, that was, the electrolyte. Next on each side of the diaphragm they placed punched strips of platinum coated with a thin film of platinum black. Their cell achieved 6 $A.ft^{-2}$ at 0.73 (V) in 1889. Freidrich Ostwald (Ortiz-Rivera 2009) provided the theoretical understanding of how Grove's fuel cell operated, thus determining the role of each component with respect to electrodes, electrolytes, anions, cations and oxidizing and reducing agents. He showed that chemical reactions within a gas diffusion electrode took place in a contact area where the catalyst, reactant gas and electrolyte met.

From this point on, the fuel cell might well have developed rapidly, if it had not been for the invention of the internal combustion engine and the discovery of petroleum. In contrast to the technologically advanced fuel cell concept, internal combustion engines were a simpler technology. With the option of petroleum as fuel, and an internal combustion engine as the energy transformation machine, almost all other forms of transforming energy were suspended for the time being.

The second period began shortly after World War II when Francis T. Bacon of Cambridge, England, successfully developed a high-pressure cell (Bacon 1973). A functioning device was demonstrated in 1954. But serious interest in the fuel cell as a practical generator of electrical energy did not begin until the 1960s, when the National Aeronautics and Space Administration (NASA) (Fitzgerald 2005) chose fuel cells over riskier nuclear power and more expensive solar energy for the first manned flight into space (Apollo and Gemini projects). Since their adoption by the space program, fuel cell technology has achieved widespread recognition by industry and government as a clean energy source for the future.

In recent years the technology has developed significantly and now appears promising in offering inexpensive and clean energy. The demand for highly-efficient, low to zero emission processes converting fossil and renewable combustibles into rapidly-available energy increased constantly during the last two decades. This demand originated from growing environmental problems caused by air pollutants and other reasons. Fuel cells present an attractive alternative for both stationary as well as mobile applications in industry and in the transportation sector.

2.2 Fuel Cell Phenomena

Understanding the phenomena in fuel cells through advancements in the areas of thermodynamics, electrode kinetic, transport processes and their applications, has continued since the time of Grove's discovery. In this section the basic fundamentals of fuel cells are discussed.

In a fuel cell an overall combustion reaction takes place through two so-called half-cell reactions. For example in solid oxide fuel cell:

Half-cell reaction (Cathode) $0.5O_2 + 2e^- \rightarrow O^{2-}$ (2 – 1)

Half-cell reaction (Anode) $H_2 + O^{2-} \rightarrow H_2O + 2e^-$ (2 – 2)

Fuel cells are typically fed with hydrogen as the fuel and air as the oxidant. The conventional physical structure of all fuel cells consists of an electrolyte layer in contact with an anode where the fuel (typically hydrogen) is electrochemically oxidized and a cathode at which the oxygen (typically from air) is reduced. The electrode structure is porous, and is used to maximize the length of the three-phase boundary between the electrode, electrolyte and the gas or liquid reactant, and also to separate the bulk gas phase and the electrolyte. The main functions of the electrolyte are to (a) prevent the direct contact of fuel and oxidant such that no thermal combustion takes place, and (b) conduct the reductant/oxidant to the other side of the electrolyte where it takes part in the electrochemical reaction. The gas/liquid ionization or de-ionization reactions take place on the surface of the electrode, and the reactant ions are conducted away from or towards the three-phase boundary. A solid or liquid electrolyte layer provides a physical barrier to prevent the direct mixing of the fuel and the oxidant, allows the conduction of ionic charge between the electrodes, and transports the dissolved reactants to the electrode.

Depending on the type of the fuel cell there are two mechanisms for migration through electrolyte:

- Conducting Ions Supplied from Cathode

In this case oxidant is supplied to the cathode. With the help of the catalyst, the oxidant dissociates and accepts electrons from the cathode to become diffusing anions (usually O^{2-}). The anions then diffuse across the electrolyte and react with the fuel at the anode, to produce the final product (usually water). An example of this kind of mechanism is a solid oxide fuel cell (SOFC) that uses O^{2-} as an oxidant and H_2 as fuel. The half reactions are shown in Equation $(2-1)$ and $(2-2)$.

- Conducting Ions Supplied from Anode

In this case fuels are dissociated, give up electrons to the anode, and become cations (usually H^+). The ions diffuse across the electrolyte and then react with the oxidant on the cathode, releasing the final product. An example of this fuel cell mechanism is the proton exchange membrane fuel cell that uses O_2 as an oxidant and H_2 as a fuel separated by a thin polymer membrane acting as the electrolyte. The half reactions are as follows:

$$\text{Anode: } H_2 \rightarrow 2H^+ + 2e^- \qquad (2-3)$$

$$\text{Cathode: } 0.5O_2 + 2H^+ + 2e^- \rightarrow H_2 \qquad (2-4)$$

The electrons produced at the anode are gathered by the current collectors and passed through an external circuit to a load where the energy is used. Finally the electrons flow from the load to the cathode side. Along with production of electrical energy, heat is also produced as a by-product of fuel cell operation. Both the reversible entropy change and the irreversibility resistances within the fuel cell system cause the heat production.

2.2.1 Differences between Conventional Electric Power Generation and a Fuel Cell

The overall reaction in a fuel cell is identical to a combustion reaction. However; the difference is that in a fuel cell the oxidation of the fuel and reduction of the air/oxygen are spatially separated from each other in order to prevent all the free energy of reaction from being converted to thermal energy.

Fuel cells have many advantages compared to conventional electric power generation systems. They include high intrinsic efficiency, which is relatively independent of size, and environmental compatibility. Furthermore, vibration-free operation of fuel cells (no moving parts in a fuel cell) also eliminates the noise usually associated with conventional power generation systems.

In fuel cells, unlike other power generation systems, electricity is produced directly through a chemical reaction. Although fuel cells are limited by the Carnot cycle efficiency, they do not have the severe materials limitation of combustion processes. The theoretical efficiency η_{th}, of an electrochemical process is defined as the ratio of the Gibbs free energy ΔG for the reaction and the reaction enthalpyΔH (Services 2000).

Theoretical efficiency of a fuel cell: $$\eta_{th} = {}^{\Delta G}/_{\Delta H} \qquad (2-5)$$

For combustion engines the theoretical efficiency $\eta_{th,Carno}$ is determined by their heat source working temperature T_H and heat sink working temperature TC in the Carnot-process.

Theoretical efficiency of a combustion engine: $$\eta_{th,Carno} = 1 - {}^{T_C}/_{T_H} \qquad (2-6)$$

The maximum value for T_H is the adiabatic flame temperature. The materials normally used in combustion processes are normally limited to a maximum of 900 K.

2.2.2 Ideal Performance

The maximum efficiency of a fuel cell occurs at an electrical potential known as the open circuit potential. The open circuit potential is generally described by the Nernst equation which is derived from thermodynamics equations. The maximum electrical work of a fuel cell is defined by the change in the overall Gibbs free energy for the electrochemical reactions taking place in an anode and a cathode of a typical fuel cell (Bockris 2008).

For a typical equation: $\mathrm{aA} + \mathrm{bB} \rightarrow \mathrm{cC} + \mathrm{dD}$ the useful work that can be obtained from a process is defined as

$$\mathrm{W_{el}} = \Delta\mathrm{G} = -\mathrm{nFE} \qquad (2-7)$$

While the change in free Gibbs energy is:

$$\Delta\mathrm{G} = \Delta\mathrm{H} - \mathrm{T}\Delta\mathrm{S} \qquad (2-8)$$

It is also represented by the definition of chemical potential (Gibbs energy per mole) in the following equation:

$$\Delta\mathrm{G} = \Delta\mathrm{G}^{\circ} + \mathrm{RT}\ln\frac{\mathrm{A^aB^b}}{\mathrm{C^cD^d}} \qquad (2-9)$$

Therefore:

$$\mathrm{E} = \mathrm{E}^{\circ} + \frac{\mathrm{RT}}{\mathrm{nF}}\ln\frac{\mathrm{A^aB^b}}{\mathrm{C^cD^d}} \qquad (2-10)$$

In this general form of the Nernst equation $\Delta\mathrm{G}^{\circ}$ and E° refer to the free energy of the standard state and the standard electrochemical potential of the reaction at 298 K. Ideal cell performance is defined by the ideal cell electrical potential (E). The Nernst equation gives the ideal performance of a fuel cell in terms of the standard electrochemical potential, E^0, (the potential at concentrations of the reactant and product species of 1 atm and T=25°C. The open circuit potential is electrical potential of a fuel cell when no current is flowing. It is generally 10 –20 % less than the value of E^0.

2.2.3 Actual Performance

During operation of a real system, as the current flows through the cell, the resistances within the system (electrolyte, electrodes, and current collector) cause a drop in potential. This wasted chemical energy is released as heat. The losses usually originate from four sources: (1) electrode resistance (2) ohmic resistance, (3) diffusion in the gas and/or liquid phase, and (4) the difference between the standard electrochemical potential and the open circuit potential, as shown in Figure 2.1.

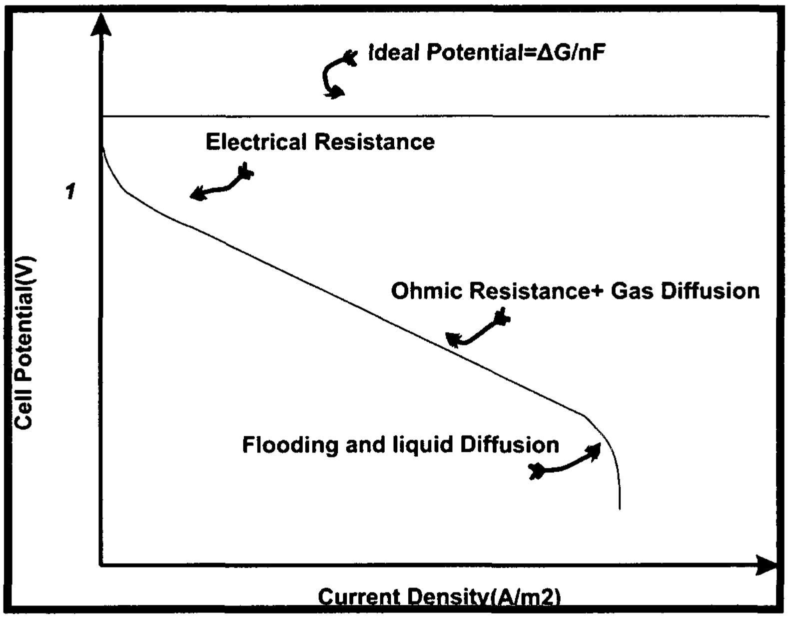

Figure 2. 1 Ideal and Actual Fuel Cell Potential/Current Characteristic

2.2.3.1 Electrode Resistance

The Electrode resistance can be observed at low current densities when surface processes, adsorption, reaction, desorption occur. In electrochemical reactions, like chemical reactions activation energy is necessary to form the transition state (a reaction intermediate). The energy of the transition state is greater than the energy of the reactants.

2.2.3.2 Ohmic Resistance

Ohmic polarization occurs because of the natural resistance to the flow of charges through the fuel cell materials. There is resistance to the movement of ions inside the electrolyte and there is also a resistance towards the movement of electrons inside the electrode and through the external circuit. The dominant ohmic losses are often through the electrolyte. They are reduced by decreasing the electrolyte thickness and by improving the ionic conductivity of the electrolyte. Ohm's law describes the losses in both the electrolyte and fuel cell electrodes.

2.2.3.3 Diffusion Resistance

This kind of resistance is caused by a decrease in concentration of the fuel or oxidant at the surface of the electrodes. As a reactant is consumed at the electrode by electrochemical reaction, a loss of chemical potential occurs. This phenomenon is due to the concentration gradient that is related to the rate of diffusion. Several diffusion processes may contribute to the overall diffusion resistance: slow diffusion in the gas phase in the electrode pores is one. Solution/dissolution of reactants/products into/out of the electrolyte, and diffusion of reactants/products through the electrolyte to/from the electrochemical reaction site are others. The rates of these diffusion processes cause potential losses over the entire current density range.

2.2.4 Efficiency

The overall energy efficiency of the fuel cell can be defined as the useful electrical energy produced divided by the heat that would have been obtained through the combustion of the fuel (enthalpy of fuel conversion to CO_2 and H_2O). In the ideal case, the maximum efficiency (or thermodynamic efficiency) of a fuel cell operating reversibly can be expressed as the ratio of Gibbs free energy of formation divided by the enthalpy of formation, where ΔG is the change in Gibbs free energy and ΔH is the change in the enthalpy for the reaction, as shown in Equation (2 – 5).

A single fuel cell typically operates at a potential of 0.6-0.8 (V) (Hoogers 2002). In order to produce more electrical power a number of cells are attached to each other in series to form the so-called "fuel cell stack". Stacks producing 1W to 250 (kW) power (Kordesch 1996) are available commercially.

Hydrogen can be produced and stored for future consumption in a fuel cell. However, there are challenges and costs associated with transforming fuel into hydrogen and its subsequent storage. On-site production of hydrogen (fuel processing) includes both steam reforming of hydrocarbons and hydrogen purification. The hydrogen must be purified, by removing sulphur and carbon monoxide, for use in low temperature fuel cells while high temperature fuel cells can tolerate larger CO contents in the feed.

System components other than the fuel conversion and conditioning systems are also required. Thermal management and electric power conditioning components are necessary for the operation of the fuel cell system. These components together form what is called the balance of plant and are added to the fuel cell stack and the fuel processor to build a complete system.

2.2.5 Advantages and Disadvantages of Fuel Cell

2.2.5.1 Advantages

- Efficiency: Theoretically Fuel cells could be more efficient than combustion engines for the conversion of chemical energy directly into electrical energy. They do not have the material limitation of the heat engine. For high temperature fuel cells all the exhaust gas from the fuel cell can be used to generate even more power, increasing the efficiency even higher.

- Simplicity: Fuel cells have few or no moving parts. In some cases high reliability may be attained with operational lifetimes exceeding 40,000 hours. (the operational life is formally over when the rated power of the fuel cell is no longer satisfied)

- Low/Zero emissions: Fuel cells running on hydrogen and air produce only water as the by-product. The reaction inside the fuel cell occurs between specific reactant species only. It limits release of NO_x because the temperature in fuel cells is less that in combustion engines. Fuel cells produce lower concentrations of SO_X because the fuel being fed to the fuel cell contains less sulphur than that being fed to combustion engines.

- Quiet operation: Fuel cells operate quietly with only a few moving parts if any. They also require less maintenance. This is in strong contrast with the combustion engine.

- Flexibility: Modular installations can be used to match the load and increase reliability of the system

2.2.5.2 Disadvantages

Since different types of fuel cells have significantly different operating regimes, they have their own individual disadvantages. Many of them are associated with their materials of construction, fabrication techniques, and specific system requirements. But some of these disadvantages are similar for the majority types of the fuel cells.

- Cost: The most important disadvantage of almost all types of fuel cells at the present time is the cost. The cost and energy requirements associated with production, storage, and distribution of hydrogen decreases the attractiveness of fuel cells and is a significant challenge in commercialization of these systems

- Endurance and Reliability: Although fuel cells are highly environmental friendly devices which can produce energy with reasonable efficiency, improvements in the long term performance of most types of fuel cells are wanted. Many research projects are currently underway in order to improve reliability and durability.

- Other disadvantages include catalyst deactivation, catalyst poisoning by fuel impurities or reaction products, carbon sediment, material incompatibility within fuel cells or fuel cell stacks; limitations in infrastructure for the delivery of fuels suitable for many fuel cells; and their acceptance into the existing marketplace as safe energy devices.

2.2.6 Application

The three major categories of fuel cells are portable, stationary and mobile. Examples of these applications include using alkaline fuel cells in space application, applying proton exchange membrane fuel cells in cars, buses and locomotives, employing SOFCs in commercial heat and power production. Some of the most important application areas are as follows:

2.2.6.1 Stationary Applications (~ 10-500 (kW))

Fuel cells have possible applications as stationary power generation units. Large fuel cells might become an alternative to conventional combustion power plants. Fuel cells can also be used as a backup power source or an emergency power system in a crisis (eg. When regular systems fail in hospitals, laboratories, telecommunication sites and data centers). A smaller fuel cell of capacity up to 7 (kW) of power can be used to generate power for houses.

2.2.6.2 Transportation (Vehicular Applications ~ 50-100 (kW))

Another major application of fuel cells is in transportation. From cars and scooters, to locomotives, trains and planes, fuel cell vehicles have already been developed to the prototype stage. Fuel cell vehicles can be fuelled either with pure hydrogen gas stored onboard in high-pressure tanks or with hydrogen-rich fuels; such as methanol, natural gas, or even gasoline. However, these fuels must first be converted into hydrogen gas by a fuel processor. The latter produce air pollutants CO_2 during steam reforming. While hydrogen fuel produces no pollutants; only water and heat, CO_2 was emitted to the atmosphere when hydrogen was manufactured.

Almost all the major car companies have R&D units to investigate and test fuel cell applications in the transportation industry. Some of them like Toyota plan commercial production of a fuel-cell vehicle by 2015. After US President Barak Obama declared (Scoggins 2008) that there would be government fuel cell funding, several car companies, including General Motor Corp. and Honda Motor Co. decided to continue their research.

2.2.6.3 Portable Power (Mobile/Portable Applications ~ 10-100 W)

For portable power applications such as lap-top computers, smart cell-phones, and personal digital assistants, fuel cells must compete with batteries. Nevertheless, this application promises to be one of the early commercial markets for fuel cell technology. Fuel cells were first explored as portable power units in the 1960s. Casio, HP, NEC and Motorola all have fuel cell programs (Bove 2007). Fuel cell manufacturing companies like Medis, Mechanical Technology, and Enable Fuel Cell, are developing miniature fuel cell solutions to power portable electronics.

2.3 Types of Fuel cell

Fuel cells are usually categorized according to their electrolyte type. The following are the five different types of fuel cells:

2.3.1 The Phosphoric Acid Fuel Cell (PAFC)

The operation temperature of the phosphoric acid fuel cell (PAFC) is in the range of 150°C to 220°C. The specific electrolyte used for this type of fuel cell is phosphoric acid. The acid is contained in the porous structure of silicon carbide diaphragms. A Pt catalyst is used in both the anode and cathode. Protons, (H^+), the charge carrier in this type of fuel cell, migrate from the anode, through the electrolyte, to the cathode where they combine with the oxygen. The final product of this reaction is water. The electrons produced flow out of the fuel cell through an external circuit.

The basic reactions taking place in a typical PAFC are shown below:

Anode: $H_2 \rightarrow 2H^+ + 2e^-$ (2 − 11)

Cathode: $0.5O_2 + 2H^+ + 2e^- \rightarrow H_2O$ (2 − 12)

Overall: $H_2 + 0.5O_2 \rightarrow H_2O$ (2 − 13)

Some of the advantages of PAFC's are high efficiency in cogeneration mode, simple construction, low electrolyte volatility, long-term stability and minimum corrosion problems.

2.3.2 The Proton Exchange Membrane Fuel Cell (PEMFC)

The fuel cell type proposed for the automobile industry is the proton exchange membrane fuel cell (PEMFC). They operate at low temperature 60°C -80°C. The electrolyte that is used in this type of fuel cell is a proton conductor membrane, normally Nafion.

The fuel for the PEMFC is normally hydrogen and the charge carrier is the hydrogen ion (H^+, proton). The hydrogen ions flow from the anode, through the electrolyte, to reach the cathode while the electrons flow through an external circuit and produce electric power. Oxygen, usually in the form of air, is supplied to the cathode and combines with the electrons from the external circuit and the hydrogen ions from the electrolyte to produce water. The electrode reactions that take place are:

Anode: $H_2 \rightarrow 2H^+ + 2e^-$ (2 − 14)

Cathode: $0.5O_2 + 2H^+ + 2e^- \rightarrow H_2O$ (2 − 15)

Overal: $H_2 + 0.5O_2 \rightarrow H_2O$ (2 − 16)

Fast start times, minimum hardware corrosion, more power for a given volume or weight of fuel cell compared to other types of fuel cell, long cell and stack life due to their solid electrolyte are the merits of PEMFCs.

2.3.3 The Molten Carbonate Fuel Cell (MCFC)

Molten carbonate fuel cell (MCFC) is a high-temperature fuel cell. The electrolyte is a combination of alkali carbonates. In order to provide mechanical stability to the structure of the electrolyte a ceramic network of $LiAlO_2$ is usually used to contain the molten carbonate.

When heated to a temperature of around 650°C, alkali carbonates melt and become conductive to carbonate ions (CO_3^{2-}). In order to produce water at the anode of the fuel cell the carbonate ions flow from the cathode, through the electrolyte, to the anode where they react with hydrogen. The electrons flow from the anode, through an external circuit, to the cathode. Carbon dioxide produced at the anode must be moved to the cathode where it is consumed. The electrode reactions taking place in the anode and cathode are:

Anode: $H_2 + CO_3^{2-} \rightarrow H_2O + CO_2 + 2e^-$ (2 − 17)

Cathode: $0.5O_2 + CO_2 + 2e^- \rightarrow CO_3^{2-}$ (2 − 18)

Overall: $H_2 + 0.5O_2 \rightarrow H_2O$ (2 − 19)

Some of the advantages of MCFC's are internal fuel reforming of natural gas, the ability to use standard materials for construction of fuel cell, and the possibility of using nickel-based catalysts on the electrodes.

2.3.4 The Alkaline Fuel Cell (AFC)

As mentioned in 2.2 (history of the fuel cell) the alkaline fuel cell is one of the oldest types of the fuel cells. It was used in the mid 1960 by NASA (National Aeronautics and Space Administration) in the Apollo program and later in the Space Shuttle program. KOH is the electrolyte used in this type of fuel cell. One of the other features of this type is the wide variety of catalysts that can be applied from Ni, Ag, metal oxides, to many noble materials.

One of the drawbacks of these fuel cells is the fuel supply purity. CO is a poison. CO_2 will react with the KOH to form K_2CO_3, thus altering the electrolyte. The charge carrier for an AFC is the hydroxyl ion (OH^-) that migrates from the cathode to the anode where it reacts with hydrogen to produce water and electrons. Water formed at the anode migrates back to the cathode to regenerate hydroxyl ions. The set of reactions in the fuel cell is:

Anode: $H_2 + 2OH^- \rightarrow 2H_2O + 2e^-$ (2 − 20)

Cathode: $0.5O_2 + 2OH^- + 2e^- \rightarrow 2OH^-$ (2 − 21)

Overall: $H_2 + 0.5O_2 \rightarrow H_2O$ (2 − 22)

The major advantage of this type of fuel cell is its low cost.

2.3.5 The Direct Methanol Fuel Cell (DMFC)

Direct methanol fuel cells are a recent (1954) technology compared to hydrogen fuel cells, and are almost at the stage of commercial development. DMFCs are very similar to

PEMFC in that both use a polymer electrolyte and the charge carrier is the hydrogen ion (proton). Liquid or vapour phase methanol (CH_3OH) is oxidized in the presence of water at the anode producing CO_2, hydrogen ions, and electrons that travel through the external circuit to the cathode. The hydrogen ions flow through the electrolyte and react with oxygen from the air and the electrons from the external circuit to form water at the anode. The reactions are as follows

Anode: $CH_3OH + H_2O \rightarrow CO_2 + 6H^+ + 6e^-$ (2 − 23)

Cathode: $1.5O_2 + 6H^+ + 6e^- \rightarrow 3H_2O$ (2 − 24)

Overall: $CH_3OH + 1.5O_2 \rightarrow CO_2 + 2H_2O$ (2 − 25)

The main advantage of this type of fuel cell is the fact that the fuel is stored in the liquid phase and thereby avoids the problems of storing gaseous hydrogen.

2.3.6 The Solid Oxide Fuel Cell (SOFC)

Solid oxide fuel cells operate at very high temperature (600°C -1000°C). The high operating temperature of SOFC attracts attention from power generation industries because the high temperature gas leaving the fuel cell can be used to generate additional electrical power. They are also being considered as auxiliary power units for diesel trucks. The in-situ production of hydrogen from hydrocarbon fuels at the high temperature inside SOFC's is also being studied.

The basic half reactions of SOFC are as follows:

Anode: $2H_2 + 2O^{2-} \rightarrow 2H_2O + 4e^-$ (2 − 26)

Cathode: $O_2 + 4e^- \rightarrow 2O^{2-}$ (2 − 27)

Overall: $2H_2 + O_2 \rightarrow 2H_2O$ (2 − 28)

Like any other fuel cell, SOFCs are made up different components. The major distinct characteristic of solid oxide fuel cell is that the electrolyte is made of ceramic. The materials used are solid ion conductors. Furthermore the materials for the electrodes need to meet a number of requirements. High electrical conductivity, sufficient ionic conductivity, good catalytic activity, and compatible thermal expansion coefficient are the main characteristics required for anode and cathode materials. Various components of SOFC will be discussed in detail in the next sections.

2.3.6.1 History of Solid Oxide Fuel Cell

The idea of using a stabilized zirconia material as an electrolyte stemmed from the experiments by Nernst in 1899. In the late 1930s, Emil Baur et al. (Baur 1937), carried out some experiments using solid oxide electrolyte. The solid substances used were zirconium, yttrium, cerium, lanthanum, and tungsten. Their designs were not successful and frequently experienced unwanted chemical reactions between the electrolytes and various gases, including carbon monoxide.

In the 1940s, O. K. Davtyan's (Davtyan 1947) experimental results on solid electrolytes for high-temperature fuel cells were published. He and his colleagues designed a new ceramic material that increased the conductivity and mechanical strength. Davtyan's designs, however, also experienced unwanted chemical reactions and short life ratings.

Toward the end of the 1950s several different research institutions worked on improving solid oxide conditions (CONSOL Energy, General Electric). A 1959 discussion of fuel cells, mentioned by (Stambouli 2002), pointed out those problems with solid electrolytes included relatively high internal electrical resistance, melting, and short-circuiting due to semi-conductivity. However the promise of a high-temperature cell that would be tolerant of carbon monoxide and use a stable solid electrolyte continued to attract attention (Janardhanan 2007). More recently, increasing energy prices and achievements in materials technology have revived work on SOFCs, and a recent report (Stambouli 2002) noted about 40 companies working on these fuel cells.

2.3.6.2 Advantage and Disadvantage of SOFC's

The high temperature of the outlet streams of an SOFC offers the possibility of co-generation using gas turbine power systems to produce electricity from the high temperature heat in the fuel cell product off-gas. Once a SOFC is combined with a gas turbine, efficiencies of up to 74% can be achieved (Singhal 2000). In addition the high operating temperature enables the fuel cell to operate without precious metal electro catalysts at the electrodes. The use of solid oxygen conductors as the electrolyte eliminates corrosion and electrolyte management problems.

However, there are also disadvantages associated with SOFCs. The major demerits are the time needed for heating an SOFC system to the operating temperature during start up, sealing failure, and safety issues. SOFCs require expensive materials of construction.

2.3.6.3 Anode

The function of an SOFC anode is to electrochemically oxidize hydrogen contained within the fuel. The anode must meet the following requirements:

- Stability: The anode should have stability and compatibility with the adjacent materials. Several chemical and phase changes, that cause dimensional changes, take place during the operation of the fuel cell. These changes may occur due to interactions with other SOFC components, or by the production of water vapour at the high operating temperature. SOFCs should also be capable of operating with impurities in the feed streams.
- Catalytic activity: The anode should have a high catalyst activity for the oxidation of fuel gas.
- Conductivity: In order to minimize the ohmic loss a large electrical conductivity is desired.
- Porosity: The porosity of the anode must be tailored with regard to mass transport considerations as well as mechanical strength.

The anode material is usually a combination of Ni (nickel) and YSZ (yttrium stabilized zirconia) (Zhu 2003). Usage of the ceramic material in the anode is (a) to ensure that the thermal expansion coefficient of the composite electrode is close to that of the other components of the cell, (b) to prevent the nickel particles in the porous structure from sintering, and (c) to have a three dimensional electrode where there is intimate contact for reaction between the electrons (Ni phase) and the ions (YSZ phase). Ni/YSZ is the conventionally used cermet anode, where Ni plays the dual role of hydrogen (or hydrocarbon) oxidation catalyst and electric current conductor.

2.3.6.4 Cathode

It is important for the cathode materials to meet the following criteria:

- Stability and compatibility: Cathode compatibility refers to (a) preventing high temperature reactions that form undesired phases at the cathode-electrolyte and cathode interconnect interfaces, (b) ensuring matching thermal expansion of different materials over the entire SOFC operating range, as well as (c) the rapid incorporation of oxygen ions into vacancies within the electrolyte.

- Catalytic activity: The cathode should have a high catalyst activity for the half-cell reaction at the cathode: the dissociative adsorption of oxygen and its reduction at the surface. Since the O^{2-} ion formation is an energy demanding reaction, the electrode resistance at the cathode is very high. Any material that can effectively catalyze the formation of O^{2-} ions can reduce the overpotential.

- Conductivity: The cathode should usually have a good ionic conductivity. Ionic properties can significantly improve the performance and electrode overpotential.

- Porosity: It should have some porosity for an adequate gas transport rate. A porous structure allows rapid mass transport of reactant and product gases.

The cathode is composed of a perovskite mixed with YSZ. The perovskite is both the electro catalyst and the electronic conductor. It is composed of strontium doped lanthanum manganite (LSM) with the formula $La_{(1-x)}Sr_xMnO_3$ (LSM) (Minh 1995).

2.3.6.5 Electrolyte

The electrolyte in SOFC is a ceramic material sandwiched between the anode and the cathode. An electrolyte should have the following requirements:

- Conductivity: The electrolyte should be a very good ionic conductor for the transport of the oxygen ions that are formed at the cathode/electrolyte interface and subsequently transported towards the electrolyte-anode interface. On the other hand the electrolyte should have no conductivity for electrons
- Stability: The electrolyte has to be stable under the oxidizing atmosphere prevailing at the cathode and under the reducing atmosphere at the anode.
- Electrolyte materials also must be electrically insulating and gas impermeable (microstructurally dense).

The most common electrolyte material is zirconia with 8% yttria added as dopant (yttrium-stabilized zirconia or YSZ). It is a polycrystalline ceramic, exhibiting excellent stability in both oxidizing and reducing atmospheres. YSZ is not the only electrolyte material being investigated for SOFCs. Other materials such as rare earth oxide doped ceria's and lanthanum gallates have higher ionic conductivities than YSZ, however they also have higher costs and have experienced some reaction and phase stability issues. (Singhal 2004)

2.3.6.6 Fuels

Most fuel cells demand quite pure hydrogen as fuel. SOFCs have the ability to work with other fuels like hydrocarbons. Nevertheless SOFC fuel cells, that can use other fuels, normally work best with hydrogen. Operating fuel cells directly with hydrocarbons has drawn considerable attention recently. The large availability of hydrocarbon fuels like natural gas, make them a good choice for stationary applications. Although there are some reports on the operation of SOFCs using fuels such as ethane, propane, butane and octane, these have been limited to laboratory studies. When operating SOFCs with hydrocarbon fuels, the higher hydrocarbons, break down to smaller molecules, and the electrochemical charge transfer proceeds through hydrogen and CO oxidation (Singhal 2004).

2.3.6.7 Types of Solid Oxide Fuel Cell (SOFC)

SOFCs can be categorized based on their manufacturing process. They can be either electrolyte or electrode supported which means either the electrolyte or the electrode provides the mechanical strength for the cell.

- Electrolyte Supported Cells

In the electrolyte-supported SOFCs, the anode and cathode are very thin but the electrolyte thickness is thick enough to provide the necessary mechanical strength, generally 100-200 (μm). Electrolyte supported cells are appropriate at 850-1000°C (1123 -1273 (K)) where the thick electrolyte will have adequate conductivity for the oxygen anions. Electrolyte-supported cells have the disadvantage that due to the high Ohmic losses in the solid electrolyte they require a much higher operating temperature and their power density is comparatively low.

- Electrode Supported Cells

Electrode supported cells can be cathode or anode-supported. The thickness of the electrolyte in these systems can be decreased to 5-10 (μm) and thus they can operate at lower temperatures (700°C -800°C). Either the anode or cathode must be thick enough to support the cell. It is usually between 0.3 and 1.5 (mm). In cathode-supported cells, there are mass transfer limitations, manufacturing problems, and higher costs are issues. Anode supported cells are the most attractive, because the Ni/YSZ anode material provides higher thermal and electrical conductivity, better mechanical strength, and minimal chemical interaction with the electrolyte. In addition cathode-supported cells are more expensive to produce than anode-supported cells since perovskite cathode material is more expensive than the anode material.

SOFC can also be classified based on the shape and geometry of the cell

- Planar (Bipolar)Solid Oxide Fuel Cell

The planar geometry is the sandwich type utilized by most types of fuel cells including SOFCs, where the electrolyte is in between the electrodes. A flat shape is one of the main advantages of the planer SOFCs (Costamagna 2004). Flat shapes are easy to handle, fabricate, and assemble in stacks. In addition the current collection is easier when the surface is flat. The main disadvantage however, is the appropriate sealing of the different layers of the cell to prevent cross-over of the fuel and oxidant, and to prevent leaks to the cell exterior. In the planar design the fuel and air may flow co-currently, counter-currently, or cross currently. Each of these flow patterns has its own advantages and all three cases are currently used in manufacturing planar cells. (Yamamoto 2000):

- Tubular Solid Oxide Fuel Cell

In the tubular design of SOFCs either air or fuel passes through the inside of the tube and the other gas passes along the outside of the tube. Tubular cells have the advantage that their geometry results in a natural seal between layers of the structures, and fabrication can be simple. Nevertheless, these cells tend to be long and small in diameter, and are vulnerable to consistency and failure issues due to induced thermal stresses (Yamamoto 2000).

2.3.6.8 The Application of Solid Oxide Fuel Cell

Solid oxide fuel cells are expected to be used in three major energy applications: stationary, transportation, and military. SOFCs have great promise for the stationary power generation sector. They can be the primary or auxiliary power source for many facilities like homes, office buildings, and industrial power plants. Since SOFCs, like molten carbonate fuel cells, require high operating temperatures, cogeneration–using waste heat to generate steam for space heating, industrial processing, or in a steam turbine to make more electricity is possible.

In the transportation sector, recent developments suggest that SOFCs could play an important role. In diesel trucks, they will probably be used as auxiliary power units to run electrical systems like air conditioning and on-board electronics (Singhal 2002). Such units would eliminate the need to leave diesel trucks running at rest stops, thereby leading to a savings in diesel fuel expenditures and a significant reduction in both diesel exhaust and truck noise.

The above fuel cell types can also be categorized by their operating temperatures:

- High Temperature Fuel Cells: MCFC (550°C -700°C) and SOFC (600°C -1000 °C)
- Low Temperature Fuel Cells: PEMFC (60°C - 80°C), AFC, and PAFC (150°C -220°C)

Bibliography

Amory, L., B. Williams. "A Strategy for Hydrogen Transition." Paper presented to the 10 th Annual U.S. Hydrogen Meeting. Vienna,VA, April 7-9 1999.

Bacon, Francis T. and T. M. Fry., "The Development and Practical Application of Fuel Cells." Proceedings of the Royal Society of London, Series A. Mathematical and Physical Sciences, 1973:431.

Baur, E., H. Preis., "Solid. Electrolyte Fuel Cells." Z. Elektrochem. 43, 1937: 727.

Blum, L., W. A. Meulenberg, H. Nabielek, R. Steinberger-Wilckens. "Worldwide SOFC Technology Overview and Benchmark." International Journal of Applied Ceramic Technology, 2,2005: 482-492.

Bockris, J., A. Reddy,M. Gamboa-Aldeco. Modern Electrochemistry 2A: Fundamentals of Electrodics. Springer, 2008.

Bove, R., S. Basu (Editor). "Recent Trends in Fuel Cell Science and Technology". Springer, 2007.

Chalk, S.G., J.F. Miller, F.W. Wagnerc. "Challenges for Fuel Cells in Transport Applications." Journal of Power Sources,86,1-2, 2000: 40-51.

Clean Coal & Natural Gas Power Systems,Future Fuel Cells R&D. www.fossil.energy.gov.

CONSOL Energy, America's On Switch. http://www.consolenergy.com/.

Costamagna, P., A. Selimovic, M. Del Borghi, G. Agnew. "Electrochemical Model of the Integrated Planar Solid Oxide Fuel Cell (IP-SOFC)." Chemical Engineering Journal,(102), 2004: 61.

Davtyan, O. K.,. "The Problem of Direct Conversion of the Chemical Energy of a Fuel to Electrical Energy [in Russian]." Izd. AN SSSR, 1947.

Electric Fuel : Military Batteries & Rechargeable Batteries. http://www.electric-fuel.com/.

Enable Fuel Cell Corporation. www.enablefuelcells.com (accessed 2009).

Fergus, J., R. Hui, X. Li, D. Wilkinson, J. Zhang. Solid Oxide Fuel Cells: Materials Properties and Performance. Springer, 2008.

Fitzgerald, J., N. O'Bryan. Fuel Cells: A Better Energy Source for Earth and Space. 02 11, 2005. http://www.nasa.gov/centers/glenn/technology/fuel_cells.html (accessed 7 1, 2009).

Fuel Cell Basics Application. http://www.fuelcells.org/basics/apps.html (accessed Aguest 2009).

Fuller, T.F., M.L. Perry, "A Historical Prespective of Fuel Cell Technology in the 20th Centrury", Journal of the Electrocchemical Society, 149,7, 2002: 59-57

"FY 2010 Congressional Budget Request." U.S Department of Energy. http://www.cfo.doe.gov/budget/10budget/Content/Highlights/FY2010Highlights.pdf (accessed May 2009).

General Electric, Schenectady, NY. http://www.ge.com/.

Grove, W.R., "On a New Voltaic Combination", Philosophical Magazine and Journal of Science, 13,1839: 127-130

Grove, W.R., "Note sur une Pile Voltaique grande energie, construite par M.Grove; communication de M.Becquerel", Comptes Rendus., 8,1839:497

Grove, W.R., Philosophical Magazine and Journal of Science, 1842:417-420

Holland, B.J., J.G. Zhu, L. Jamet. "Fuel Cell Technology and Application." Australasian Universities Power Engineering Conference (AUPEC-2001). Perth, Australia: Curtis University of Technology, 2001.

Hoogers, Gregor. Fuel Cell Technology Handbook. CRC press, 2002.

Janardhanan, V. A Detailed Approach to Model Transport, "Heterogeneous Chemistry, and Electrochemistry in Solid Oxide Fuel Cells". Doctoral thesis. Institute for Chemical Technology and Polymer Chemistry, 2007.

Kordesch, K., G. Simader. "Fuel Cells and Their Applications". Weinheim, Germany: Wiley-VCH, 1996.

Kreuer, K.D., T. Van Nguyen,T.Zhao. Advances in Fuel Cells, Volume 1. Elsevier Science, 2007.

Larminie, J., A. Dicks. Fuel Cell Systems Explained. SAE International, 2003.

Lovins, A.B., B.D. Williams. A strategy for the Hydrogen Transition. Rocky Mountain Institute, 2000.

Mechanical Technology Incorporated - MTI (Nasdaq MKTY), http://www.mechtech.com/company/ (accessed 03 2009).

Medis Power Pack Micro Fuel Cell Technical and Cost Analysis. Yole Developpement, 2008.

Minh, N. Q. "Ceramic Fuel Cells." Journal of the American Ceramic Society, Vol/Issue: 76:3,1993: 563-588.

Minh, N.Q.,T. Takahashi. "Science and Technology of Ceramic Fuel Cells". Amsterdam,The Netherlands: Elsevier, 1995.

National Aeronautics and Space Administration. http://history.nasa.gov/apollo.html.

National Fuel Cell research Cente, University of California, Irvine. http://www.nfcrc.uci.edu/2/fuel_cell_information/fcexplained/Fuels.aspx (accessed April 2009).

Ortiz-Rivera, E., A. Salazar-Llinas, and J.Velez-Delgado. "An Enriched Undergraduate Research Experience based on the Simulation, Experiments, and Theory of Fuel Cells." 39th ASEE/IEEE Frontiers in Education Conference. San Antonio, 2009. M4D1.

Scoggins, J. U.S. Department of Energy. May 27, 2008. http://www.energy.gov/news/6283.htm (accessed April 2009).

Services, EG&G Technical. Fuel Cell Handbook. Parsons, Inc, 2000.

Singhal, S. C. "Advances in Solid Oxide Fuel Cell Technology." Solid State Ionics(135), 2000: 307.

Singhal, S. C.,. "Solid oxide fuel cells for stationary, mobile and military applications." Solid State Ionics,(152-153), 2002: 405.

Singhal, S.C., K. Kendall. "High-temperature Solid Oxide Fuel Cells: Fundamentals, Design and Applications". Elsevier Science, 2004.

Srinivasan, S. "Fuel Cells: From Fundamentals to Applications". Springer, 2006.

Stambouli, A.B., E. Traversa, " Solid Oxide Fuel Cell: A Review of an Environmentallly Clean and Efficient Source of Energy", Renewable and Sustainable Energy Reviewa, 6, 5, 2002: 433-455.

The Business of Fuel Cells. http://www.eyeforfuelcells.com/index.asp (accessed May 2009).

Yamamoto, O. "Solid Oxide Fuel Cells: Fundamental Aspects and Prospects." Electrochimica Acta,(45), 2000: 2423.

Zhu, W.Z., S. C. Deevi. "A Review on the Status of Anode Materials for Solid Oxide." Materials Science and Engineering A,(362), 2003: 228.

Chapter 3 Literature Review

3.1 General Overview

The number of academic publications on the topic of solid oxide fuel cells (SOFCs) has been increasing. A search in databases shows that more than 8,000 papers on fuel cell related subjects have been published up to the present time. Almost 1200 papers were published last year, compared to the approximately 700 that were published in 2007. This increasing number of publications shows an increasing interest in addressing SOFC issues.

This research can be divided into several areas of interest: alternative material of electrodes and electrolytes (Steele 1990, Metcalfe 1992, Baker 1994, Irvine 1997, Slater 1997, Flot 1998, Kaiser 1998); micro-structure (Lee 1997, Jensen 2001, Clemmer 2004, Pratihar 2005, Jeon 2006, Vels Kenney 2007, Zhu et al. 2008); kinetics (Divisek 1994, Mizusak 1994, Mogensen 1996, Fouquet 2003, Modak 2007); anode and cathode modeling (Costamagna 1998, Bieberle 2002, Hussain 2006) [details of this group of papers will be discussed later]; electrochemical characteristics of the cell (Kawada 1990, Kawada 1994, Horita 1996, Patcharavorachot 2008); and TPB (Nakagawa 1995, Nakagawa 1999, Deng 2005, O'Hayre 2005, Hertz 2007, Janardhanan 2008, Lynch 2008, Zhu 2008); reforming (Meusinger 1998, Finnerty 1998, Ormerod 1999, Finnerty 2000, Peters 2002, Atkinson 2004); low temperature SOFCs (De Souza 1997, Huebner 1999, Yuan 2009); hydrocarbon fuels (Lu 2002, Lu 2004, Pil Yoon 2004, Kee 2005).

3.2 Modeling

One of the major topics of interest among researchers is quantitative modeling of SOFCs. Finding an appropriate mathematical model is important, since it can diminish the need for expensive and time consuming experiments. Quantitative models are also valuable because they can examine and evaluate the effects of particular designs and operating conditions on the overall performance of SOFC.

The first SOFC model appeared in 1985. Vayenas et al. (1985) presented a paper in which a 2D model of a monolith SOFC was constructed in order to describe the distribution of the species concentrations, current density and temperature. One of the other early significant publications on SOFC modeling was published by Bossel (1992). Since then the number of papers on modeling SOFCs has been increasing rapidly. Up to the time of writing this thesis there were more than 330 papers on modeling SOFCs (Vandersteen 2004).

One major drawback of all numerical simulations is that models do not guarantee an exact representation of natural phenomena of each cell, especially if there are arbitrary unknowns incorporated into the model. Numerical approximations can cause errors and the possibility of inaccurate simulation results. However, a comparison of predicted numerical values with measured experimental data permits researchers to validate the simulations. Numerical results reported by different researchers using commercial modeling software packages such as COMSOL, Fluent and the like often show reasonable correlations with experimental data.

Mathematical models can be divided into different types. A typical SOFC can be treated as:

- A heat and mass exchanger from the viewpoint of fluid dynamics and transport phenomena.
- An electrochemical generator from the viewpoint of electrochemical modeling.
- A chemical reactor from the viewpoint of chemical reactions including the influence of fuel composition and heat effects associated with irreversibilities during electrochemical conversion.
- A system of components by combining stack models with system models such as a reformer, a contaminant removal unit, and compressors,

The models presented in the literature are: one dimensional, (Suwanwarangkul 2003, Zhu et al. 2003, Iora et al. 2004, Costamagna et al. 2004, Hernández-Pacheco et al. 2004); two dimensional (Stiller et al. 2005); or three dimensional (Yakabe et al. 2000, Yuan et al. 2003, Ferguson et al. 1996, Recknagle et al. 2003, Achenbach1994, Hussain et al.2006 and Shi et al. 2006). They take into account charge transport phenomena, mass, momentum, and energy transport; and in some case the combination of all of these phenomena.

The following models simulate only the anode (Yakabe et al. 2000, Xia et al. 2001, Suwanwarangkul et al. 2003, Yakabe 2004, Xia 2004, Ni 2007, Suzue 2008, Tseronisa 2008, Bessler 2008); only the cathode (Svensson et al. 1996, Chan et al. 2004, X. S. Chen 2004) and a single SOFC (Achenbach 1994, Iwata et al. 2000, Zhu et al. 2003, Inui et al. 2006, and Ji et al. 2006), or the whole stack (Recknagle et al. 2003, Petruzzi et al. 2003, Burt et al. 2004, and Chan et al. 2005).

Models include both steady state models (Aguiar et al. 2002, Aguiar 2005) and dynamic models (Petruzzi et al. 2003, Iora et al. 2004, Aguiar et al. 2005, Magistri et al. 2005 and Bhattacharyya 2009).

There are a large number of researchers that wrote software programs using established computer languages such as Fortran, C++, or MATLAB (ZhongHua 2007, Li 2008 and Yu 2009). Others used commercially available computational fluid dynamics programs like Fluent® (Lockett et al. 2004, Iora et al. 2004, Opera 2005) gPROMS® (Aguiar et al. 2005), and COMSOL (Suwanwarangkul 2003, Chaisantikulwat 2008, Ciano 2008). Finally some used a combination of methods (Tseronis 2006).

The distinction between micro-modeling and macro-modeling is another way to classify models. Macro-models deal with the macroscopic or overall operational behaviour of SOFCs. Micro-models, consider the micro-scale behaviour. There are several models that concentrated on SOFC component performance, especially electrodes. Micro-structure is important because it influences the performance of the electrodes. The porosity, the pore size, and the tortuosity factor can affect the transport of gaseous species through porous electrodes.

- Simple Pore Model

This model is one of the physicochemical models for porous gas diffusion electrodes used with liquid phase electrolytes. In this model the gas must first dissolve in the liquid phase electrolyte and then be transported to the surface of the electrode that is covered with liquid phase electrolyte. This model is referred to as the pore model (Austin 1965).

- Thin Film Model

In the case of thin film model for a gas diffusion electrode, used with liquid phase electrolytes, it is postulated that a thin film covers the interior surface of pores within a porous electrode (Austin 1965, Tanner 1997). A uniform cylindrical pore as in the case of the simple pore model and a uniform structure of a thin film within each pore are the essential features. The thin film model proved to be more realistic than the pore gas model. Pore model is used in micro-structuring model of SOFC (Kuo 1995).

- Random Resistor Network Model

In a random resistor network model particles of ionic and electronic conductors are randomly distributed by a Monte Carlo technique, and modeled as a resistor network. Then, the overpotential at the electrode is obtained by solving Kirchoff's law for this resistor network (Sunde 1995, Maddox 1985, Costamagna 2004).

- Random Packing Sphere Model

This is an advanced model in comparison with the classical electrode models (Na 2006). Percolation theory (Stauffer 1994) and coordination number theory (Bouvard 1991) were were applied to a system of randomly packed spheres to calculate ionic and electronic conductivities, length of the TPB, and density. Most of these models rely on the macroscopic homogeneity of composite electrode media. Their results are not consistent with experimental results using the real micro-scale electrode structures.

3.3 Modeling the Electrodes

Numerous quantitative models have been developed to relate SOFC electrode micro-structure to performance

3.3.1 Mass Transport

The mass conservation law can be written as:

Net rate of accumulation of species i in the control volume (C.V.)
= Net rate of mass efflux of species i from the (C.V.)
+ Rate of chemical production of species i within the (C.V.)

$$\frac{\partial C_i}{\partial t} = -\nabla . N_i + R_i \qquad (3-1)$$

Where C_i is the concentration of species i, N_i is the flux of species i, and R_i is the rate of reaction of species i.

Models for mass transport inside a porous SOFC anode/cathode were developed based on Fick's model (FM), the dusty-gas model (DGM) and the Stefan–Maxwell model (SMM) to predict the concentration overpotential (Suwanwarangkul 2003).

3.3.1.1 The Fick's Law Model (FM)

FM is the simplest form used to describe the transport of components through the gas phase and within porous media. The general extended form of this model (Suwanwarangkul 2003) takes into account diffusion and convection transport and is given by:

$$N_i = -D_i^e \Delta C_i + vC_i \qquad (3-2)$$

and if the convection transport term is described by the Darcy equation:

$$N_i = -D_i^e \Delta C_i + C_i \frac{\beta_\circ}{\mu_{mix}} \nabla p \qquad (3-3)$$

Where D_i^e is the effective diffusion coefficient which includes both bulk diffusion and Knudsen diffusion for the species i. v is the convection velocity $\beta_\circ$ is the permeability; p is the pressure and μ_{mix} is the viscosity of the mixture. d_m is the diameter of the molecules and n is the number of molecule per unit volume. Molecular diffusion is dominant for large pore sizes and high system pressures while Knudsen diffusion becomes important when the mean-free path of the molecular species is larger than the pore diameter d_p.

The mean-free path λ is (Suwanwarangkul 2003):

$$\lambda = \frac{1}{\sqrt{2}\pi d_m^2 n} \qquad (3-4)$$

The relative importance of bulk diffusion and Knudsen diffusion is determined by calculating the Knudsen number (N_{kn}).

$$N_{kn} = \frac{\lambda}{d_p} \qquad (3-5)$$

For Knudsen numbers less than 0.01 molecular diffusion is dominant. For Knudsen numbers greater than 10 the Knudsen diffusion is dominant. For the numbers in between, both types diffusion will contribute. By assuming equimolar counter diffusion of reactant and product species the effective diffusivity of the mixture, D_i^e (Veldsink 1999) will be

$$D_i^e = \left[\frac{1}{D_{im}^e} + \frac{1}{D_{ik}^e}\right]^{-1} \qquad (3-6)$$

D_{im}^e and D_{ik}^e are the effective molecular and Knudsen diffusion coefficients respectively.

$$D_{im}^e = \frac{d_p}{3}\frac{\varepsilon}{\tau}\sqrt{\frac{8RT}{\pi M}} \text{ (Mason 1983)} \qquad (3-7)$$

R= Universal gas constant

T= Absolute temperature

and

$$D_{ik}^e = \frac{1 - X_i}{\sum_{j \neq i} D_{ij}^e} \text{ (Yakabe 2000)} \qquad (3-8)$$

D_{ij}^e is the ordinary molecular binary diffusion and can be obtained from the following equation (Krishna 1997):

$$D_{ij}^e = \frac{\varepsilon}{\tau} D_{ij} \qquad (3-9)$$

ε is porosity and τ, is tortuosity.

$$\varepsilon = \frac{V_V}{V_{\text{Total}}} \tag{3 - 10}$$

where V_V is the volume of void-space and V_{Total} is the total or bulk volume of material, and the following equation can be used to calculate tortuosity. τ can be calculated from the following equation:

$$\tau = \left(\frac{l^e}{l}\right)^2 \tag{3 - 11}$$

where l^e , is the length of the tortuous path through the pores between two points and l is the straight line distance between the same two points. The permeability $\beta_\circ$ in Equation $(3 - 3)$ is a characteristic of the porous matrix structure and ideally should be obtained experimentally. If a bed of spherical particles (with diameter d_p) represents a porous electrode, then the permeability $\beta_\circ$ can be calculated from the Cozeny- Carman equation (Bear 1972).

$$\beta_\circ = \frac{d_p^2}{180} \frac{\varepsilon^3}{(1 - \varepsilon)^2} \tag{3 - 12}$$

The ordinary molecular binary diffusion coefficient D_{ij} can be calculated from kinetic theory and the Champan-Enskog equation (Chapman 1970),

$$D_{ij} = K \frac{\sqrt{T^3 \left(\frac{1}{M_i} + \frac{1}{M_j}\right)}}{p\, \sigma^2 \Omega_{D,ij}} \tag{3 - 13}$$

in which K is a constant of the equation, $\Omega_{D,ij}$ is a function of the temperature and the Boltzman constant, k (Bird 2002). M_i and M_j are the molecular weight of species i and j respectively and σ is the collision diameter of molecules.

The viscosity of each species can be calculated by (Bird 2002)

$$\mu_i = 8.4411 * 10^{-5} \frac{\sqrt{MT}}{\sigma^2 \Omega_\mu} \tag{3-14}$$

The mixture viscosity is given by

$$\mu_{mix} = \sum_{i=1}^{n} \frac{X_i \mu_i}{\sum_{j=1}^{n} X_j \theta_{i,j}} \tag{3-15}$$

In which $\theta_{i,j}$ is a function of each species viscosity (Bird 2002)

$$\theta_{ij} = \frac{1}{\sqrt{8}} \left(1 + \frac{M_i}{M_j}\right)^{-0.5} \left(1 + \left(\frac{\mu_i}{\mu_j}\right)^{0.5} \left(\frac{M_j}{M_i}\right)^{0.25}\right)^2 \tag{3-16}$$

3.3.1.2 The Stefan-Maxwell Model (SMM)

The SMM is a well-known mass transport model applied to nonporous medium. The SMM expresses species concentrations in terms of fluxes; it is given by (Lehnert 2000):

$$-\nabla . X_i = \sum_{j=1\, j\neq i}^{n} \frac{X_j N_i - X_i N_j}{C D_{i,j}^{e}} \tag{3-17}$$

Where X_i and X_j are the mole fractions of species i and j respectively. $0.5\, n(n-1)$ binary diffusivities are required. The viscous diffusivity can be added to the general equation to give the total fluxes.

3.3.1.3 The Dusty Gas Model (DGM)

The DGM includes three transport mechanisms: molecular diffusion, Knudsen diffusion, and viscous transport where the Stephan-Maxwell formulation is used to describe molecular diffusion. The total diffusive flux in the DGM is molecular diffusion acting in series with Knudsen diffusion. The viscous porous media flow (Darcy flow) acts in parallel with diffusive flux (Janardhanan 2007).

$$-\nabla . X_i - X_i \frac{\beta_\circ}{\mu_{mixD^{e}_{ik}}} \nabla p = \frac{N_i}{D_{i,k}} + \sum_{j=1\ j\neq i}^{n} \frac{X_j N_i - X_i N_j}{CD_{i,j}} \qquad (3-18)$$

In general the DGM is often the preferred way to describe a system consisting of all three types of transport. Comparing the DGM equation$(3-18)$ with the SMM equation $(3-17)$ shows that there are two additional terms in the DGM equation, $\frac{N_i}{D_{i,k}}$ accounts for the interaction between the gas species and the pore wall. The second additional term describes viscous transport. It is assumed from this model that pore walls consist of giant molecules "dust" uniformly distributed in space. These dust molecules are considered to be a dummy, or pseudo, species in the mixture (Arnost 1999).

3.3.2 Ion/Electron Transport

Another key aspect of an SOFC electrode model is ion transport. It is sometimes assumed that the electrolyte layer is the only cause of ohmic losses. In addition, charge transport in the ion conducting component of electrodes is important. Ionic transport is a fundamental process of fuel cell operation since ions must be present at the reaction site where the electrochemical reaction occurs.

3.3.2.1 Ionic Transport: Nernst-Plank Equation

Ions respond to both the concentration gradient and the electrical potential gradient (Lightfoot 1965). The total flux is therefore the sum of diffusion, and migration or drift, (electrophoresis phenomena) that moves ions in electric fields:

Based on Equation $(3-2)$:

Diffusion $= -D_i\ \nabla . C_i$ and

Convection = vC_i

There will be another term due to the potential difference for charge species:

$$\text{Electrophoresis} = -\varkappa_i\ C_i\ z_i\ \nabla . \varphi \qquad (3-19)$$

Where $\varkappa_i$ is the mobility

So the total flux will be:

$$\text{Total Flux } (N_i) = vC_i - D_i\ \nabla . C_i - \varkappa_{i_i}\ C_i\ z_i\ \nabla . \varphi \qquad (3-20)$$

The Nernst-Einstein relation:

$$\frac{\varkappa_{i_i} k T}{q} = D_i \qquad (3-21)$$

$$q = \text{elementary charge} = \frac{F}{N_A} \qquad (3-22)$$

k= Boltzmann constant

F= Faraday constant

replacing $\varkappa_i$ and q:

$$N_i = vC_i - D_i \nabla C_i - z_i \frac{D_i F}{RT} \nabla \varphi\ C_i \qquad (3-23)$$

z_i, is an integer ionic charge (the moles of charge per mole of ion).

$$\text{Total Flux } (N_i) = vC_i - D_i\ \nabla . C_i - \varkappa_{i_i}\ C_i\ z_i\ \nabla . \varphi \qquad (3-24)$$

3.3.2.2 Electronic and Ionic Transport: Ohm's Law

The governing equation for the charge transport of electrons is Ohm's law:

$$i_{el} = \sigma_{el} \nabla \varphi_{el} \qquad (3-25)$$

It is based on the conservation of charge in the electron conducting phase of the electrode. Wherei_{el}, is the electronic current density and σ_{el} is the conductivity of the electronic material. The governing equation for the charge transport of ions is

$$i_{io} = \sigma_{io} \nabla \varphi_{io} \qquad (3-26)$$

It is based on the conservation of charge in the ion conducting phase of the electrode. Where i_{io}, is the ionic current density and σ_{io} is the conductivity of the ionic material.

3.3.3 Anode

Xia et al. (2001) developed a one-dimensional micro-model of an anode in a SOFC. It includes the transport of electrons, ions, and gas molecules and the electrochemical reaction at the TPB of the anode. They identified a particular particle size that caused a minimum overall polarization. Very little anode polarization occurred when pure hydrogen was used. Finally they found a strong link between the anode thickness and particle size in the anode design. The bigger the particle size, the thicker the anode required to provide a sufficient number of reaction sites.

Xia et al. (2004) improved their previous work (Xia et al. 2001) by considering all possible polarizations that govern the complex interdependency among the various transport phenomena and the electrochemical reaction. They included variations in the micro-structure of the anode. The true internal exchange current density in the charge transfer equation accounted for the reaction rates at all anode locations. They validated their predicted anode resistance by comparing it with experimental data collected using different cermet particle sizes, anode thicknesses, and water content in the hydrogen. They obtained good agreement between the predicted results and the experimental data. They postulated that their model can be used as a guide for cell component design, component matching, and optimization of performance and operating conditions.

3.3.4 Cathode

In 2004, Chan et al. developed a cathode micro-model. They added the micro-structure of the electrode to the various transport phenomena and electrochemical reaction. These combined effects on the cathode overpotential at different operating conditions were studied. Their results showed that to decrease the cathode overpotential (a) the larger the ratio of yttrium stabilized zirconia (YSZ) particle size, to lanthanum strontium manganite (LSM) particle size, in the composite cathode, the smaller the optimum YSZ volume fraction, and (b) the larger the absolute particle sizes, the thicker the optimum cathode. A reduced overpotential was predicted for a thin cathode consisting of small particle sizes. Their results were in good agreement with experimental findings from the literature.

Chen et al. (2004) developed a mechanistic model to simulate a composite SOFC cathode. Their model incorporated oxygen reduction at the YSZ/LSM interface, and a complete micro-model for the YSZ/LSM composite cathode. Their numerical model also described the interrelationship among the transport phenomena, the electrochemical processes, and the micro-structure of the composite cathode. They estimated a TPB length in a pure LSM cathode from the micro-structure of the YSZ surface after the LSM cathode was washed with HCl acid.

3.3.5 TPB

The concept of the TPB is frequently employed in the fuel cell literature, especially with respect to SOFCs. The TPB concept holds that electrochemical reactions only occur at confined spatial sites, or ''triple phase boundaries'' where electrolyte, gas, and catalyst regions contact.

The most important reactions of a typical fuel cell are thought to occur at the TPB. Therefore improving the performance of the fuel cell is highly dependent on understanding, characterizing, and optimizing the TPB length. From a technology perspective the TPB zone can be increased by decreasing the size of catalyst particles in the electrode. By using nanoscale composites of catalyst material, conductive support, solid electrolyte, and gas pore space, the length of TPB can be increased (Steele 2001). The longer the TPB the better the kinetic performance of the fuel cell.

Most of the papers published on the nature and properties of a TPB in a SOFC agree that TPB is not a line. Rather it is a zone in which diffusion through materials and reactions between components take place. There are several papers on TPB in SOFCs (Mizusaki 1991, Petitbon 1996, Bieberle 2001, Brichzin 2002, Fleig 2002 and Fleig 2003). Most of results have focused on the cathode. In contrast few studies have considered the TPB at SOFC anodes.

3.3.5.1 TPB Length

The TPB length is widely viewed as a key electrode structural parameter. Deng et al. (2005) described a geometrical model that predicted the influence of solid grain size, pore size, and porosity on the TPB length in electronic composite SOFC electrodes. Their results showed that the TPB length is inversely proportional to grain size and can be optimized by the pore size and porosity. They concluded that the TPB length is a function of size and volume fraction of the three phases. A finer solid grain size increased the TPB length exponentially. The TPB length can be maximized at optimal values for the pore size and porosity. Their optimal values depended on grain size, pore size, and on porosity.

J.R. Wilson et al. (2006) used a dual-beam focused ion beam–scanning electron microscope to make a three-dimensional reconstruction of a SOFC electrode. They used these data to calculate critical micro structural features including the TPB length. The volume-specific TPB length was found to be 4.28×10^6 ($m.m^{-3}$).

Deng et al. (2005) described a mathematical model to calculate the TPB length for mono sized particles. Their expression leads to a TPB length with units of ($m.m^{-4}$). The unit of their TPB length is not well-defined in terms of physical quantities. For a composite electrode, one is interested in the volume-specific TPB length.

Deseure et al. (2007) developed an analytical model that calculated the TPB length for a composite electrode. They claimed that the maximum TPB length is obtained when the volume fraction of ionic conducting particles is 50%.

Janardhanan et al. (2008) described a mathematical model to calculate the volume specific TPB length in the porous composite electrodes of a SOFC that was based on simple geometrical concepts. Their model accounts for porosity, particle diameter, particle size distribution, and solids phase distribution. Their results were based on both a uniform particle size distribution as well as a non-uniform particle size distribution.

3.3.5.2 TPB at an Anode

It has been shown by several electrochemical and surface science techniques that the oxidation process is not strictly limited to the TPB of the anode. Instead the reaction zone extends beyond the Ni catalyst surface over several hundreds of Angstroms (Williford 2003).

Williford et al. (2003) claimed that anodic concentration polarization originates in the immediate vicinity of the reactive TPB sites near the anode/electrolyte interface. They first presented experimental evidence that supports tortuosities in the range of 2.5-3 for modern SOFC anode materials. This was followed by a description of the proposed mechanisms responsible for concentration polarization: competitive adsorption and surface diffusion near the TPBs. Then an anode mathematical model was described showing how concentration polarization is controlled by two localized phenomena. One is competitive adsorption of reactants in areas adjacent to the reactive TPB sites. The other phenomenon is relatively slow surface diffusion. The mathematical model was then fitted to experimental fuel cell performance data and showed good agreement when model parameters were filled with independent experimental data.

3.3.5.3 Mechanism

The major species present at the anode side of a SOFC are H_2 and H_2O in the gas phase. The reaction taking place at the interface of the three phases - metallic Ni, gaseous H_2- H_2O, and ceramic YSZ - is the oxidation of hydrogen which results in the production of water. The electrochemical reaction at the anode is:

$$H_2 \rightarrow 2H^+ + 2e^- \qquad (3-27)$$

However, the detailed mechanism of the reaction is more complicated, and less investigated in the literature. Despite the fact that materials and micro-structural properties of the anode have been investigated and optimized properly, very little information is available on the intermediates, the reaction mechanism or the kinetics.

The electrode kinetics were studied experimentally using either Ni-YSZ cermet anodes or metallic Ni anodes, such as Ni pattern (Mizusak 1994, Mizusaki 1994) Ni point (Nakagawa 1995), or porous Ni anodes (Jiang 1997, Jianga 1999). Electrochemical information was obtained from electrochemical impedance spectroscopy (EIS) measurements and from fitting these data to equivalent circuits. Several phenomena, the dissociative adsorption of hydrogen, the formation of hydroxyl, the charge transfer reaction, and desorption of water were examined as possible rate limiting steps (Mizusak 1994, Kawada 1990).

Despite the difficulties concerning the interpretation of the EIS data, various reaction mechanisms have been proposed in the literature. Major differences were found by variying (a) the location where the chemical and the electrochemical reactions take place (either merely on the Ni surface or equally on the Ni and on the YSZ surface, respectively), (b) the reactions of the interstitial oxygen in the YSZ, (c) the adsorption and desorption behaviour of water, and (d) the charge transfer step.

Many different reaction steps have been studied. Mizusaki et al. (1994) consider the Ni surface to be exclusively electrochemically active. Jiang et al. (1997) include surface reactions on the YSZ surface in their model. De Boer et al. (2000) and Holtappels et al. (1999) suggest that interstitial hydrogen and hydroxyl are formed. The removal of oxygen from the YSZ is assumed to proceed rather differently: (a) if the oxygen becomes adsorbed onto the YSZ surface, (b) if it forms a hydroxyl interstitial, (c) if a negatively charged hydroxyl is formed on the Ni surface, or (d) if water is immediately formed without any intermediate steps.

De Boer et al. (2000) postulated the following sequence of reactions at the porous nickel anode:

$$H_{2gas} + 2S_{Ni} \rightarrow 2H_{Niad} \qquad (3-28)$$

$$H_{Niad} + O^{2-} + S_{YSZ} \rightarrow OH^{-}_{YSZad} + V_{0}^{''} + e^{-} + S_{Ni} \qquad (3-29)$$

$$H_{Niad} + OH^{-}_{YSZad} \leftrightarrow H_2O_{YSZad} + e^{-} + S_{Ni} \qquad (3-30)$$

$$H_2O_{YSZad} \leftrightarrow H_2O_{gas} + S_{YSZ} \qquad (3-31)$$

Where the subscript YSZ indicates species that are adsorbed on YSZ, Ni represent species adsorbed on nickel, S_{Ni} and S_{YSZ} denote vacant sites on the nickel electrode surface and the YSZ surface. $V_{0}^{''}$, denotes oxygen vacancies and O^{2-} stands for the lattice oxygen anions.

The assumptions for the models were:

1. Dissociative adsorption of hydrogen occurs on the Ni surface.
2. Charge transfer between hydrogen and both lattice oxygen and hydroxyl ions occurs at the TPB.
3. Water molecules are desorbed from the YSZ surface.

Equations in which protons act as mediators in the reaction were reported by Mogensen et al. (1996) and later by (Brown 2000, Vels Jensen 2001)

$$H_{2gas} + 2S_{Ni} \leftrightarrow 2H_{Niad} \qquad (3-32)$$

$$H_{Niad} \leftrightarrow H_{Niad}^{+} + e^{-} \qquad (3-33)$$

$$H_{Niad}^{+} + O^{2-} \leftrightarrow OH_{YSZad}^{-} + V_O^{''} + S_{Ni} \qquad (3-34)$$

$$2OH_{YSZad}^{-} + V_O^{''} \leftrightarrow H_2O_{YSZad} + O_O^{x} + S_{YSZ} \qquad (3-35)$$

$$H_2O_{YSZad} \leftrightarrow H_2O_{gas} + S_{YSZ} \qquad (3-36)$$

Mizusaki et al. (1994), proposed the following scheme for the electrode reaction, which proceeded only via the nickel surface:

$$H_{2gas} + 2S_{Ni} \leftrightarrow 2H_{Niad} \qquad (3-37)$$

$$O^{2-} + S_{Ni} \leftrightarrow O_{Niad}^{2-} + V_O^{''} \qquad (3-38)$$

$$H_{Niad} + O_{Niad}^{2-} \leftrightarrow 2OH_{Niad}^{-} + S_{Ni} \qquad (3-39)$$

$$H_{Niad} + OH_{Niad}^{-} \leftrightarrow H_2O_{Niad} + S_{Ni} + e^{-} \qquad (3-40)$$

$$H_2O_{Niad} \leftrightarrow H_2O_{gas} + S_{Ni} \qquad (3-41)$$

The assumptions for their models were:

1. Oxygen adsorbs on Ni near the TPB via charge transfer.
2. All surface intermediates involved bear no charge.

Bieberle et al. (2000, 2002) altered the scheme proposed by Mizusaki et al. (1994). They introduced one more, step in which two hydroxyl groups react to form water and an oxygen anions:

$$2OH^{-}_{Niad} \leftrightarrow H_2O_{Niad} + O^{2-}_{Niad} \qquad (3-42)$$

Ihara et al. (2000) presented a model for Ni/YSZ cermets in which all reaction steps take place on nickel with surface coverage of H, O and H_2O in equilibrium. They replaced the third and fourth reaction introduced by Mizusaki et al. (1994) by:

$$2H_{Niad} + O^{2-}_{Niad} \leftrightarrow H_2O_{Niad} + 2S_{Ni} \qquad (3-43)$$

Holtappels et al. (1999) claimed that the electrochemical reaction would extend beyond the area of the Ni/YSZ interface. That is possible because hydrogen is permeable in Ni and protons are conducted in YSZ. The first step was the dissociative adsorption of H_2 on Ni. Two different reaction pathways were assumed for the oxidation of the adsorbed hydrogen atoms. H_{Niad} was oxidized both on the Gas/Ni interface and in the region of the TPB. The water formation reaction proceeded via intermediates, e.g., hydroxides on the Ni surface. In the area of the Ni/YSZ interface, hydrogen dissolved in Ni. H_{Niad}, was oxidized by forming interstitial protons (H_i°) or hydroxides (OH_i°) in the electrolyte. The transport of H_{Niad} and (H_i°) may occur via diffusion in the Ni and the electrolyte phase, respectively. The remaining processes, e.g., formation, dissociation, as well as adsorption and desorption of water took place in the TPB region. Gas transport limitations were not considered because the porosity of the Ni-YSZ cermets electrode was small and the high binary diffusion coefficients of the hydrogen/water mixtures were sufficiently large.

Jiang et al. (1997) developed a model in which the interaction of water with a Ni surface proceeded via a dissociative adsorption or a molecular adsorption step. They found that interaction of H_2O with Ni leads to complete dissociation at elevated temperatures:

$$H_2O_{gas} \leftrightarrow O^{2-}_{Niad} + H_{2gas} \qquad (3-44)$$

Oxygen species could be thermodynamically stable on the Ni surface either in the form of adsorbed O^{2-}_{Niad} or as a suboxide on the Ni surface. Dissociative adsorption/diffusion processes of hydrogen could be very different on an oxidized surface compare to that on a clean Ni surface.

In summary, it should be noted that a variety of reaction steps have been investigated at the interface of Ni, YSZ, and a gas phase. All the models discussed here were developed from AC and DC electrochemical impedance spectroscopy.

3.3.5.4 Modeling

TPB is rarely modeled separately in the literature. It has been treated as a boundary condition for mass transport equations in modeling the whole anode/ cathode (Bieberle 2002). It has been discussed from a kinetics analysis view point. On the other hand some models examine the possibility of having a wider TPB than the original concept of single line. Williford et al. (2006) discussed a model that described concentration polarization in areas adjacent to the reactive TPB sites.

In general the TPB term usually appears in the literature that studied the micro-structure of a SOFC anode. Several groups have developed microscopic models to study charge-transfer processes in the vicinity of the TPB (Mizusak 1994, Bronin 2004, Bessler 2008). These TPB models may include adsorption/desorption of the gas-phase species, surface reactions, diffusion of the adsorbed species, and the charge-transfer electrochemical reactions.

Bieberle et al. (2002) developed an electrochemical model for the Ni/YSZ interface that only considered the Ni surface. They studied the polarization resistance, as a function of the TPB length. R. Bove et al. (2006) assumed that the TPB is small enough compared to electrode and electrolyte thickness to be treated as a boundary condition (Bove 2005).

A variety of geometries have been studied. Presvytes et al. (2007) developed a diffusion-reaction model having spherical coordinates to describe the steady-state operation of nickel cermet anodes in SOFCs. Sund (2000) presented two models. One was based on random packing of particles. Their thin film model used TPB length model to simulate the conductivity, polarization resistance, and impedance of composite electrodes. Zue et al. (2005) described a computational framework for modeling porous media transport in electrodes. Charge transfer chemistry was presented using a modified Butler-Volmer equation. The TPB was included in their model as a boundary condition at the electrode-electrolyte interface for the electrochemical charge-transfer reaction.

Zue et al (2008) also presented a one dimensional model to examine the effect of micro-structure on the performance of a SOFC anode. They took a similar approach to O'Hayre et al. (2005) in dealing with the effect of surface diffusion along the width of the interface adjacent to the TPB.

Bibliography

Achenbach, E. "Response of a Solid Oxide Fuel Cell to Load Change." Journal of Power Sources,57,1-2, 1995: 105-109.

Achenbach, E.,. "Three-Dimensional and Time-Dependent Simulation of a Planar Solid Oxide Fuel Cell Stack." Journal of Power Sources 49, 1994: 333–348.

Aguiar, P., C.S. Adjiman , N.P. Brandon. "Anode-Supported Intermediate Temperature Direct Internal Reforming Solid Oxide Fuel Cell. I: Model-Based Steady-State Performance." Journal of Power Sources ,147,1-2, 2005: 136-147.

Aguiar, P., D.Chadwick, L .Kershenbaum. "Modelling of an Indirect Internal Reforming Solid Oxide Fuel Cell." Chemical Engineering Science,57,10, 2002: 1665-1677.

Arnost, D., P. Schneider. "Dynamic Transport of Multicomponent Mixtures of Gases in Porous Solids." Chemical Engineering Journal 57, 1999: 91-99.

Atkinson, A., T. Ramos. "Assessment of Ceramic Membrane Reforming in a Solid Oxide Fuel Cell Stack." Journal of Power Sources,130,1-2, 2004: 129-135.

Austin, L.G., Mario Ariet, R. D. Walker, G. B. Wood, R. H. Comyn. "Simple-Pore and Thin-Film Models of Porous Gas Diffusion Electrodes." Ind. Eng. Chem. Fundamen,4,3, 1965: 321–327.

Baker, R.T., I.S. Metcalfe, P.H. Middleton, B.C.H. Steele. Solid State Ionics,72, 1994: 328.

Bear, J."Dynamics of fluids in porous media. New York: American Elsevier Pub. Co,1972.

Bessler, W.G., S. Gewiesz. "Physically Based Impedance Modeling of Ni/YSZ Cermet Anodes." Journal of The Electrochemical Society, 155 ,9, 2008: B937-B952.

Bhattacharyya, D., R. Rengaswamy. "A Review of Solid Oxide Fuel Cell (SOFC) Dynamic Models." Ind. Eng. Chem. Res,48,13, 2009: 6068–6086.

Bieberle, A. "The Electrochemistry of Ni Pattern Anodes Used as Solid Oxide Fuel Cell Model Electrodes." J. Electrochem. Soc.,148,6, 2001: A646-A656.

Bieberle, A., L.Gauckler. "Reaction Mechanism of Ni Pattern Anodes for Solid Oxide Fuel Cells." Solid State Ionics 135, 2000: 337–345.

Bieberle, A., L.J. Gauckler. "State-Space Modeling of the Anodic SOFC System, Ni, H2–H2O,YSZ." Solid State Ionics 146, 2002: 23–41.

Bird, R.B, W.E Stewart ,E.N.Lightfoot. Transport Phenomena 2nd ed. New York John Wiley & Sons Inc, 2002.

Bossel, U.G. "Final International Energy Agency Report." Berne, 1992.

Bouvard, D., F.F. Lange. "Relation between Percolation and Particle Coordination in Binary Powder Mixtures." Acta Metall Mater. 39, 1991: 3083–3090.

Bove, R., N.M. Sammes. "The Effect of Current Collectors Configuration on the." Proceedings of the Ninth International Symposium on Solid Oxide Fuel Cells (SOFC IX). Quebec City, Canada, 2005.

Bove, R., S.Ubertin. "Modeling Solid Oxide Fuel Cell Operation: Approaches, Techniques And Results." Journal of Power Sources 159, 2006: 543–559.

Brichzin, V., J. Fleig, H. U. Habermeier, G. Cristiani, J. Maier. "The Geometry Dependence of the Polarization Resistance of Sr-Doped Lamno3 micro-electrodes on Yttria-Stabilized Zirconia." Solid State Ionics, 152, 2002: 499.

Bronin, D.I., I. Yu. Yaroslavtsev , H. Näfe and F. Aldinger. "Identification of the Reaction Mechanism of the Pt,O2/La(Sr)Ga(Mg)O3−α Electrode System." Electrochimica Acta,49,15, 2004: 2435-2441.

Brown, M., S. Primdahl, M. Mogensen. "Structure/Performance Relations for Ni/Yttria-Stabilized Zirconia Anodes for Solid Oxide Fuel Cells." Journal of The Electrochemical Society, 147 ,2, 2000: 475-485.

Burt, A.C., I. B. Celik, R. S. Gemmen,A. V. Smirnov. "A Numerical Study of Cell-to-Cell Variations in a SOFC Stack." Journal of Power Sources,126,1-2, 2004: 76-87.

Campanari, S., P. Iora. "Definition and Sensitivity Analysis of a Finite Volume SOFC Model for a Tubular Cell Geometry." Journal of Power Sources,132,1-2, 2004: 113-126.

Chaisantikulwat, A., C. Diaz-Goano,E.S. Meadows. "Dynamic Modelling and Control of Planar Anode-Supported Solid Oxide Fuel Cell." Computers & Chemical Engineering,32,10, 2008: 2365-2381.

Chan, S. H., O. L. Ding. "Simulation of a Solid Oxide Fuel Cell Power System Fed by Methane." International Journal of Hydrogen Energy,30,2, 2005: 167-179.

Chapman, S., T. Cowling. Mathematical Theory on Non-Uniform Gases. Cambridge: Cambridge Univ. Press, 1970.

Chen, X.J., S. H. Chan, K. A. Khor. "Cathode Micro Model of Solid Oxide Fuel Cell." Journal of The Electrochemical Society, 151, 2004: A164-A172.

Chen, X.J., S.H. Chan, K.A. Khor. "Simulation of a Composite Cathode in Solid Oxide Fuel Cells." Electrochimica Acta 49, 2004: 1851–1861.

Ciano, C. "A Model for Tubular Solid Oxide Fuel Cells." Proceedings of the COMSOL Users Conference 2006. Milano, 2008.

Clemmer, R.M.C., S.F.Corbin. "Influence of Porous Composite Microstructure on the Processing and Properties Of Solid Oxide Fuel Cell Anodes." Solid State Ionics, 166,3-4, 2004: 251-259.

Costamagna, P., A. Selimovic, M. Del Borghi, G. Agnew. "Electrochemical Model of the Integrated Planar Solid Oxide Fuel Cell (IP-SOFC)." Chemical Engineering Journal,102, 2004: 61.

Costamagna, P., P. Costa, V. Antonucci. "Micro-Modelling of Solid Oxide Fuel Cell Electrodes." Electrochimica Acta,43,3-4, 1998: 375-394.

De Boer, B., M. Gonzalez, H.J.M. Bouwmeester, H. Verweij. "The Effect of the Presence of Fine YSZ Particles on the Performance of Porous Nickel Electrodes." Solid State Ionics 127, 2000: 269–276.

De Souza, S., S.J. Visco, L. C. De Jonghe. "Thin-Film Solid Oxide Fuel Cell with High Performance at Low-Temperature." Solid State Ionics,98,1-2, 1997: 57-61.

Deng, X., A. Petric. "Geometrical Modeling of the Triple-phase-boundary in Solid Oxide Fuel Cells." Power Sources 140, 2005: 297.

Deng, X., A.Petric. "Geometrical Modeling of the Triple-Phase-Boundary in Solid Oxide Fuel Cells." Journal of Power Sources 140, 2005: 297–303.

Deseure, J., Y. Bultel , L. Dessemond, E. Siebert,P. Ozil. "Modelling the Porous Cathode of a SOFC: Oxygen Reduction Mechanism Effect." Journal of Applied Electrochemistry,37, 2007: 129-136.

Divisek, J., L.G.J. de Haart, P. Holtappels, T. LennaT, W. MallCnerb. "The Kinetics Of Electrochemical Reactions on High Temperature Fuel Cell Electrodes." Journal of Power Sources, 49, 1994: 257-270.

Ferguson, J.R., J.M.Fiard,R.Herbin. "Three-Dimensional Numerical Simulation for Various Geometries of Solid Oxide Fuel Cells." Journal of Power Sources 58, 1996: 109–122.

Finnerty, C.M., R.H. Cunningham, K. Kendall , R.M. Ormerod. "A Novel Test System For in Situ Catalytic and Electrochemical Measurements on Fuel Processing Anodes in Working Solid Oxide Fuel Cells." J. Chem. Soc. Chem. Commun, 1998.

Finnerty, C.M., R.M. Ormerod. "Internal Reforming Over Nickel/Zirconia Anodes in SOFCS Oparating on Methane: Influence of Anode Formulation, Pre-Treatment and Operating Conditions." Journal of Power Sources,86,1-2, 2000: 390-394.

Fleig, J. "Solid Oxide Fuel Cell Cathodes: Polarization Mechanisms and Modeling of The Electrochemical Performance." Annu. Rev. Mater. Res,33, 2003: 361.

Fleig, J.,. "On the Width of the Electrochemically Active Region in Mixed Conducting Solid Oxide Fuel Cell Cathodes." Journal of Power Sources,105,2, 2002: 228-238.

Flot, D.M., J.T.S. Irvine. Ionics,4, 1998: 175.

Fouquet, D., A.C. Miiller, A. Weber , E. lvers-Tiffte. "Kinetics of Oxidation and Reduction of Ni/YSZ Cermets." International Journal of Ionic,9,1-2, 2003: 103-108.

Hernández-Pacheco, E., D. Singh,P.N.Hutton,N.Patel,M.D,Mann. "A Macro- Level Model for Determining the Performance Characteristics of Solid Oxide Fuel Cells." JournalofPowerSources,138, 2004: 174-186.

Hertz, J.L., H. L. Tuller. "Measurement and Finite Element Modeling of Triple Phase Boundary Relatedcurrent Constriction in YSZ." Solid State Ionics 178, 2007: 915–923.

Holtappels, P., L.G.J.de Haart, M.Mogensen, U.Stimming, I.C.Vinke. "Reaction of CO/CO2 Gas Mixtures on Ni - YSZ Cermet Electrodes." J.Appl.Electrochem. 29, 1999: 561.

Horita, T., N. Sakai, H. Yokokawa, M. Dokiya, T. Kawada. Solid State Ionics 86-88, 1996: 1259.

Huebner, W., H. U. Anderson. Anode, Cathode and Thin Film Studies for Low Temperature SOFC's. Technical Report, Pittsburgh, US: Federal Energy Technology Center, 1999.

Hussain, M.M., X.Li,I.Dincer. "Mathematical Modeling of Planar Solid Oxide Fuel Cells." Journal of Power Sources 161, 2006: 1012–1022.

Inui, Y., A. Urata, N. Ito, T. Nakajima , T. Tanaka. "Performance Simulation of Planar SOFC Using Mixed Hydrogen and Carbon Monoxide Gases as Fuel." Energy Conversion and Management,47,13-14, 2006: 1738-1747.

Iora, P., P. Aguiar, C.S. Adjiman, N.P. Brandon. "Comparison of Two IT DIR-SOFC Models: Impact of Variable Thermodynamic, Physical, and Flow Properties. Steady-State and Dynamic Analysis." Chemical Engineering Science,60,11, 2005: 2963-2975.

Irvine, J.T.S, D.P. Fagg, J. Labrincha, F.M.B. Marques. Catal. Today,38, 1997: 467.

Iwata, M., T.Hikosaka, M. Morita,T. Iwanari, K.Ito, K. Ond,Y.Sakaki and S.Nagata. "Performance Analysis of Planar-Type Unit SOFC Considering Current and Temperature Distributions." Solid State Ionics,132,3-4, 2000: 297-308.

Janardhanan, V. A Detailed Approach to Model Transport, Heterogeneous Chemistry, and Electrochemistry in Solid Oxide Fuel Cells. Doctoral thesis. Institute for Chemical Technology and Polymer Chemistry, 2007.

Janardhanan, V. M. , V.Heuveline, O.Deutschmann. "Three-Phase Boundary Length in Solid-Oxide Fuel Cells: A Mathematical Model." Journal of Power Sources ,178, 2008: 368–372.

Jeon, D.H., J. H.Nam, C. Kim. "Microstructural Optimization of Anode-Supported Solid Oxide Fuel Cells by a Comprehensive Microscale Model." Journal of The Electrochemical Society,153, 2006: A406-A417.

Ji, Y., K. Yuan, J.N. Chung. "Effects of Transport Scale on Heat/Mass Transfer and Performance Optimization for Solid Oxide Fuel Cells." Journal of Power Sources ,161,1, 2006: 380-391.

Jiang, S. P., S. P. S. Badwalab. "Hydrogen Oxidation at the Nickel and Platinum Electrodes on Yttria-Tetragonal Zirconia Electrolyte." J. Electrochem. Soc.144, 1997: 3777.

Jianga, S.P., S. Badwalb. "An Electrode Kinetics Study of H Oxidation On Ni/YSZ Cerment Electrode Of The Solid Oxide Fuel Cell." Solid State Ionics 123, 1999: 209–224.

Kaiser, A., A.J. Feighery, D.P. Fagg, J.T.S. Irvine. Ionics 4, 1998: 215.

Kawada, T., B.A. van Hassel, T. Horita, N. Sakai, H. Yokokawa,M. Dokiya. Solid State Ionics 70/71, 1994: 65.

Kawada, T., N. Sakai, H. Yokokawa, M. Dokiya, M. Mori, T. Iwata. "Structure and Polarization Characteristics of Solid Oxide Fuel Cell Anodes." Solid State Ionics,40/41, 1990: 402.

Kee, R.J., H. Zhu, D.G. Goodwin. "Solid-Oxide Fuel Cells with Hydrocarbon Fuels." Proceedings of the Combustion Institute. 2005. 2379-2404.

Kenney, B., K. Karan. "Engineering of Microstructure and Design of a Planar Porous Composite SOFC Cathode: A Numerical Analysis." Solid State Ionics,178, 2007: 297–306.

Krishna, R., J. A. Wesselingh. "The Maxwell-Stefan Approach to Mass Transfer." Chemical Engineering Science,52,6, 1997: 861-911.

Kuo, C.H, P.K.Gupita. "Rigidity And Conductivity Percolation Thresholds In Particulate Composites." Acta MetalL, 1995: 397-403.

Lee, C., H. Lee, S. M. Oh. "Microstructure and Anodic Properties of Ni/YSZ Cermets in Solid Oxide Fuel Cells." Solid State Ionics,98,1-2, 1997: 39-48.

Lehnert, W., J. Meusinger , F. Thom. "Modeling of Gas Transport Phenomena in SOFC Anodes." Journal of Power Sources 87, 2000: 57-63.

Li, J.,Y. Kang, G. Cao, X. Zhu, H. Tu, J. Li. "Numerical Simulation of a Direct Internal Reforming Solid Oxide Fuel Cell Using Computational Fluid Dynamics Method." Journal of Zhejiang University - Science A,9,7, 2008: 961-969.

Lightfoot, E.N., E. M. Scattergood. "Suitability of the Nernst-Planck Equations for Describing Electrokinetic Phenomena." A.1.Ch.E. Journal,11, 1965: 175.

Lockett, M., M. J. H. Simmons, K. Kendall. "CFD to Predict Temperature Profile for Scale Up of Micro-Tubular SOFC Stacks." Journal of Power Sources,131,1-2, 2004: 243-246.

Lu, C., S. An, W.L. Worrell, J.M. Vohs, R.J. Gorte. "Development of Intermediate-Temperature Solid Oxide Fuel Cells for Direct Utilization of Hydrocarbon Fuels." Solid State Ionics ,175,1-4, 2004: 47-50.

Lu, C., W.L.Worrell, C.Wang,S. Park, H. Kim,J. M. Vohs, R. J. Gorte. "Development of Solid Oxide Fuel Cells for the Direct Oxidation of Hydrocarbon Fuels." Solid State Ionics,152-153, 2002: 393-397.

Lynch, M.E., D. S. Mebane,Y. Liu,M. Liu. "Triple-Phase Boundary and Surface Transport in Mixed Conducting Patterned Electrodes." Journal of The Electrochemical Society, 155(6), 2008: B635-B643.

Maddox, R.N., A. L. Hines. Mass Transfer: Fundamentals and Applications. Englewood Cliffs: Prentice-Hall, Inc., 1985.

Magistri, L., A. Traverso , F. Cerutti , M. Bozzolo , P. Costamagna , A. F. Massardo. "Modelling of Pressurised Hybrid Systems Based on Integrated Planar Solid Oxide Fuel Cell (IP-SOFC) Technology." Fuel cells,5,1, 2005: 80 - 96.

Mason, E.A., A.P. Malinauskas. "Gas Transport in Porous Media: The Dusty-Gas Model." New York Elsevier, 1983.

Metcalfe, I.S., P.H. Middleton, P. Petrolekas, B.C.H. Steele. Solid State Ionics,57, 1992: 257.

Meusinger, J., E. Riensche, U. Stimming. "Reforming of Natural Gas in Solid Oxide Fuel Cell Systems." Journal of Power Sources,71,1-2, 1998: 315-320.

Minh, N.Q., T. Takahashi. Science and Technology of Ceramic Fuel Cells. Amsterdam,The Netherlands: Elsevier, 1995.

Mizusak, J., H.Tagawa, T.Saito, T.Yamamura. "Kinetic Studies of the Reaction at The Nickel Pattern Electrode on YSZ In H2-H20 Atmospheres." Solid State Ionics 70/71, 1994: 52-58.

Mizusaki, J. "Reaction Kinetics and Microstructure of the Solid Oxide Fuel Cells Air Electrode La0.6Ca0.4MnO3/YSZ." J. Electrochem. Soc.,138, 1991: 1867.

Mizusaki, J., H. Tagawa, K. Isobe, M. Tajika, I. Koshiro,H. Maruyama,K.Hirano,. "Kinetics of The Electrode Reaction at The H2-H2O Porous Pt/Stabilized Zirconia Interface." J. Electro chem., 1994: 1674.

Modak, U., T. Lusk. "Kinetic Monte Carlo Simulation of a Solid-Oxide Fuel Cell I. Open-Circuit Voltage and Double Layer Structure." Energy Conversion and Management 48, 2007: 1544–1553.

Mogensen, M. "Kinetic and Geometric Aspects of Solid Oxide Fuel Cell Electrodes." Solid State Ionics 86-88, 1996: 1151-1160.

Na, J.H., D.H.Jeon. "A Comprehensive Micro-Scale Model for Transport and Reaction in Intermediate Temperature Solid Oxide Fuel Cells." Electrochimica Acta,51,17, 2006: 3446-3460.

Nakagawa, N., H. Sakurai, K. Kondo,T. Morimoto,K.Hatanaka, K. Kato. "Evaluation of the Effective Reaction Zone at Ni(NiO)/Zirconia Anode by Using an Electrode with a Novel Structure." J. Electrochem. Soc,142, 1995: 3474.

Nakagawa, N., K. Nakajima, M. Sato, K. Kato. "Contribution of the Internal Active Three-Phase Zone of Ni-Zirconia Cermet Anodes on the Electrode Performance of SOFCs." J. Electrochem. Soc ,146, 1999: 1290.

Ni, M., M. K. H. Leung,D. Y. C. Leung. "Micro-Scale Modeling of a Functionally Graded Ni-YSZ Anode." Chem. Eng. Technol,30,5, 2007: 587–592.

O'Hayre, R., D.M. Barnett, F. B. Prinzc. "The Triple Phase Boundary:A Mathematical Model and Experimental Investigations for Fuel Cells." Journal of The Electrochemical Society, 152,(2), 2005: A439-A444.

Opera, C. "Fuel Cell Modeling With Fluent Software." 1st Meeting of "Romanian Hydrogen and Fuel Cell Technology Platform, 2005.

Ormerod, R.M. "Internal Reforming in Solid Oxide Fuel Cells." Studies in Surface Science and Catalysis,122, 1999: 35-46.

Patcharavorachot, Y., A. Arpornwichanop, A. Chuachuensuk. "Electrochemical Study of a Planar Solid Oxide Fuel Cell: Role of Support Structures." Journal of Power Sources, 177 ,2, 2008: 254-261.

Peters, R., R. Dahl, U. Klüttgen, C. Palm, D. Stolten. "Internal Reforming of Methane in Solid Oxide Fuel Cell Systems." Journal of Power Sources, 106,1-2, 2002: 238-244.

Petitbon, M., F. Kleitz. "Optimized SOFC Electrode Microstructure." Solid State Ionics, 92, 1996: 65.

Petruzzi, L., S. Cocchi , F. Fineschi. "A Global Thermo-Electrochemical Model for SOFC Systems Design and Engineering." Journal of Power Sources,118,1-2, 2003: 96-107.

Pil Yoon, S. , J.Han, S. W. Nam, T. Lim, S. Hong. "Improvement of Anode Performance by Surface Modification for Solid Oxide Fuel Cell Running on Hydrocarbon Fuel." Journal of Power Sources,136,1, 2004: 30-36.

Pratihar, S.K, A. Dassharma, H.S. Maiti. "Processing Microstructure Property Correlation of Porous Ni-YSZ Cermets Anode for SOFC Application." Material research bulletin, 2005.

Presvytes, D., C. G. Vayenas. "Mathematical Modeling of the Operation of SOFC." Ionics, 13, 2007: 9-18.

Recknagle, K.P., R.E.Williford,L.A.Chick,D.R.Rector. "Three- Dimensional Thermo-Fluid Electrochemical Modeling of Planar SOFC Stacks." Journal of Power Sources 113, 2003: 109–114.

Shi, Y., N. Cai. "A General Mechanistic Model of Solid Oxide Fuel Cells." Tsinghua Science & Technology,11,6, 2006: 701-711.

Siam, J. "Triple Phase Boundaries in Solid-Oxide Cathodes." J. Appl. Math.70,2, 2009: 510-530.

Slater, P.R., D.P. Fagg, J.T.S. Irvine, J. Mater. chem,7, 1997: 2495.

Stauffer, D., A. Aharony. Introduction To Percolation Theory. CRC, 1994.

Steele, B.C.H. "Material Science and Engineering: the Enabling Technology for the Commercialization of Fuel Cell Systems." J. Mater. Sci.,36, 2001: 1053.

Steele, B.C.H., P.H. Middleton, R.A Rudkin. "Material Science Aspects of SOFC Technology with Special Reference to Anode Development." Solid State Ionics,40/41, 1990: 388.

Stiller, C., B.Thorud,B.S.Seljeb,H. Karoliussen,O.Bolland,. "Finite-Volume Modeling and Hybrid-Cycle Performance of Planar and Tubular Solid Oxide Fuel Cells." Journal of Power Sources,141, 2005: 227–240.

Sund, S. "Simulations of Composite Electrodes in Fuel Cells." Journal of Electroceramics, 5,2, 2000: 153-182.

Sunde, S,. "Calculation Of ConductivityAnd Polarization ResistanceOf Composite SOFCs Electrodes from Random Resistor Networks." Journal of The Electrochemical Society ,142, 4, 1995: L50-L52.

Sunde, S.,. "Calculations of Impedance of Composite Anodes for Solid Oxide Fuel Cells." Electrochim. Acta 42, 1997: 2637–2648.

Suwanwarangkul, R., E. Croiset, M.W. Fowler, P.L. Douglas, E. Entchev. "Performance Comparison of Fick's, Dusty-Gas and Stefan-Maxwell Models to Predict the Concentration Overpotential of a SOFC Anode." J. Power Sources,122, 2003: 9-18.

Suwanwarangkul, R., E. Croiset,E. Entchev,S. Charojrochkul,M.D. Pritzker,M.W. Fowler,P.L. Douglas,H. Mahaudom. "Experimental and Modeling Study of Solid Oxide." Journal of Power Sources,161,1, 2006: 308-322.

Suzue, Y., N. Shikazono, N.Kasagi. "Micro Modeling of Solid Oxide Fuel Cell Anode Based on Stochastic Reconstruction." Journal of Power Sources 184, 2008: 52-59.

Suzuki, M., H. Sasaki, S. Otoshi, A. Kajimura ,M. Ippommatsu. "HighPower Density Solid Oxide Fuel Cells Using Ru/Y,03 Stabilized Zirconia Cermet Anodes." Solid State Ionics 62, 1993: 125.

Svensson, A.M., S. Sunde, K. Nisancioglu. "A Mathematical Model of the Porous SOFC Cathode." Solid State Ionics 86–88, 1996: 1211–1216.

Tanner, C.W, K.Z Fung , A.V Virkar. "The Effect of Porous Composite Electrode Structure on Solid Oxide Fuel Cell Performance. I. Theoretical Analysis." J. Electrochem. Soc.,144,21, 1997.

Tsai, T., E. Perry, sa Barnett. "Effect of Mixed-Conducting Interfacial Layers on Solid Oxide Fuel Cell Anode Performance." J. Electrochem. Soc.,145, 1998: 1696.

Tseronis, K., I. Kookos, K. Theodoropoulos. "Modelling and Design of the Solid Oxide Fuel Cell Anode." Proceedings of the COMSOL Users Conference. Birmingham, 2006.

Tseronisa, K., I.K.Kookosb, C.Theodoropoulos. "Modelling Mass Transport in Solid Oxide Fuel Cell Anodes:A Case For a Multidimensional Dusty Gas-Based Model." Chemical Engineering Science 63, 2008: 5626--5638.

VanderSteen, J.D.J, B.Kenney ,J.G Pharoah ,K. Karan. "Mathematical Modeling of the Transport Phenomena and the Chemical/Electrochemical Reactions in Solid Oxide Fuel Cells: A Review." Proceedings of hydrogen and fuel cells. Toronto, Canada, 2004.

Vayenas, C.G., P.G . Debenedett. "Cross-Flow, Solid-state Electrochemical Reactors: A Steady-State Analysis." Ind. Eng. Chem. Fundam,24, 1985: 316-324.

Veldsink, J.W., R.M.J. Vandamme, G.F. Versteeg and W.P.M. Vanswaaij. "The Use of Dusty-Gas Model for the Description of Mass Transport With Chemical-Reaction in Porous Media." Chem Eng J Biochem Eng J 57,2, 1999: 115–125.

Vels Jensen, K., S. Primdahl, I. Chorkendorff , M. Mogensen. "Microstructural and Chemical Changes at the Ni/YSZ Interface." Solid State Ionics,144, 2001: 197–209.

Williford, R.E. "Modeling of Environmentally Significant Interfaces: Two Case Studies." Journal of Electron Spectroscopy and Related Phenomena, 150, 2006: 171–184.

Williford, R.E., L. A. Chick, G. D. Maupin, S. P. Simner, and J. W. Stevenson. "Diffusion Limitations in the Porous Anodes Of SOFCs." J. Electrochem. Soc,150,8, 2003: A1067-A1072.

Wilson, J.R, W Kobsiriphat, R Mendoza, H Chen, JM Hiller, DJ Miller. "Three-Dimensional Reconstruction of a Solid-Oxide Fuel-Cell Anode." Nature materials 5,7, 2006: 541-544.

Xia, S.H., Z. T.Chan. "Anode Micro Model of Solid Oxide Fuel Cell." Journal of The Electrochemical Society, 148, 2001: A388-A394.

Xia, Z.T., S.H.Chan , K.A.Khor. "An Improved Anode Micro Model of SOFC." Electrochem Solid-State Lett,7,3, 2004: A63–A65.

Yakabe, H., M. Hishinuma, M. Uratani, Y. Matsuzaki, I. Yasuda. "Evaluation and Modeling of Performance of Anode-Supported Solid Oxide Fuel Cell." Journal of Power Sources,86,1-2, 2000: 423-431.

Yakabe, H., Y. Baba,T.Sakurai,Y.Yoshitaka. "Evaluation of the Residual Stress for Anode-Supported SOFCs." Journal of Power Sources ,135, 2004: 9–16.

Yu, Z., J. Han,X. Cao, W. Chen, B. Zhang. "Analysis of Total Energy System Based on Solid Oxide Fuel Cell for Combined Cooling and Power Applications." International Journal of Hydrogen Energy,In press, 2009.

Yuan, J., B. Sundén, M. Hou ,H. Zhang. "Three-Dimensional Computational Analysis of Gas and Heat Transport Phenomena in Ducts Relevant for Anode-Supported Solid Oxide Fuel Cells." International Journal of Heat and Mass Transfer,46, 2003: 809–821.

Yuan, K., Y.Ji, J.N. Chung. "Physics-Based Modeling of a Low-Temperature Solid Oxide Fuel Cell with Consideration of Microstructure and Interfacial Effects." Journal of Power Sources, 2009: in Press, Corrected Proof.

ZhongHua, D., L.Xi. "The Design for Model and Control of Solid Oxide Fuel Cell Electrical Characteristic." Control Conference. 2007. 264 - 266.

Zhu, H., R. J. Kee, V.M. Janardhanan,O. Deutschmann, D. G. Goodwinc. "Modeling Elementary Heterogeneous Chemistry and Electrochemistry in Solid-Oxide Fuel Cells." Journal of The Electrochemical Society,152,12, 2005: A2427-A2440.

Zhu, H., R.J. Kee. "A General Mathematical Model for Analyzing the Performance of Fuel-Cell Membrane-Electrode Assemblies." Journal of Powe rSources,117, 2003: 61-74.

Zhu, W., D.Ding,C. Xia. "“Enhancement in ThreePhase Boundary of SOFC Electrodes by an Ion Impregnation Method: A Modelling Comparison." Electrochemical and solid-state letters,11, 2008: B83-B86.

Zhu,H.,Kee, R.J. "Importance of Anode Microstructure in Modeling Solid Oxide Fuel Cells." Journal of The Electrochemical Society,155, 2008: B538-B546.

Chapter 4 Description of the Model

4.1 Introduction

Solid Oxide fuel cells (SOFC) are a promising power source option due to their high electrical efficiency and low emission of polluting gas compared to the other kinds of fuel cells. For the past few decades, there has been substantial research and development of SOFC technology all over the world. Its objectives have been to lower production costs, increase reliability and durability, and improve both design and operating conditions.

One important step in minimizing costs and maximizing efficiency of a fuel cell is to optimize the performance of the TPB. The TBP is the locus of points common to a gas phase in which hydrogen diffuses (Gas), a solid phase which conducts electrons (metallic Ni) and a solid phase in which oxide ions migrate (ceramic YSZ)]. This contact line is where the electrochemical reaction takes place. Therefore it can be considered to be the core of the fuel cell.

The various aspects of the model for the triple phase boundary (TPB) are described in this chapter. In this work the geometry of the TPB model evolved from an initial version to a final version. The assumptions used for the final geometry are listed. A summary of the equations that were used in the model is then presented. The coupling between the variables in the differential equations is shown and the boundary conditions are listed. Finally, the values for the parameters that are held constant are presented at the end of the chapter.

A framework is presented for the simulation of reaction dynamics in the vicinity of the TPB of the SOFC composite anode. This model is a physically based, numerical predictive model that can be used for understanding SOFC phenomena. The model coupled diffusion, migration and reaction phenomena for the chemical components in the vicinity of the TPB.

In this model a two dimensional geometry was considered. In order to find the best representation of the actual physical structure three geometries were examined. The first attempt was the simple geometry in Figure 4.1

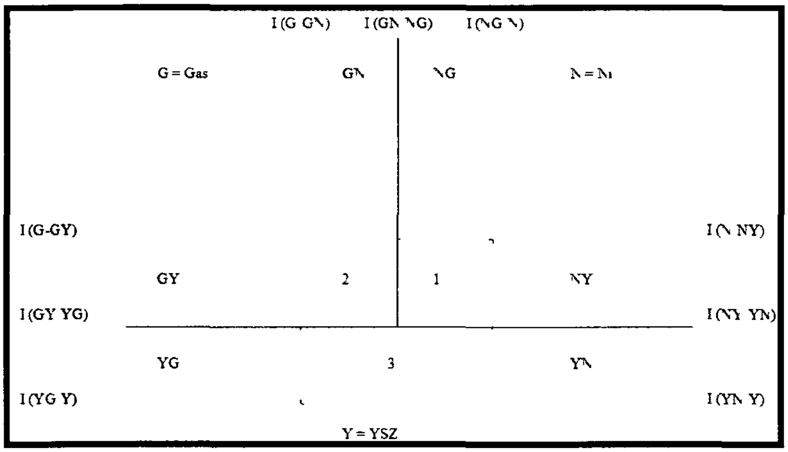

Figure4 1 First Proposed TPB Geometry 1

In this geometry G, N and Y represent gas, nickel metal, and YSZ, where all components (species participating in reactions) have uniform bulk concentrations. The letter I is used for interfaces. I(G-GN) represents the position at which the concentration of a component in the GN region is equal to the bulk gas phase concentration (G). I (G-GY) is the position at which the concentration of a component in the GY region is equal to the bulk gas phase concentration (G). I (N-NY) is the position at which the concentration of a component in the NY region is equal to the bulk phase concentration in the nickel metal phase, (N). I (NG-N) is the position at which the concentration of a component in the NG region is equal to the bulk concentration in the nickel metal phase, (N). I (GY-Y) is the position at which the concentration of a component in the GY region is equal to the bulk concentration in the YSZ phase, (YSZ). I (YN-Y) is the position at which the concentration of a component in the YN region is equal to the bulk concentration in the YSZ phase, (YSZ).

The geometry described above was eventually discarded. It was inadequate in representing the external boundaries of the TPB. In addition it had too many subdomains (eleven regions). Each additional subdomain adds more complexity to the model.

The other proposed geometry is shown in Figure 4.2. In this representation the region between the two bulk phases was visualized. The YSZ within the anode cermet is treated here as regularly spaced corrugations shown in Figure 4.2, where ΔL is the thickness of the composite electrode$\Delta L = a \times \Delta w$, and a is an adjustable parameter. Δw is the periodic spacing between corrugations in the electrode and it is the width of a corrugation. As Δw approaches zero, the boundary region between the two bulk phases (the line that defines the TPB between the two bulk phases) will approach a straight line (the interface line) of length = r (the radius of the domain). For a region having a finite thickness, the length of the interface line will be n (2Δw + 2aΔw) where n is the number of interface segments. ΔL = a × Δw where a is an adjustable parameter.

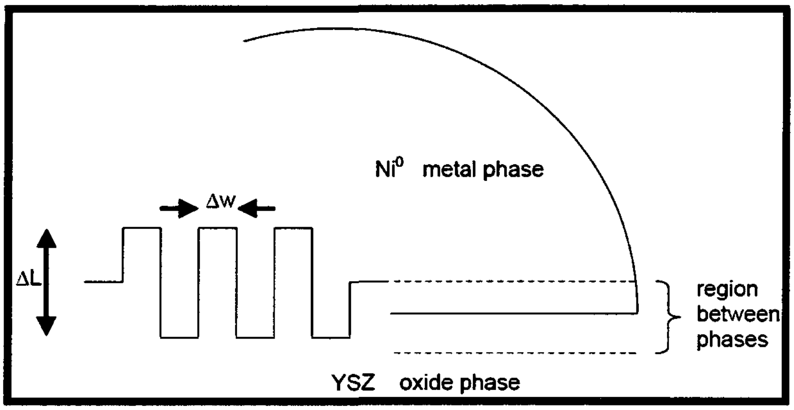

Figure4. 2 Second Proposed TPB Geometry

This representation was also discarded. It was difficult to implement this TPB configuration in the software. Overpotential and boundary conditions were hard to specify in each domain

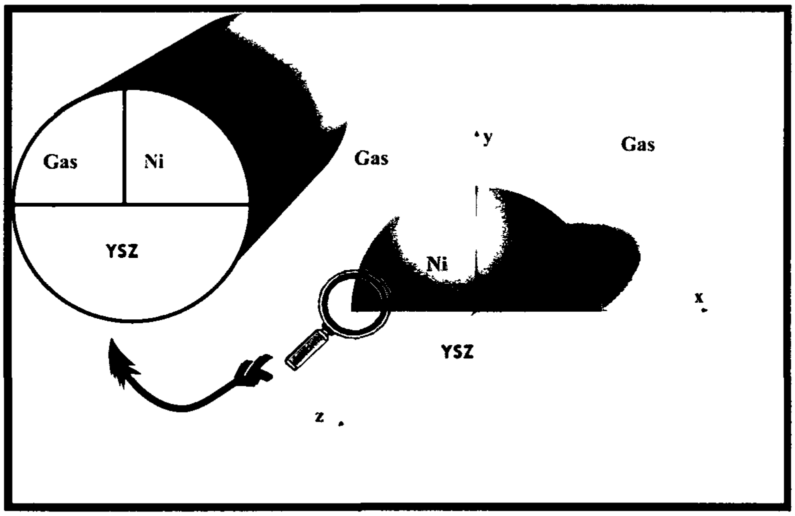

Figure4. 3 Schematic Picture of a Ni Particle in the Vicinity of YSZ and Gas of Anode Side of SOFC

Another representation is shown in Figure 4.3. A semi-spherical solid nickel particle on the surface of a semi-infinite YSZ solid is shown on the right hand side of Figure 4.3. There is a gas phase above the nickel particle and the YSZ solid. The location where the gas, nickel, and YSZ are in contact is magnified on the left hand side of Figure 4.3. This physical model defined the external boundaries, which is a definite advantage over the previous geometry. The 3D schematic geometry on the left side of Figure 4.3 is a very long and thin cylinder. It simplifies the representation by being a 2D model. The same two dimensional geometry is shown in Figure 4.4 with additional labels for domains and boundaries. The contact line common to the three phases is shown as a single point at the origin of the two dimensional domain. The domain comprises a circular neighbourhood with a radius that will be varied to investigate phenomena that occur in the region of the TPB.

In Figure 4.4 the symbol Ω is used to represent subdomains and the symbol Γ is used to represent interfaces. (Ω_{YSZ}), (Ω_{Ni}), and (Ω_G) represent domains for the YSZ, Ni, and gas phases respectively. $\Gamma_{Bulk/G}$ is the interface between the bulk gas and the Ω_G in the TPB model. $\Gamma_{Bulk/Ni}$ is the interface between the bulk nickel and the Ω_{Ni} in the TPB model. $\Gamma_{Bulk/YSZ}$ is the interface between the bulk YSZ and the Ω_{YSZ} in the TPB model.

Although simplified, this geometry can be used to describe the transport of multiple components. This type of schematic diagram has been used previously by mathematicians for PEMFC and SOFC models (Berg et al. 2008, Fehribach 2009). One feature of this geometry is that it is only necessary to change one variable (the radius) to be able to examine the distance from the origin in all three regions where phenomena occur.

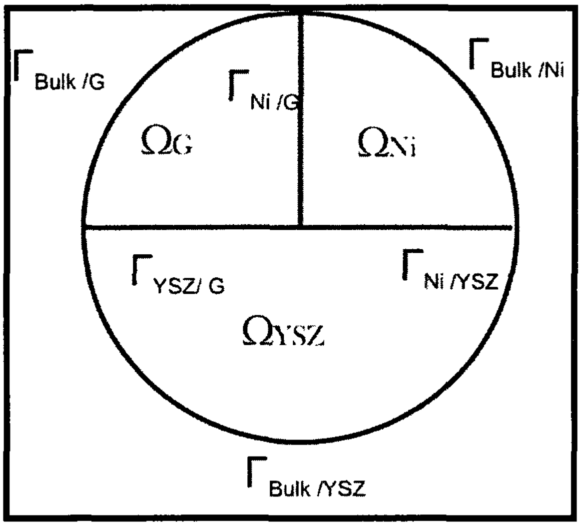

Figure4. 4 Geometric Modeling of the TPB Contact Point

The mathematical formulation for the model is based on the following physical assumptions:

1. The system is assumed to be at steady state.
2. The behaviour of different chemical components (hydrogen, oxygen, water, etc) is described by the macroscopic conservation laws for species, i.e. a system of equations for reaction-diffusion-migration continuum mechanics. Thus, nanoscale phenomena including the quantum size effect are not modelled explicitly. The Ω_{Ni} is not porous and Ω_{YSZ} is a dense phase (impermeable to gas).
3. x and y have been represented in the geometry of the system and z coordinate in the thickness direction has been eliminated.
4. Each conducting phase is considered continuous and homogenous, having a constant conductivity throughout each subdomain.
5. The molecular hydrogen supplied to the gaseous subdomain and the water produced by the reaction exists in Ω_G and behave as ideal gases.
6. The gas pressure at the $\Gamma_{Bulk/G}$ is assumed to be constant and equal to 1 atmosphere.
7. Thermal effects are negligible and the temperature is taken to be constant and uniform throughout the domain. The temperature is 1273 K.

8. Molecular hydrogen is assumed to adsorb dissociatively on Ni. The diffusion of molecular hydrogen in YSZ is very small and is therefore neglected.
9. Surface diffusion is not implemented into the model.
10. The diffusive fluxes of gases are described using Fick's Law since it is simpler to implement than the Dusty Gas model or the Stephan Maxwell model.

The first step in finding the distribution of different species that exist at the TPB was to write a general mass conservation equation for a three dimensional element:

Net rate of accumulation of i within the element

= Net rate of mass efflux of i from the element

+ Rate of chemical production of i within the element

A representative elementary volume is shown in Figure 4.5. The lengths of the three sides are Δx, Δy and Δz. The time step used for the discretization of the continuity equation was dt. Then the mass conservation equation will be:

$$N_{i,x+\Delta x}\Delta y\Delta z|_{x+\Delta x} - N_{i,x}\Delta y\Delta z|_{x} + N_{i,y+\Delta y}\Delta x\Delta z|_{y+\Delta y} - N_{i,y}\Delta x\Delta z|_{y} + N_{i,z+\Delta z}\Delta y\Delta x|_{z+\Delta z}$$

$$-N_{i,z}\Delta y\Delta x|_{z} + \frac{\partial\rho}{\partial t}\Delta x\Delta y\Delta z - R\Delta x\Delta y\Delta z = 0 \qquad (4-1)$$

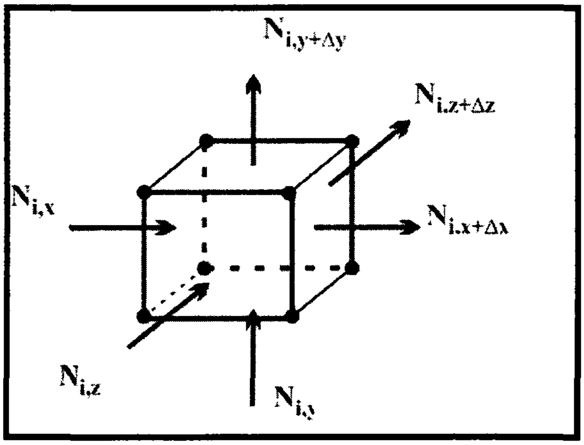

Figure4. 5 An Elementary Control Volume

Therefore mass conservation can be analytically described by the following transportation equation:

$$\nabla \cdot (\mathrm{N_i}) + \frac{\partial \rho}{\partial t} = \mathrm{R} \qquad (4-2)$$

Since the system is assumed to be at steady state:

$$\frac{\partial \rho}{\partial t} = 0 \qquad (4-3)$$

$\mathrm{N_i}$, consists of three terms representing (a) the movement of species based on concentration gradients (Diffusion), (b) the movement of species due to potential gradient (Migration), (c) and the convective flux.

$$\nabla \cdot (-\mathrm{D_i} \nabla \mathrm{C_i} - \alpha_i \mathrm{C_i} + \mathrm{C_i} v) = \mathrm{R_i} \qquad (4-4)$$

The expression that is used for alpha is related to the nature of the mass transfer:

$$\alpha_i = \begin{cases} 0 & \mathrm{i = H_2, H, H_2O, Ni} \quad \text{Fick's law} \\ -\mathrm{D_i}\frac{\mathrm{F}}{\mathrm{RT}}\nabla\varphi & \mathrm{i = OH^-, H^+, O^{2-}, Ni^{2+}} \quad \text{Nernst} - \text{Plank} \end{cases} \qquad (4-5)$$

For neutral species Equation$(4-4)$ becomes a simple Fick's law equation. For charged species Equation $(4-4)$becomes the Nernst-Plank equation. In Equation $(4-4)$, $\mathrm{R_i}$ is the rate of production/consumption of species i.

The following equation is used for electron conservation:

$$\mathrm{C_{dl}} \frac{\partial \nabla \varphi}{\partial t} + \nabla \cdot (\sigma_l \nabla \varphi) = \mathrm{j_{far} L_{TPB}} \qquad (4-6)$$

The double-layer capacitance per unit total volume $\mathrm{C_{dl}}$only impacts transient calculations and thus has no effect on the steady-state modeling (Mitterdorfer 1999, Adler 2004).

$$C_{dl}\frac{\partial \nabla \varphi}{\partial t} = 0 \qquad (4-7)$$

j_{far}, the Faradaic current, is the local charge transfer rate between phases at the TPB. The Faradic current, j_{far} is caused by charge-transfer electrochemistry. L_{TPB} is the TPB length which has the units of meter per meter cubed (Deng 2005, Janardhanan 2008). It should be mentioned that outside of the electrochemically active region, TPB, $j_{far} = 0$ so in Equation $(4-6)$ the electric potential in the bulk collapses to a simple Ohm's law equation.

The Faradaic current is a function of overpotential and concentration of reactants. This function is usually described via an empirical global kinetic, Butler-Volmer equation. The Butler-Volmer equation usually describes the kinetics of the electrode (half-cell) reactions in a single-step reaction. While The Butler-Volmer equation does account for the complex electrochemical processes at the reaction interface, it does not account for all the other processes at the three-phase boundaries. Here the Butler-Volmer equation is used explicitly as part of the rate constant expressions; as described by Bessler et al. (2008) is used. The rate expressions forR_i, in Equation$(4-4)$:

$$R_i = k_{fwd}\prod C_i - k_{bwd}\prod C_j \qquad (4-8)$$

where $k_{fwd}$and k_{bwd} are for forward and reverse reaction. For reactions involving one electron charge transfer, the rate constants are:

$$k_{fwd} = k_{ifwd} \times \exp\left(z \times \alpha_{fwd} \times \eta \times \frac{F}{RT}\right) \qquad (4-9)$$

$$k_{bwd} = k_{ibwd} \times \exp\left(-z \times (1-\alpha_{fwd}) \times \eta \times \frac{F}{RT}\right) \qquad (4-10)$$

The reaction in which losing an electron (oxidation) occurs, is considered as a forward reaction. The reverse reaction or backward reaction is considered to be the process of gaining an electron (reduction). η is the local overpotential. T is the temperature. R and F are the universal gas and Faraday constants, respectively. The forward and backward symmetry parameters are $\alpha_{fwd} = \alpha_{bwd} = 0.5$. k_i, is the rate constant for the thermal component of the rate expression, expressed in Arrhenius form:

$$k_i = A \times T^{\beta} \exp\left(\frac{-E_a}{RT}\right) \qquad (4-11)$$

This may be included in the expression for the overall rate expression as:

$$k_{bwd} = \left(\frac{1}{F}\right) \times A \times T^{\beta} \exp\left(\frac{-E_a}{RT}\right) \times \exp\left(-z \times \alpha_{fwd} \times \eta \times \frac{F}{RT}\right) \qquad (4-12)$$

where E_a (J mol^{-1}) is the activation energy for the chemical (thermal) reaction and A is the pre-exponential factor (Schichlein 2002). The first and second exponential terms thus represent chemical (thermal) and electrochemical contributions, respectively, to the overall reaction rate.

Generally, the electrode potential is expressed in terms of overpotential

$$\eta = \phi_{Ni} - \phi_{YSZ} - (\phi_{Ni} - \phi_{YSZ})_{EQ} = \phi_{NiEQ} - \phi_{Ni} - \left(\phi_{YSZ} - \phi_{YSZEQ}\right) \qquad (4-13)$$

where ϕ_{Ni} and ϕ_{NiEQ} for the electrode are defined with respect to the hydrogen half-cell potential and therefore have specific values. In contrast, ϕ_{YSZ} for the electrolyte is only defined with respect to ϕ_{YSZEQ}. Since the only potentials that can be measured are potential differences, ϕ_{YSZEQ} can be defined relative any arbitrary value. For this work, $\phi_{YSZ\text{-}EQ}$ has been set equal to ϕ_{NiEQ}. Therefore η becomes:

$$\eta = \phi_{Ni} - \phi_{YSZ} \qquad (4-14)$$

which is a negative number. The local overpotential however, is expressed by $\eta = \varphi_{YSZ} - \varphi_{Ni}$ in the literature (Kenney 2006). This is the potential in the electrolyte (ionic) minus the potential in the electrode (electronic). If the overpotential is unequal to zero, the forward and backward rates of each reaction step Equation $(4-9)$ and Equation $(4-10)$ are no longer the same and when the overpotential becomes sufficiently different from zero, the reverse reaction becomes insignificant.

4.2 Models

Two models (the complete model and the simple model) describing the distribution of species near the TPB of a SOFC anode half cell are presented in this chapter. In both models molecular hydrogen is supplied by gaseous diffusion through the anode gas phase; the oxygen anions are supplied by a solid state vacancy transport mechanism through the electrolyte and the YSZ phase of the anode. For the case of the simple model, the system of equations was solved twice, for two different radii.

In order to determine proper rate expressions and boundary conditions for the model, the mechanism (reaction pathway) for the species should be identified first. Different mechanistic models for the chemical and electrochemical reactions at the Ni/YSZ cermets have been proposed in the literature (Chapter 3, Section 3.3.5.3.2). Based on these models a detailed reaction mechanism was presented in Section 4.2. Intermediate species have been included in this mechanism, for example$0H^{-}_{Ni}$, H^{+}_{Ni}, Ni^{2+}_{Ni}, $0H^{-}_{YSZ}$and H^{+}_{Ni} as well as basic species.

Modeling SOFC is an inherently complex task. Any physically realistic model should account for coupled reaction and mass transport. Since solving the whole system with all of the species present in all subdomains is almost an impossible task, different combinations of one or two elementary charge-transfer reactions were investigated. A simpler mechanism was ultimately used for the simple model. The Simple model is described in Section 4.2.2. Even though the equations describing the detailed model were not used in the present study, they are documented here, in Section 4.2.1, for possible future use.

4.2.1 Complete Model

The anode system was assumed to consist of three Ω_G species (H_{2gas}, H_{gas} and H_2O_{gas}), eight species in the Ω_{Ni} (H_{Ni}, H^+,H_{2Ni},O^{2-}_{Ni}, OH^-_{Ni},H_2O_{Ni},Ni^{2+}_{Ni},Ni), and six species in the Ω_{YSZ} (H_{2YSZ}, O^{2-}_{YSZ}, H_2O_{YSZ}, H_{YSZ}, OH^-_{YSZ}, H^+_{YSZ}) in the complete model. Various reaction mechanisms were proposed in the complete model for the TPB of an anode. In this model chemical and electrochemical reactions take place on the surfaces of the Ni and in the Ω_{YSZ}. Bulk reactions were also considered, including the formation of interstitial hydrogen and hydroxyl radicals in the Ω_{YSZ}. Bulk transport of (O^{2-}_{YSZ}) interstitial species takes place by a vacancy diffusion mechanism whereas (H^+_{YSZ}, H_{YSZ}, H_{2YSZ}) transport occurs by interstitial diffusion.

The movements of reaction gases and ions are composed of several elemental steps. Some of the mechanisms that occur include: Diffusion of reaction species (H_2 and H_2O) in Ω_G, dissociative adsorption of reaction gases at the solid surfaces (formation of H, on metal surfaces), diffusion of H radicals, O^{2-} and OH^- in the anode, diffusion of H in the anode metals to the reaction sites, charge transfer reactions, and the formation of H_2O at reaction sites. In principle any one of these steps can be rate determining for the anodic reaction.

The rate determining reaction step was assumed to be one of the following: the dissociative adsorption of hydrogen, the formation of hydroxyl, a charge transfer reaction, or the desorption of water. The complete model considers all of the possible mechanisms, which makes it very complex to solve. The reactions and rate expressions as well as boundary conditions for the complete model are presented in the following sections.

4.2.1.1 Reactions

The reactions in the three domains Ω_G, Ω_{Ni} and Ω_{YSZ} are shown below in Equation($4-15$), Equations ($4-16$) to($4-22$), and Equations ($4-23$) to ($4-27$). No interface reaction between one species in the Ω_{Ni} and one species in the Ω_{YSZ} has been considered for the complete model. It was assumed that O^{2-} and OH^- in Ω_{Ni} and H_2, H^+ and H in Ω_{YSZ} can diffuse far enough to be considered bulk species.

- Reaction in Ω_G

$$H_{2gas} \leftrightarrow 2H_{gas} \qquad k_{G1}/k_{G1b} \qquad (4-15)$$

- Reactions in Ω_{Ni}

$$H_{2Ni} \leftrightarrow 2H_{Ni} \qquad k_{Ni1}/k_{Ni1b} \qquad (4-16)$$

$$H_{Ni} \rightarrow H^+_{Ni} + e^- \qquad k_{Ni2} \qquad (4-17)$$

$$H_{2Ni} + 2O^{2-}_{Ni} \rightarrow 2OH^-_{Ni} + 2e^- \qquad k_{Ni3} \qquad (4-18)$$

$$H_{Ni} + OH^-_{Ni} \rightarrow H_2O_{Ni} + e^- \qquad k_{Ni4} \qquad (4-19)$$

$$H^+_{Ni} + O^{2-}_{Ni} \leftrightarrow OH^-_{Ni} \qquad k_{Ni5}/k_{Ni5b} \qquad (4-20)$$

$$H^+_{Ni} + OH^-_{Ni} \leftrightarrow H_2O_{Ni} \qquad k_{Ni6}/k_{Ni6b} \qquad (4-21)$$

$$Ni \rightarrow Ni^{2+}_{Ni} + 2e^- \qquad k_{Ni7} \qquad (4-22)$$

- Reactions in Ω_{YSZ}

$$H_{2YSZ} \leftrightarrow 2H_{YSZ} \qquad k_{YSZ0}/k_{YSZ0b} \qquad (4-23)$$

$$H_{2YSZ} + O^{2-}_{YSZ} \leftrightarrow H_2O_{YSZ} + 2e^- \qquad k_{YSZ1}/k_{YSZ1b} \qquad (4-24)$$

$$H_{YSZ} + O^{2-}_{YSZ} \leftrightarrow OH^-_{YSZ} + e^- \qquad k_{YSZ2}/k_{YSZ2b} \qquad (4-25)$$

$H_{YSZ} + OH^{-}_{YSZ} \leftrightarrow H_2O_{YSZ} + e^{-}$ k_{YSZ3}/k_{YSZ3b} (4 − 26)

$H^{+}_{YSZ} + OH^{-}_{YSZ} \leftrightarrow H_2O_{YSZ}$ k_{YSZ4}/k_{YSZ4b} (4 − 27)

$H^{+}_{YSZ} + O^{2-}_{YSZ} \leftrightarrow OH^{-}_{YSZ}$ k_{YSZ5}/k_{YSZ5b} (4 − 28)

4.2.1.2 Reaction Rate Expression

The kinetic rate equations for the above stoichiometric reactions are shown below:

- Reaction rate expressions in Ω_G

5.3.1.3.1 Based on reaction (4 − 15) above:

$$R_{H_{2gas}} = -k_{G1} P_{H_2} + 0.5k_{G1b} (P_H)^2 \qquad (4-29)$$

$$R_{Hgas} = 2k_{G1} P_{H_2} - k_{G1b} (P_H)^2 \qquad (4-30)$$

- Reaction rate expressions in Ω_{Ni}

Based on reactions (4 − 16) and (4 − 18):

$$R_{H_2Ni} = -k_{Ni1}C_{H_{2Ni}} + 0.5k_{Ni1b}(C_{HNi})^2 - k_{Ni3}(C_{O^{2-}Ni})^2 C_{H_{2Ni}} \qquad (4-31)$$

Based on reactions (4 − 17) and (4 − 19):

$$R_{HNi} = 2k_{Ni1}C_{H_{2Ni}} - k_{Ni1b}(C_{HNi})^2 - k_{Ni2}C_{HNi} + k_{Ni4}C_{HNi}C_{OH^-Ni} \qquad (4-32)$$

Based on reactions(4 − 17), (4 − 20) and (4 − 21):

$$R_{H^+Ni} = k_{Ni2}C_{HNi} - k_{Ni3}C_{H^+Ni}C_{O^{2-}Ni} - k_{Ni6}C_{H^+Ni}C_{OH^-Ni} + k_{Ni6b}C_{H_2ONi} \qquad (4-33)$$

Based on reactions(4 − 18),(4 − 19), (4 − 20) and (4 − 21):

$$R_{OH^-Ni} = 2k_{Ni3}C_{H_2Ni}(C_{O^{2-}Ni})^2 + k_{Ni5}C_{H^+Ni}C_{O^{2-}Ni} - k_{Ni5b}C_{OH^-Ni} - k_{Ni6}C_{H^+Ni}C_{OH^-Ni} - k_{Ni4}C_{HNi}C_{OH^-Ni} + k_{Ni6b}C_{H_2ONi} \quad (4-34)$$

Based on reactions $(4-19)$ and$(4-21)$:

$$R_{H_2ONi} = k_{Ni4}C_{OH^-Ni}C_{HNi} - k_{Ni5b}C_{H_2ONi} + k_{Ni5}C_{H^+Ni}C_{OH^-Ni} \quad (4-35)$$

Based on reaction$(4-22)$:

$$R_{Ni^{2+}Ni} = k_{Ni7}C_{Ni} \quad (4-36)$$

$$R_{Ni} = -k_{Ni7}C_{Ni} \quad (4-37)$$

Based on reactions$(4-18)$,$(4-20)$:

$$R_{O^{2-}Ni} = -2k_{Ni3}\,C_{H_2Ni}(C_{O^{2-}Ni})^2 - k_{Ni5}C_{H^+Ni}C_{O^{2-}Ni} + k_{Ni5b}C_{OH^-Ni} \quad (4-38)$$

- Reaction rate expressions in Ω_{YSZ}

Based on reactions$(4-23)$,$(4-24)$:

$$R_{H_2YSZ} = k_{YSZ1}\,C_{H_2YSZ}C_{O^{2-}YSZ} + k_{YSZ1b}\,C_{H_2OYSZ} \quad (4-39)$$

Based on reactions$(4-23)$, $(4-25)$,$(4-26)$:

$$R_{HYSZ} = -k_{YSZ2}\,C_{HYSZ}\,C_{O^{2-}YSZ} - k_{YSZ3}\,C_{OH^-YSZ}C_{HYSZ} + k_{YSZ2b}\,C_{OH^-YSZ} + k_{YSZ3b}\,C_{H_2OYSZ} \quad (4-40)$$

Based on reactions$(4-26)$,$(4-27)$:

$$R_{H^+YSZ} = k_{YSZ5}\,C_{H^+YSZ}\,C_{O^{2-}YSZ} - k_{YSZ4}\,C_{H^+YSZ}\,C_{OH^-YSZ} + k_{YSZ5b}\,C_{OH^-YSZ} \quad (4-41)$$

Based on reactions$(4-25)$,$(4-26)$,$(4-27)$,$(4-28)$:

$$R_{OH^{-}YSZ} = k_{YSZ2}\, C_{HYSZ}C_{O^{2-}YSZ} - k_{YSZ3}\, C_{HYSZ}C_{OH^{-}YSZ} - k_{YSZ4}\, C_{H^{+}YSZ}C_{OH^{-}YSZ} + k_{YSZ5}\, C_{H^{+}YSZ}C_{O^{2-}YSZ} - k_{YSZ4b}\, C_{OH^{-}YSZ} + k_{YSZ5b}\, C_{H_2OYSZ} - k_{YSZ2}\, C_{OH^{-}YSZ} + k_{YSZ3b}\, C_{H_2OYSZ} \qquad (4-42)$$

Based on reactions(4 – 24), (4 – 26), (4 – 27):

$$R_{H_2OYSZ} = k_{YSZ4}\, C_{H^{+}YSZ}C_{OH^{-}YSZ} - k_{YSZ4b}\, C_{H_2OYSZ} + k_{YSZ3}\, C_{HYSZ}\, C_{OH^{-}YSZ} - k_{YSZ1b}\, C_{H_2OYSZ} - k_{YSZ3b}\, C_{H_2OYSZ} \qquad (4-43)$$

Based on reactions(4 – 24), (4 – 25) and (4 – 26):

$$R_{O^{2-}YSZ} = k_{YSZ1}\, C_{H_{2YSZ}}C_{O^{2-}YSZ} - k_{YSZ2}\, C_{HYSZ}C_{O^{2-}YSZ} - k_{YSZ2}\, C_{HYSZ} - k_{YSZ5}\, C_{H^{+}YSZ} + k_{YSZ5b}\, C_{OH^{-}YSZ} + k_{YSZ1b}\, C_{H_2OYSZ} + k_{YSZ2b}\, C_{OH^{-}YSZ} \qquad (4-44)$$

4.2.1.3 Boundary Conditions

Several boundary conditions must be specified. The boundary conditions could be of several types. As it is shown in Figure 4.4 there are 6 borders and interfaces that need to be specified. The Dirichlet boundary condition and the Neumann boundary condition are the two types of boundary conditions, applied here.

4.2.1.3.1 Boundary Conditions at $\Gamma_{Bulk/G}$

Two boundary conditions were specified at the$\Gamma_{Bulk/G}$. The flux of atomic hydrogen radicals is equal to zero. The partial pressure of the hydrogen molecules is constant:

Neuman Boundary Condition $\qquad n \cdot (N_i) = 0 \qquad i = H_{gas}$

in which n is the normal to the surface and N is the flux

Dirichlet Boundary Condition $P_i = \text{constant}$ $i = H_{2gas}$

4.2.1.3.2 Boundary Conditions at $\Gamma_{Bulk/YSZ}$

Two boundary conditions were specified at the $\Gamma_{Bulk/YSZ}$. For all species the flux at $\Gamma_{Bulk/YSZ}$ was equal to zero. For all species either the concentration or the pressure was constant at the $\Gamma_{Bulk/YSZ}$:

Neumann Boundary Condition $n \cdot (N_i) = 0$ $i = H_{YSZ}, H^{+}_{YSZ}, H_2O_{YSZ}, H_{2YSZ}$

Dirichlet Boundary Condition $C_i = \text{constant}$ $P_i = \text{constant}$ $i = O^{2-}_{YSZ}, OH^{-}_{YSZ}, H_2O_{YSZ}, Ni^{2+}_{YSZ}, \varphi, H_{2gas}$

4.2.1.3.3 Boundary Conditions at $\Gamma_{Bulk/Ni}$

Two boundary conditions were specified at the $\Gamma_{Bulk,Ni}$. For all species the flux at $\Gamma_{Bulk,Ni}$ was equal to zero. For all species the concentration was constant at $\Gamma_{Bulk,Ni}$

Neumann Boundary Condition $n \cdot (N_i) = 0$ $i = H_{Ni}, H^{+}_{Ni}, H_2O_{Ni}, H_{2Ni}, O^{2-}_{Ni}, OH^{-}_{Ni}, Ni^{2+}_{Ni}$

Dirichlet Boundary Condition $C_i = \text{constant}$ $i = H_2O_{Ni}, Ni, \varphi$

4.2.1.3.4 Boundary Conditions at $\Gamma_{G/YSZ}$

Three different types of boundary conditions were used at $\Gamma_{G/YSZ}$. For all charged species and for the potential the flux at $\Gamma_{G/YSZ}$ was equal to zero (Neumann boundary condition).

In case of a Dirichlet boundary condition the least complex model in the literature assumed minor deviations from equilibrium between the adsorbed species and gaseous species (Wang 1981, Murygin 1991, Adler 2004). As a result Henry's law or Sievert's law was used for the concentration of dissociatively adsorbed H and H_2O at the $\Gamma_{G/YSZ}$. Sievert's law states that the concentration of species in the solid phase is proportional to the square root of the pressure of that species in the Ω_G. This assumption is only true if the concentrations of dissociated species in the solid phase were low.

And finally for several neutral species ($H_{2gas}, H_{gas}, H_{YSZ}, H_2O_{YSZ}$) the flux is continuous from the Ω_G to the Ω_{YSZ}.

Neumann Boundary Condition	$n \cdot (N_i) = 0$	$i = H^+, OH^-, O^{2-}, \varphi$
Dirichlet Boundary Condition	$C_i = P_i^n \times k_i$ $n = 1$ Henry's law $n = 0.5$ Sievert's law	$i = H_2O, H$
Continuity of the Flux	$n \cdot \left(N_{igas} - N_{iYSZ}\right) = 0$	$i = H_2, H, H_2O$

In the above tables, the concentrations or pressures have been specified as constants. At the $\Gamma_{G/YSZ}$, the gaseous species can react to form dissociated species that are adsorbed on the solid YSZ surface.

eg. $H_{2gas} \leftrightarrow 2\,H_{YSZ}$

Furthermore these dissociation reactions are assumed to be at equilibrium (not rate determining). The equilibrium concentrations of the dissociated adsorbed species (Dirichlet bondary conditions) are related to the concentrations of their corresponding molecules in the Ω_G, by an equation.

4.2.1.3.5 Boundary Conditions at $\Gamma_{G/Ni}$

At the $\Gamma_{G/Ni}$, the gaseous species can react to form dissociated species that are adsorbed on the solid Ni surface.

eg. $H_{2gas} \leftrightarrow 2\, H_{Ni}$

Furthermore these dissociation reactions are assumed to be at equilibrium (not rate determining). The equilibrium concentrations of the dissociated adsorbed species (Dirichlet boundary conditions) are related to the concentrations of their corresponding molecules in the Ω_G, by an equation.

Neuman Boundary Condition	$n \cdot (N_i) = 0$	$i = H^+_{Ni}, OH^-_{Ni}, O^{2-}_{Ni}, \varphi, Ni, Ni^{2+}_{Ni}$
Dirichlet Boundary Condition	$P_i = (C_i/k_i)^2$	$i = H_{2gas}, H_2O_{gas}, H_{gas}$
Continuity of the Flux	$n \cdot \left(N_{igas} - N_{iYSZ}\right) = 0$	$i = H_{2Ni}, H_{Ni}, H_2O_{Ni}$

4.2.1.3.6 Boundary Conditions at $\Gamma_{Ni/YSZ}$

The boundary conditions at the $\Gamma_{Ni/YSZ}$ are more complex than those at other interfaces, because this is the interface at which the rate-determining step occurs. Furthermore many different reaction intermediates are included at this interface because it is the interface at which the rate determining step occurs.

Equations$(4-17)$, $(4-20)$ and $(4-21)$ involve the consumption/production of H^+ in Ω_{Ni}, and Equations$(4-27)$, $(4-28)$ involve the consumption/production of H^+ in the Ω_{YSZ}. The appropriate rate expressions are as follows:

$$n \cdot (N_{H^+YSZ}) - n \cdot (N_{H^+Ni}) = L_{TPB}(k_{Ni2}\, C_{HNi} - k_{Ni3} C_{H^+Ni} C_{O^{2-}Ni} - k_{Ni6} C_{H^+Ni} C_{OH^-Ni} + k_{Ni6b} C_{H_2ONi} + k_{YSZ5}\, C_{H^+YSZ} C_{O^{2-}YSZ} + k_{YSZ4}\, C_{H^+YSZ} C_{OH^-YSZ} - k_{YSZ5b}\, C_{OH^-YSZ} - k_{YSZ4b}\, C_{H_2OYSZ})$$

Equations$(4-18)$,$(4-19)$, and $(4-21)$ involve the consumption/production of OH^- in the Ω_{Ni}, and Equation $(4-25)$- Equation $(4-28)$ involve the consumption/production of OH^- in the Ω_{YSZ}. The appropriate rate expressions are as follows:

$$n \cdot (N_{OH^-YSZ}) - n \cdot (N_{OH^-Ni}) = L_{TPB}(k_{YSZ2}\, C_{HYSZ} C_{O^{2-}YSZ} - k_{YSZ3}\, C_{HYSZ} C_{OH^-YSZ} - k_{YSZ4}\, C_{H^+YSZ} C_{OH^-YSZ} + k_{YSZ5}\, C_{H^+YSZ} C_{O^{2-}YSZ} - k_{YSZ5b}\, C_{OH^-YSZ} + k_{YSZ4b}\, C_{H_2OYSZ} - k_{YSZ2b}\, C_{OH^-YSZ} + k_{YSZ3b}\, C_{H_2OYSZ} - 2k_{Ni3} C_{H_{2Ni}} C^2_{O^{2-}Ni} - k_{Ni5} C_{H^+Ni} C_{O^{2-}Ni} + k_{Ni5b} C_{OH^-Ni} + k_{Ni6} C_{H^+Ni} C_{OH^-Ni} + k_{Ni4} C_{HNi} C_{OH^-Ni} - k_{Ni6} C_{H_2ONi})$$

Equations$(4-18)$, $(4-20)$ involve the consumption/production of O^{2-} in the Ω_{Ni}, and Equations$(4-24)$, $(4-25)$, $(4-28)$ involve the consumption/production of O^{2-} in the Ω_{YSZ}. The appropriate rate expressions are as follows:

$$n \cdot (N_{O^{2-}YSZ}) - n \cdot (N_{O^{2-}Ni}) = L_{TPB}(-k_{YSZ1}\, C_{O^{2-}YSZ} C_{H_{2YSZ}} - k_{YSZ2}\, C_{HYSZ} - k_{YSZ5}\, C_{H^+YSZ} + k_{YSZ5b}\, C_{OH^-YSZ} + k_{YSZ1b}\, C_{H_2OYSZ} + k_{YSZ2b}\, C_{OH^-YSZ} - C_{O^{2-}Ni}(-2k_{Ni3}\, C_{H_{2Ni}} C_{O^{2-}Ni} - \mathrm{kNi5CH{+}Ni{-}kNi5bCOH{-}Ni})$$

Equations$(4-16)$, $(4-18)$ involve the consumption/production of H_2 in the Ω_{Ni}, and Equations$(4-23)$, $(4-24)$ involve the consumption/production of H_2 in the Ω_{YSZ}. The appropriate rate expressions are as follows:

$$n \cdot (N_{H_{2YSZ}}) - n \cdot (N_{H_{2Ni}}) = L_{TPB}(k_{YSZ1}\, C_{H_{2YSZ}} C_{O^{2-}YSZ} + k_{YSZ1b}\, C_{H_2OYSZ} + k_{Ni1} C_{H_{2Ni}} - 0.5k_{Ni1b} C^2_{HNi} + k_{Ni3} C^2_{O^{2-}Ni} C_{H_{2Ni}})$$

Equations$(4-17)$, $(4-19)$ involve the consumption/production of H in Ω_{Ni}, and Equations$(4-23)$, $(4-25)$, $(4-26)$ involve the consumption/production of H in the Ω_{YSZ}. The appropriate rate expressions are as follows:

$$n \cdot (N_{HYSZ}) - n \cdot (N_{HNi}) = L_{TPB}(C_{HYSZ}\,(-k_{YSZ2}\,C_{O^{2-}YSZ} - k_{Ni3}C_{OH^{-}YSZ}) + k_{YSZ2b}\,C_{OH^{-}YSZ} + k_{YSZ3b}\,C_{H_2OYSZ} - 2k_{Ni1}C_{H_2Ni} + k_{Ni1b}C_{HNi}^{2} + k_{Ni2}C_{HNi} + k_{Ni4}C_{HNi}C_{OH^{-}Ni})$$

Equations(4 − 19) and (4 − 21) involve the consumption/production of H_2O in Ω_{Ni}, and Equations(4 − 24), (4 − 26) and (4 − 27) involve the consumption/production of H_2O in the Ω_{YSZ}. The appropriate rate expressions are as follows:

$$n \cdot \left(N_{H_2OYSZ}\right) - n \cdot \left(N_{H_2ONi}\right) =$$
$$L_{TPB}(k_{YSZ4}\,C_{H^{+}YSZ}C_{OH^{-}YSZ} - k_{YSZ4b}\,C_{H_2OYSZ} + k_{YSZ3}\,C_{HYSZ}C_{OH^{-}YSZ} - k_{YSZ1b}\,C_{H_2OYSZ} - k_{YSZ1b}\,C_{H_2OYSZ} - k_{Ni4}C_{OH^{-}Ni}C_{HNi} + k_{Ni6b}C_{H_2ONi} - k_{Ni6}C_{H^{+}Ni}C_{OH^{-}Ni})$$

Equation (4 − 22) involves the consumption/production of H^{+} in the Ω_{Ni}. The appropriate rate expression is as follows:

$$n \cdot (N_{Ni^{2+}YSZ}) - n \cdot (N_{Ni^{2+}Ni}) = L_{TPB}(-k_{Ni7}C_{Ni^{2+}Ni})$$

4.2.2 Simple Model: Coupled Mass Transport and Reactions, at $\Gamma_{G/Ni}$and at $\Gamma_{Ni/YSZ}$

The above detailed complete model was converted into the simplest model that might adequately represent the TPB, having only two reactions one at $\Gamma_{G/Ni}$ and one at $\Gamma_{Ni/YSZ}$. There is one solid-gas chemical reaction at the $\Gamma_{G/Ni}$and one electrochemical reaction at the$\Gamma_{Ni/YSZ}$. The reaction that occurs at $\Gamma_{Ni,YSZ}$ between hydrogen radicals and oxygen anions is the rate limiting step in the overall reaction. The reaction that occurs at $\Gamma_{G/Ni}$ is assumed to be the faster of the two and was treated as an equilibrium reaction. It is assumed that the simple model of the anode system consists of two mobile species (H_{2gas},H_2O_{gas}) in the gas phase, one mobile specie in the Ω_{Ni} (H_{Ni}), and two mobile species in the Ω_{YSZ} (O_{YSZ}^{2-},H_2O_{YSZ}). Reactions and boundary conditions are discussed in Section 4.2.2.1 and 4.2.2.2 respectively.

4.2.2.1 Reaction

- Reaction at $\Gamma_{Ni,YSZ}$

In the vicinity of the $\Gamma_{Ni/YSZ}$, diffusing hydrogen atoms may hop to either a hydroxyl ion or an oxygen ion Equation $(4-45)$ on the YSZ side of the $\Gamma_{Ni,YSZ}$. In this study the second possible reaction was chosen. The pathway was proposed in several literature sources (Bieberle 2001, Bieberle 2002, Zhu 2005, Bessler 2005, Bessler 2007). As a result the rate limiting electrochemical reaction occurring at the $\Gamma_{Ni,YSZ}$ is written as:

$$2H_{Ni} + O_{YSZ}^{2-} \rightarrow H_2O_{YSZ} + 2e^- \qquad (4-45)$$

- Reaction at $\Gamma_{G/Ni}$

The reaction at the $\Gamma_{G/Ni}$ was considered fast enough to be at equilibrium:

$$H_{2gas} \leftrightarrow 2H_{Ni} \qquad (4-46)$$

- Reaction Rate Expressions

Based on reaction$(4-45)$:

$$R^* = k^* \, C_{O^{2-}YSZ} C_{HNi}{}^2 \qquad (4-47)$$

Based on reaction$(4-46)$:

$$R' = k_f * P_{H_2gas} - \left(C_{HNi}{}^2\right) * k_r \qquad (4-48)$$

4.2.2.2 Boundary Conditions

Boundary conditions for the simple model are the same as for the complete model at the $\Gamma_{Bulk/G}$,$\Gamma_{Bulk/YSZ}$, $\Gamma_{Bulk/Ni}$ and $\Gamma_{G/YSZ}$. Boundary conditions at $\Gamma_{G/YSZ}$ and $\Gamma_{Ni/YSZ}$ are as follows:

4.2.2.2.1 Boundary Condition at $\Gamma_{G/Ni}$

At the $\Gamma_{G/Ni}$ the flux of hydrogen atoms entering the Ω_{Ni} was set equal to the rate expression of reaction$(4-46)$. So all the hydrogen molecules that reached the $\Gamma_{G/Ni}$would react and be converted to H radicals that eventually diffused into the Ω_{Ni}.

Flux Boundary Condition $\quad N_i = -0.5R' \quad i = H_{Ni}$

4.2.2.2.2 Boundary Condition at $\Gamma_{Ni/YSZ}$

At $\Gamma_{Ni/YSZ}$ the flux was set equal to the rate expression that was appropriate for each of the reacting species, based on reaction$(4-45)$.

Neuman Boundary Condition $\quad n \cdot \left(N_{O^{2-}_{YSZ}}\right) = 0.5R^* \quad i = O^{2-}_{YSZ}$

Neuman Boundary Condition $\quad n \cdot \left(N_{H_{Ni}}\right) = R^* \quad i = H_{Ni}$

Neuman Boundary Condition $\quad n \cdot \left(N_{H_2O_{YSZ}}\right) = -0.5R^* \quad i = H_2O_{YSZ}$

4.3 Electrochemical, Physical and Chemical Properties

Many different electrochemical and physical properties are required to apply the mathematical model. Experimental data for some parameters could be found in the literature.

Unfortunately there were no references available for others, and they have not been measured experimentally. In these cases an estimation technique was applied (Bieberle 2000).

Obtaining accurate data was sometimes difficult and sometimes impossible. For example, the diffusivity of chemical species depends strongly on the structural characteristics of the electrolyte, catalyst layer and gas diffusion layer, which form the cermet. Because variations in these properties from one SOFC to another are expected, the values used would not be universally applicable. Furthermore the solubility constants and rate constants for several reaction intermediates are not known. Therefore, there is some uncertainty in the results from this numerical simulation.

4.3.1 Diffusion Coefficient

Some of the diffusion parameters needed for the model are: the diffusion coefficient of H_2 in the Ω_G, the diffusion coefficient of H atoms in nickel particles, the diffusion coefficients of H_2O in both the Ω_{YSZ} and Ω_G and the diffusion coefficient of O^{2-} in the Ω_{YSZ}. Some of these constants were calculated using an accepted equation and some of them were experimental values, measured by researchers and presented in papers. A summary of the literature found for diffusion coefficient values is given in Table 4.1.

The diffusion coefficient D in the table was calculated from the following equation:

$$D = D^{\circ} \exp\left(\frac{-E}{RT}\right) \qquad (4-49)$$

in which D° is the pre-exponential factor, E is the activation energy, R is the gas constant and T is the temperature in Kelvin.

Species	Exponential Factor($m^2.s^{-1}$)	Activation Energy ($J.mol^{-1}$)	Diffusion Coefficient ($m^2.s^{-1}$)	References
H (Ni)	$3.70*10^{-7}$	$1.13*10^{4}$	$1.27*10^{-7}$	(Bhatia 2005)
	$2.80*10^{-7}$	$1.89*10^{4}$	4.69E-08	(Cao 1997)
	$6.00*10^{-7}$	$1.44*10^{4}$	$1.54*10^{-7}$	(Rossmeisl 2008)
	$6.00*10^{-7}$	$1.30*10^{4}$	$1.76*10^{-7}$	(Watson 2001)
	$4.60*10^{-7}$	$1.44*10^{4}$	$1.18*10^{-7}$	(Horita et al. 2006)
O^{2-}(Ni)	$7.00*10^{-7}$	$5.50*10^{4}$	$3.87*10^{-9}$	(Inderwildi 2005)
	$6.00*10^{-7}$	$5.51*10^{4}$	$3.29*10^{-9}$	
	$6.00*10^{-7}$	$1.17*10^{5}$	$9.14*10^{-12}$	(Barczak 2004)
	$6.30*10^{-7}$	$6.13*10^{4}$	$1.92*10^{-9}$	
OH^{-}(Ni)	$6.00*10^{-7}$	$5.52*10^{4}$	$3.26*10^{-9}$	(Barczak 2004)
	$6.00*10^{-7}$	$5.80*10^{3}$	$3.47*10^{-7}$	(Vogler 2009)
	$6.00*10^{-7}$	$3.05*10^{4}$	$3.36*10^{-8}$	
H_2O(Ni)	$6.00*10^{-7}$	$5.59*10^{4}$	$3.05*10^{-9}$	(Barczak 2004)
	$6.00*10^{-7}$	0	$6.00*10^{-7}$	(Vogler 2009)
	$6.00*10^{-7}$	$2.80*10^{4}$	$4.26*10^{-8}$	
O^{2-}(YSZ)	$5.50*10^{-11}$	$9.00*10^{4}$	1.1210^{-14}	(Martin 1996)
		$2.70*10^{4}$	0	(Galdikas 2004)
	$3.00*10^{-13}$	$2.90*10^{4}$	$1.94*10^{-14}$	(Wahlstrom 2004)
	$5.50*10^{-11}$	$9.00*10^{4}$	$1.12*10^{-14}$	(Horita et al. 2006)
OH^{-}(YSZ)	$1.30*10^{-6}$	$5.50*10^{4}$	$7.20*10^{-9}$	(Raz 2001)
H_2O(YSZ)		$5.50*10^{4}$		(Raz 2001)

Table 4. 1 Kinetic Data for Calculating Diffusion Coefficient and Final Calculated Diffusion Coefficient for Different Species

4.3.1.1 Binary Gas Diffusion Coefficient of H_2 and H_2O

Expressions, used for estimating the value of D in the absence of experimental data were the Wilke-Lee modification of the Hirschfelder-Bird-Spotz method that is recommended for mixtures of nonpolar gases and the Fuller correlation that can be used for a binary mixture of gases at different pressures and temperatures.

The Wilke-Lee equation is:

$$D_{AB} = \frac{10^{-4}(1.084 - 0.249\sqrt{\frac{1}{M_A} + \frac{1}{M_B}})\sqrt{\frac{1}{M_A} + \frac{1}{M_B}}T^{1.5}}{p_t(r_{AB})^2 f(\frac{kT}{\varepsilon_{AB}})}$$

in which

D_{AB} = Diffusivity ($\frac{m^2}{s}$)

T = Temperature (K)

M_A, M_B = Molecular weight of A and B ($\frac{kg}{kmol}$)

p_t = Pressure ($\frac{N}{m^2}$)

$r_{AB} = (r_A + r_B)/2$ Molecular separation at collision (nm)

From Table 2.2 of Treybal (1968) $r_{H2} = 0.2827$ (nm), $r_{H2O} = 0.2641$ (nm)

$$r_{AB} = \frac{(0.2827 + 0.2641)}{2} = 0.2734 \text{ (nm)}$$

The value of r_{AB}, the molecular separation at collision, is given in the literature Treybal (1968). It can also be calculated from other properties of gases such as viscosities. Here, the values given in Treybal (1968) are used.

ε_{AB} =Energy of molecular attraction

$$\varepsilon_{AB} = \sqrt{\varepsilon_B \varepsilon_A} \qquad (4-50)$$

$\varepsilon_{H2} = 59.7\,k$, $\quad \varepsilon_{H2O} = 809.1\,k$

$\varepsilon_{AB} = k\sqrt{59.7 * 809.1} = 219.78k$

k = Boltzman's constant

$$f\left(\frac{kT}{\varepsilon_{AB}}\right) = \text{Collision function} \qquad (4-51)$$

$$= f\left(\frac{1273}{219.78}\right) = f(11.03) = 0.35$$

the value of $f\left(\frac{kc}{\varepsilon_{AB}}\right)$ was obtained from a specific figure in Treybal (1968) titled "collision function for diffusion". It shows $f\left(\frac{kc}{\varepsilon_{AB}}\right)$ versus $\frac{kc}{\varepsilon_{AB}}$

$$D_{AB} = \frac{0.0001(1.084 - 0.249\sqrt{\frac{1}{2} + \frac{1}{18}})\sqrt{\frac{1}{2} + \frac{1}{18}}(1273)^{1.5}}{(101.3 * 10^3)(0.2734)^2 0.35} = 1.14 * 10^{-3}\,(\frac{m^2}{s})$$

The Fuller method, on the other hand is

$$D_{AB} = \frac{0.00143T^{1.75}}{P \times M_{AB}^{0.5}(\Sigma_A^{1/3} + \Sigma_B^{1/3})^2} \qquad (4-52)$$

$$M_{AB} = 2(\frac{1}{M_A} + \frac{1}{M_A})^{-1} \qquad (4-53)$$

in which

D_{AB}= Diffusivity ($\frac{\mathrm{cm}^2}{\mathrm{s}}$)

T = Temperature (K)

M_A, M_B = Molecular weight of A and B ($\frac{g}{mol}$)

P = Pressure (bar)

$\sum =$ Sum of atomic diffusion volumes, which is a tabulated parameter. The molecular diffusion volumes of H_2O and H_2 are reported as 13.1 and 6.12 by Poling et al. (2004) respectively.

$$D_{AB} = \frac{0.00143(1273)^{1.75}}{1 \times 0.36^{0.5}(13.1^{0.33} + 6.12^{0.33})^2} = 1.18 \times 10^{-3} \left(\frac{\mathrm{m}^2}{\mathrm{s}}\right) \qquad (4 - 54)$$

The above formula for molecular diffusion coefficients is for binary gas mixtures.

4.3.1.2 Diffusion Coefficient for H_2 in the Ω_{Ni}

Hydrogen molecules can either form a stable hybrid with a particular metal or they can dissolve in the metal. When a hydrogen molecule dissolves, it dissociates into two atoms (Sieverts' Law), which are incorporated into the bulk solid at interstitial sites in the metal crystal lattice. Diffusion of hydrogen in nickel has been studied from about room temperature up to the melting point of nickel which is 1728 K. Various values, measured through different techniques are remarkably consistent. (Hanneken 1999, Carter 2001, Zoltowski 2007). In most cases the temperature dependence of the diffusion coefficient is described by an Arrhenius type equation. The diffusion coefficient equation consists of a pre exponential term and an activation enthalpy that according to Vtilkl (1978) are:

$D_0 = 6.9 \times 10^{-7} (\mathrm{cm^2 s^{-1}})$

$\Delta H = 0.420\ (\mathrm{eV})$

The diffusion coefficient of hydrogen in pure nickel was also calculated by (Ebisuzaki 1967) from the following equation:

$$D_H = (5.22 \pm 0.18) * 10^{-7} \exp\left(\frac{-(9.56 \pm 0.04)}{RT}\right) \qquad (4-55)$$

4.3.1.3 Diffusion Coefficient of O^{2-} in the Ω_{YSZ}

Oxygen ion transport in the Ω_{YSZ} involves the diffusion of oxygen ions by a vacancy exchange mechanism. Therefore the concentration of these vacancies plays an important role in the diffusivity of oxygen. The oxygen vacancies are introduced to the zirconia lattice by doping with yttrium. The diffusivity of oxygen in the Ω_{YSZ} has been investigated by many investigators using different techniques. Keneshea (1971), described the diffusion of pure oxygen at 1atm and between 600°C and 1000°C by the equation,

$$D_{O2} = 2.34 * 10^{-2} \exp - \frac{45300 \pm 1200}{R} \qquad (4-56)$$

4.3.1.4 Diffusion Coefficient of H_2O in the Ω_{YSZ}

No published data for the diffusion coefficient of water in the Ω_{YSZ} have been found. Although Wagner (1968) first reported the solubility of water in polycrystalline Ω_{YSZ}, No distinct study has been performed yet in order to determine the diffusion process or the diffusion coefficient. As the partial pressure of water increases the solubility of H_2O in the Ω_{YSZ} structure increases. The H_2O molecules occupy the oxygen anion vacancies and therefore decrease the oxygen ions conductivity due to the competition for the same sites that also transport oxygen.

4.3.2 Initial Concentration of H_2 and O^{2-}

The initial pressure of H_2 and the concentration of O^{2-} are used as boundary conditions in the model. For the initial pressure of H_2, the pressure drop of the gas has been neglected. In reality the pressure of H_2 reduces as it flows along the fuel channel from the inlet to the outlet, so the total pressure, the sum of the H_2 and H_2O partial pressures, is slightly different than 1 atm.

The initial concentration of O^{2-} was calculated based on the fact that YSZ films have a lattice constant of 5.15 (Å) (Hwang 1998, Millini 1994) and in each polymorph of ZrO_2, the unit cell contains four units of ZrO_2 (Yashara 1999). The final calculated value was 53.1 ($kmol.m^{-3}$).

4.3.3 Conductivity of YSZ and Ni

For ideal operation of SOFCs, conduction in the electrolyte must be an ionic conduction with a very low electronic transference number over a wide range of oxygen partial a pressure (Gordon 2003-2007). The most commonly used anode material is the mixture of yttria stabilized zirconia (YSZ is an ionic conductor) and nickel (Ni is an electronic conductor). Their properties are approximately 15 ($S.m^{-1}$), oxygen anion vacancy conductivity, for YSZ (σ_{YSZ}) and 2×10^6 ($S.m^{-1}$), electronic conductivity, for Ni (σ_{Ni}) at SOFC operating conditions of 1273K and 1 atm.

4.3.4 Estimation of Kinetic Parameters

The reaction rate constants for the chemical (k_f and k_r) and the electrochemical reactions (k^*) in Equation $(4 - 44)$ and Equation $(4 - 45)$ are not directly published in the literature, but have to be estimated. Bieberle et al (2002) calculated several rate constant for different reactions in an SOFC anode. Bieberle's values have been used in this thesis.

All the other parameters that are used in this simulation are presented in Table 4.2.

Parameter	Value	Description	Reference
P_{H2}	0.99×10^5 (Pa)	Hydrogen partial pressure at $\Gamma_{\mathrm{Bulk/G}}$	
P_{total}	1.03×10^5 (Pa)	Total pressure at $\Gamma_{\mathrm{Bulk/G}}$	
C_{O2-}	5.31×10^4 (mol.m^{-3})	Oxygen anions concentration at $\Gamma_{\mathrm{Bulk/YSZ}}$	(Mitterdorfer 1999) Calculated
σ_{Ni}	2×10^6 (S.m^{-1})^b $0.00003 \exp(\frac{-1392}{T})^c$	Electronic conductivity of pure Ni	[b] (Bossel UG 1992) [c] (Campanari 2004)
σ_{YSZ}	10 (S.m^{-1})^b $0.00003 \exp(\frac{10350}{T})^c$	Ionic conductivity of pure YSZ	(Bossel UG 1992) [c] (Campanari 2004)
T	1273 (K)	Temperature	
R	8.314(m^3 Pa K^{-1} mol^{-1})	Gas constant	
$k_{H_2O_{YSZ}}$	10^{-6} (mol.atm^{-1}.m^{-3})^a	Sievert's law constant	(Horita et al. 2006)
k_{H_2Ni}	10^{-7}- 10^{-5}	Sievert's law constant	
F	96485.3415 (C.mol^{-1})	Faraday Constant	

Table 4. 2 Model Parameters Used for the Simulations

a 1073°K
b 1000°K

Bibliography

Adler, S.B.,. "Factors Governing Oxygen Reduction in Solid Oxide Fuel Cell Cathodes." Chem. Rev.104 (10), 2004: 4791–4844.

Berg, P., Novruzi, A., Volkov, O., "Reaction Kinetics at the Triple-Phase Boundary in PEM Fuel Cells", J. Fuel Cell Technol. 5, 2008, 021007-1

Bessler, W. A New Computational Approach for SOFC Impedance from Detailed Electrochemical Reaction-diffusion Models. Solid State Ionics, 176:997_1001, 2005.

Bessler,W,. S. Gewies and M. Vogler. A New Framework for Physically Based Modeling of aSolid Oxide Fuel Cells. Electrochimica Acta, 53(4):1782_1800, 2007.

Bessler, W.G., S.Gewiesz. "Physically Based Impedance Modeling of Ni/YSZ Cermet Anodes." Journal of the Electrochemical Society, 2008: B937-B952.

Bieberle, A., L. Meier, and L. Gauckler. The Electrochemistry of Ni Pattern Anodes Used as Solid Oxide Fuel Cell Model Electrodes. J. Electrochem. Soc., 148:A646_A656, 2001.

Bieberle, A.,L.J. Gauckler. "State-space modeling of the anodic SOFC system Ni, H_2–H_2OYSZ." Solid State Ionics, 146, 1-2, 2002: 23-41.

Bossel UG "Facts and Figures" Final report on SOFC data, IEA report. Operating Task II, Swiss Federal Office of Energy, Berne, 1992.

Bove, R.,S.Ubertini. "Modeling Solid Oxide Fuel Cell Operation: Approaches, Techniques and Results." Journal of Power Sources,159,1, 2006: 543-559 .

Brossmann, U., Wutschmub. "Oxygen Diffusion in Ultera Fine Grained Monoclinic ZrO2." Journal of Applied Physics, 85, 11, 1999: 7646-7654.

Cao, G.X, E.Nabighian, X. D. Zhu. "Diffusion of Hydrogen on Ni(111) over a Wide Range of Temperature:Exploring Quantum Diffusion on Metals." Physical Review Letters,79,19, 1997: 3696.

Campanari S., P., Iora, "Definition and Sensitivity Analysis of a Finite Volume SOFC Model for a Tubular Cell Geometry," J. Power Sources, 2004, 132(1–2)

Chan, S. H., Z. T. Xia. "Anode Micro Model of Solid Oxide Fuel Cell ." Journal of The Electrochemical Society, 148 (4), 2001: A388-A394

Deng X., A. Petric. “Geometrical Modeling of the Triple-phase-boundary in Solid Oxide Fuel Cells” Journal of Power Sources 140 2005: 297–303

Ebisuzaki, Y.,W.J.Kass. "Diffusion and solubility of Hydrogen in Single Crystals of Nickel and Nickel-Vanadium Alloy." Journal of Chemical Physics,46, 1967: 1378-1381.

Edwar, A.G.,. "Measurment of the Diffusion Rate of Hydrogen in Nickle ." Journal of Appl. Phys. 8, 1957: 406-409.

Fehribach, J.D., O’Hayre, R., "Triple Phase Boundaries in Solid-Oxide Cathodes", SIAM J. Appl. Math. 70, 2, 2009, 510-530.

Greene E.S., W.K.S. Chiu, M.G. Medeiros. "Mass Transfer in Graded Microstructure Solid Oxide Fuel Cell Electrodes." Journal of Power Sources 161 , 2006: 225–231.

Horita, T., H. Kishimoto, K.Yamaji, Y.Xiong, N. Sakai,M.E. Brito, H.Yokokawa. "Materials and Reaction Mechanisms at Anode/electrolyteInterfaces for SOFCs." Solid State Ionics 177, 2006: 1941–1948.

Janardhanan,V., V.Heuveline, O.Deutschmann. “Three-phase Boundary Llength in Solid-oxide Fuel Cells: A mathematical Model” Wiley InterScience,2008

Kenney, B., K., Karan. "Engineering of Microstructure and Design of a Planar Porous Composite SOFC Cathode: A Numerical Analysis." Solid State Ionics 177, 2006: 2013–2021.

Mitterdorfer, A., L.J.Gauckler. "Identification of the Reaction Mechanism of the Pt, O2(g)|yttria-stabilized Zirconia System: Part I : General Framework, Modelling, and Structural Investigation." Solid state ionics, 1999: 187-202.

Schichlein, H., A. C. Müller, M. Voigts, A. Krügel and E. Ivers-Tiffée,. "Deconvolution of Electrochemical Impedance Spectra for the Identification of Electrode Reaction Mechanisms in Solid Oxide Fuel Cells." J. Appl.Electrochem. 32, 2002: 875.

Treybal, A. “Mass Transfer Operations” McGraw-Hill Companies; 3 edition (January 1, 1980)

Williford, R.E., L.A.Chick, G.D.Maupin, S.P.Simner, and J.W.Stevens. "Diffusion Limitations in the Porous Anodes of SOFCs." Journal of the Electrochemical Society,150, 2003: 1067-1072.

Williford, R.E.,. "Modeling of environmentally significant interfaces: Two case studies." Journal of Electron Spectroscopy and Related Phenomena,150,2-3, 2006: 171-184 .

Wortman, R.,. "Adsorption and Diffusion of Hydrogen on Nickel ." Journal of Chemical Physics, 27, 1957: 1099-1107.

Zhu, H, R.J. Kee,. "A General Mathematical Model for Analysing the Performance of Fuel-cell Membrane-electrode Assemblies." Journal of Power Sources,117,1-2, 2003: 61-74.

H. Zhu, R. J. Kee, V. M. Janardhanan, O. Deutschmann, and D. G. Goodwin. Modeling Elementary Heterogeneous Chemistry and Electrochemistry in Solid-oxide Fuel Cells. J. Electrochem. Soc., 152:A2427_A2440, 2005.

Chapter 5 Methodology

There are two primary tasks in modeling: understanding the physical phenomena that occur in the system, and describing those phenomena with a series of mathematical equations. For example the law of conservation of mass (reaction and transport of species) describes one of the phenomena that occur. Partial differential equations (PDEs) arise naturally from conservation laws. The solution of these PDEs provides the distribution in space of variables such as concentration and potential. Often these equations cannot be solved analytically. Because the laws are integral equations over the domain, the corresponding PDEs have a structure that is readily represented by a numerically procedure.

5.1 Numerical Methods

There are three general categories of numerical techniques. The first approach is based on the Taylor series, and is known as the finite difference method (FDM). A finite difference method uses difference equations for an array of grid points. The second approach is based on the use of conservation laws that are applied to each finite volume (elements) in space, and is known as the finite volume method (FVM). The third approach, the finite element method (FEM), was used in this work.

The finite element method (FEM) is a numerical technique that has been used for obtaining approximate solutions to a wide variety of engineering problems. In the FEM, the domain is divided into several elements. Known physical laws are then applied to each small element.

The first Finite Element Analysis (FEA) (Courant 1943) used the variational approach of numerical analysis to obtain approximate solutions to vibration systems. Later Turner (1956) established a broader definition of numerical analysis. In the years since 1960 the finite element method has received widespread acceptance in the field of engineering. Commercial FEM packages have been available since the 1980s. In FEM, problems are treated by identifying a finite number of unknowns, by dividing the domain into elements, and by expressing the unknown variables in terms of assumed approximating functions (interpolation functions) within each element. These interpolation functions are developed from the values of the variables at specific points, referred to as nodes. A description of nodes and other terms used in FEM will be given later in this chapter. Nodes are usually located along the element boundaries, where they connect adjacent elements.

Some features of the three numerical techniques mentioned above are compared below:

- In general FEM and FVM use integral forms of the governing equations, while FDM uses differential forms of the equations. Integral equations provide a more natural treatment of Neumann boundary conditions and discontinuous source terms. They also produce a smoother solution. (Peir´o 2005)

- The quality of FEM estimations is often superior to those from the corresponding FDM approach, but the validity of this statement depends on the nature of the problem and its particular specification. Therefore the use of integral formulations is an advantage that FEM and FVM may have over FDM.

- FEM is better than other techniques for complex geometries in multi-dimensional problems as the integral formulations do not rely on any special mesh structure.

- In terms of solving a diffusion equation, FEM is well suited to determining values for variable coefficients. An example is the transport properties that depend on a field variable.

- The FEM is used for multidisciplinary problems, since it can describe a variety of physics and engineering phenomena including solid mechanics, dynamics, heat transfer, fluid mechanics, and electrostatics. Where there is a coupling between two or more of the phenomena, FEM can be very useful.

In next section FEM will be described in more detail. Specifically, a PDE will be represented by a finite number of unknown parameters.

5.2 Finite Element Method

The finite element method FEM is normally described using specialized terms, some of which are explained below. Geometry or the domain is a collection of bounded geometric subdomains. A geometrical domain is the space over which a physical problem is to be solved. A mathematical domain of a function is the set of all input values for which that function is valid. The geometrical domain used for this work was the circle shown in Figure 1.3 in Chapter 1.

5.2.1 Decomposition of the Domain into a Finite Number of Elements.

Domains are connected manifolds, that is, volumes, surfaces, curves, or points. Depending on the geometry and the physical nature of the problem, the domain of interest can be discretized by employing line, area, or volume elements. The starting point for the FEM is the discretization of the original domain space into a finite number of elements. This concept introduces nodes and elements.

- Elements

Elements are the small spaces that are formed by discretizing the domain. A variety of element shapes may be used, and different element shapes may be employed in the same solution region. Some of the common element shapes in FEM are shown in Figure 5.1

- Nodes

Nodes are the end points of finite elements. Common nodes (eg X_5, Y_5 in Figure 5.2) connect elements to each other. A specific node may be common to more than one specific element. A node is a coordinate location in space where the degrees of freedom are defined.

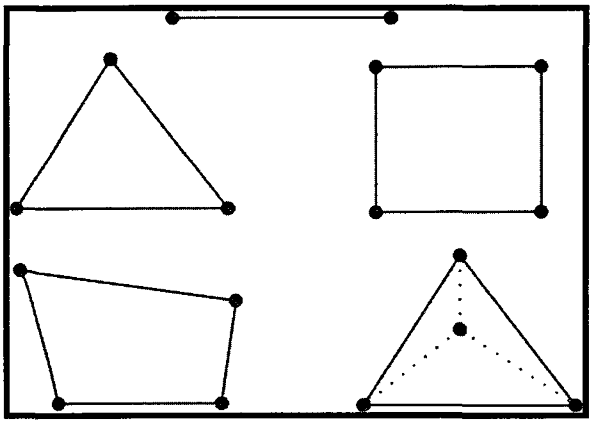

Figure 5. 1 Common Line, Area (Triangular, Rectangular, Quadrilateral, and Volume (Tetrahedral) Elements

Actions (eg. heat transfer) that occur in the geometric domain are expressed in mathematical terms at nodes. Nodes are classified as either exterior or interior, depending on their location relative to the geometry of an element. Exterior nodes lie on the boundary of an element, and they represent the points of connection between bordering elements. Nodes that exist at the corners of elements, along the edges, or on the surfaces are all exterior nodes. Interior nodes are those that do not connect with neighbouring elements.

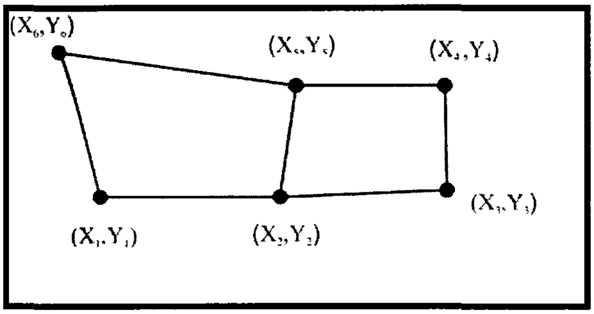

Figure 5. 2 Schematic of Two Elements and Their Nods

- Degrees of Freedom

Degrees of freedom (DOFs) are the values of a primary variable, or its derivative. In the FEM those values are expressed at common node points. A degree of freedom is identified by a name and a node point. For example, “temperature 123” represents the primary unknown variable “temperature” at node number 123. Degrees of freedom are defined at every mesh point.

- Verticies

A vertex, an end point of a subdomain shape, is analogous to a node that is an endpoint of a finite element. Specifically a vertex is either the end of a line (a straight line or an arc) or the intersection of lines in a 2D or 3D subdomain (edges or faces of a subdomain shape).

- Actions that Occur in the Geometric Domain Where the Physical Phenomena Occur

Actions that occur in the geometric domain are expressed in mathematical terms at nodes. Degrees of freedom (DOF) at a node are defined by the physical nature of the problem and the element type. For example in a heat conduction problem the degree of freedom is temperature and the action that occurs, ie, the physical phenomenon, is the heat flux. Therefore the heat flux will be expressed mathematically at each node. A schematic diagram of a discritized domain is shown in Figure 5.3. Once the domain of the problem is discretized by elements, a unique element number identifies each element and a unique node number identifies each node in the domain.

5.2.2 Selection of Interpolation Functions

The next step is to choose an appropriate interpolation function, to approximate the variation of each variable over each element. Often, polynomials are selected as interpolation functions for the variables because they are easy to integrate and differentiate. These polynomial functions should satisfy some specific criteria. For example they should be continuous within the element, and compatibility should exist along the common nodes, boundaries or surfaces between adjacent elements.

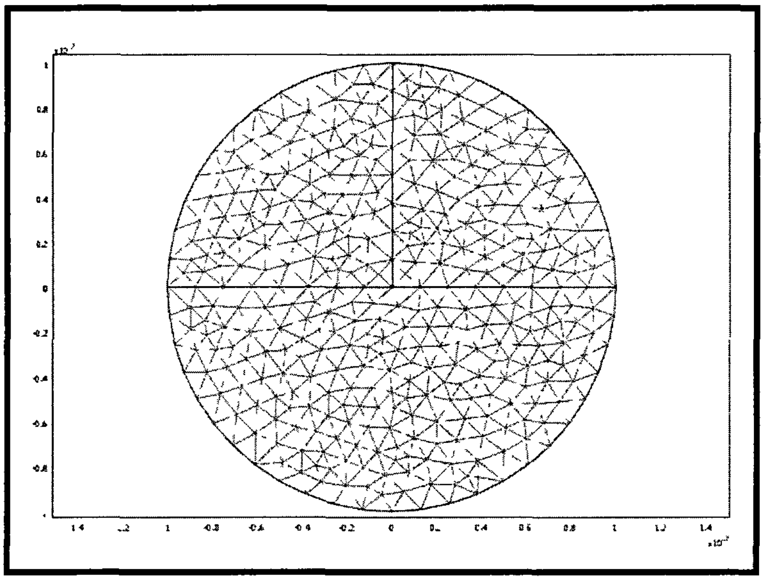

Figure 5. 3 Schematic Diagram of A Grid Discretization (Meshed) Domain Used in 2D Computational Simulations

Classical interpolation functions are Lagrange polynomials (Lagrange interpolation functions) or Hermitian polynomials. The Lagrange interpolation polynomial is a single polynomial that passes through a given set of nodes. A Lagrange polynomial is used when the interpolation function is only a function of the value of the variable it represents. A Hermitian polynomial on the other hand, is used when the interpolation function is a function of both the variable itself and derivatives of the variable it represents.

5.2.3 Determining the Element Properties

Once the elements and their interpolation functions have been selected, the matrix equations should be determined. These matrices should express the properties of the individual elements. In FEM there are three main approaches for performing this task: the direct approach, the variational approach, and the weighted residuals approach. The first is the direct approach that applies the physical concept directly to the elements. The second requires the determination of variational functionals for which a stationary state is sought. A functional is defined as a function of several other functions. Theorems such as minimization of total potential energy to achieve equilibrium in mechanical systems, or minimizing Gibbs energy to achieve thermodynamic equilibrium are examples of stationary situations. In the variational method a global energy balance of the physical phenomena is used. The third is the method of weighted residuals, alternatively known as the Galerkin procedure. It involves the governing differential equations for the physical phenomena.

5.2.3.1 Direct Approach

The direct approach originates from the direct stiffness method used for structural analysis. It applies physical concepts (e.g. force equilibrium, energy conservation, mass conservation, etc.) directly to discretized elements and, it does not need elaborate sophisticated mathematical concepts. Its applicability is limited to certain problems for which equilibrium or a conservation law can be easily stated in terms of physical quantities. Unfortunately difficulties arise when dealing with complex elements like triangular elements. For complex problems the variational approach can be considered.

5.2.3.2 Variational Approach (Rayleigh-Ritz Method)

The variational approach relies on the calculus of variations and involves finding the extremum of an integral involving a function and its derivatives (a functional). In this technique a variational principal valid over the whole domain of the problem is postulated and an integral I is defined in terms of the unknown parameters and their derivatives. The basic problem in variational calculus is to find the function $\varphi(x)$ that makes the integral stationary.

$$I = \int_{x_1}^{x_2} F(x, \varphi, \varphi_x, \varphi_{xx}).\,dx \qquad (5-1)$$

φ_x and φ_{xx} are $\frac{d\varphi}{dx}$ and $\frac{d^2\varphi}{dx^2}$ respectively. Although most physical and engineering problems can be formulated in variational format, it is not possible in all cases.

5.2.3.3 Weighted Residual Approach (Galerkin Method)

The weighted residual approach applies FEM to problems for which a functional cannot be constructed. The method of weighted residuals involves the approximation of the functional behavior of the dependent variable in the governing differential equation. When substituted into the governing differential equation, the approximate form of the dependent variable leads to an error called the residual. The goal is to eliminate or minimize this error over the whole domain. A weight function and a trial function are chosen. If both of these functions are the same, the method of weighted residuals is referred to as Galerkin's method. Otherwise, it gives the Rayleigh-Ritz formulation. The method of weighted residuals is widely used to derive element properties for nonstructural applications such as heat transfer and fluid mechanics.

After applying any of these three methods the set of linear discretized equations is rewritten as a general matrix equation having the form

$$Ku = F \qquad (5-2)$$

in which K is the system stiffness matrix, u is the vector of unknowns, and F is the force vector.

5.2.4 Assembling the Element Properties to Obtain the Global Properties for the Entire Domain.

In the next step of using FEM all the element properties are assembled to find the properties of the overall system. The matrix equations for the system have the same form as the equations for individual elements except that they include all nodes. The assembly procedure is based on the value of the field variable at a node being the same for each element that shares that node.

5.2.5 Introducing the Boundary Conditions

Before the system equations are ready for solution they must be modified to account for the boundary conditions of the problem. Known nodal values of the dependent variables are imposed at this stage.

5.2.6 Solving the System Equations

The assembly process produces a set of equations that are to be solved simultaneously. They are solved to obtain the unknown nodal values in the domain. If the problem describes steady state, then a set of linear or nonlinear algebraic equations must be solved. In the case of a time dependant problem a set of linear or nonlinear ordinary differential equations must be solved.

5.3 COMSOL

There are several open source and commercial software packages that use the FEM for solving PDE or help in the pre/postprocessing of finite element models. Choosing from these packages involves a set of criteria, usually including: analysis flexibility, ease of use, efficiency, cost, technical support, training, and availability. COMSOL was chosen for this thesis.

Many new versions of COMSOL with improved capabilities and specific features have been released over the years, as it evolved from its origin as FEMLAB software. COMSOL models and solves scientific (physics, mathematics) problems and performs engineering simulations that are based on partial differential equations. It uses finite element methods to solve linear/nonlinear problems involving several phenomena. It can handle systems of first and second order PDEs in one, two, or three dimensions. It is especially suited for modeling coupled phenomena. COMSOL in general has two methodologies: using built-in mathematical functions via a graphical user interface and writing code via COMSOL Script.

5.3.1 COMSOL Graphical User Interface (GUI)

All of COMSOL's built-in functions can be used through its graphical user interface (GUI). Complex geometries in one, two, or three dimensions can be modeled. The GUI facilitates all stages of the modeling process including the determination of the system geometry, specification of both the physics and boundary conditions of the model, creation of the mesh, solving the problem, and postprocessing of the results.

In COMOSL, the modeling process and the control of the program settings start with the Model Navigator. Selection of the Application Mode for a new model, opening an existing model, or opening an entry into the Model Library can be done through the Model Navigator dialog box that is shown in Figure 5.4. The Application Modes, listed in Figure 5.4, supply models for performing studies in areas such as acoustics, diffusion, electromagnetic, fluid mechanics, heat transfer, structural mechanics, optimization and sensitivity analysis.

The coordinate system and space dimension of the model can be selected in the Model Navigator dialog box. For example, the 2D space dimension was chosen in Figure 5.4. In COMSOL the spatial coordinate system can be either Cartesian or cylindrical. Normally the variable names are x, y, and z for Cartesian coordinates and r, φ, and z for cylindrical coordinates. In COMSOL when a 1D, 2D, or 3D space dimension is selected for a model, the coordinates of the system are by default the Cartesian coordinates x, y, and z. In 1D axisymmetric (cylindrical) geometries the default coordinate is r, the radial direction, and the x axis represents r. In 2D axisymmetric geometries the x axis represents r, the radial direction, and the y axis represents z, the height coordinate.

After the Application Mode is chosen, there are five steps in setting up a model: describing the geometry of the problem, specifying the mathematical equations, creating the mesh, solving the problem, and postprocessing of the results.

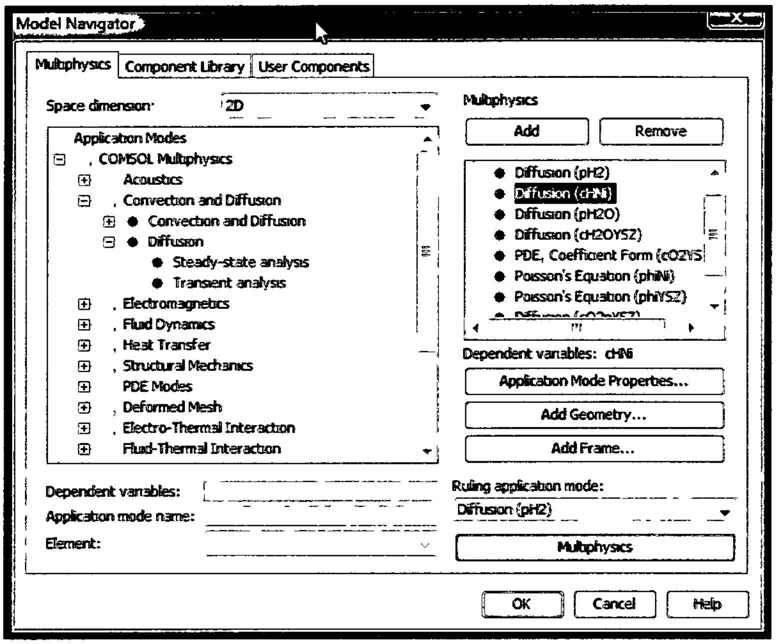

Space dimension: 2D

Dependent variables: cHNi

Ruling application mode: Diffusion (pH2)

Figure 5. 4 Model Navigator Dialog Box

In this model three types of equations were chosen. Diffusion was selected from the Convection and Diffusion Application Mode. The PDE Coefficient form and the Poisson's equation from PDE Modes were also used. All three of those terms can be seen in the window on the right-hand side of Figure 5.4.

5.3.1.1 Drawing

To create the geometry of the system in the GUI, the first step is to set up the axes. The Axes Settings dialog box for the particular model used in this work is shown in Figure 5.5. The appropriate Draw toolbar / Draw menu, 1D, 2D, or 3D can be selected in order to draw the desire geometry. In this work the x and y axis are -1.9×10^{-7}m < x axis <1.9×10^{-7} m and -1.2×10^{-7}m < y axis <1.2×10^{-7}m. The axis has equal steps of 0.5×10^{-7}(m). The 2D Draw toolbar / Draw menu was used.

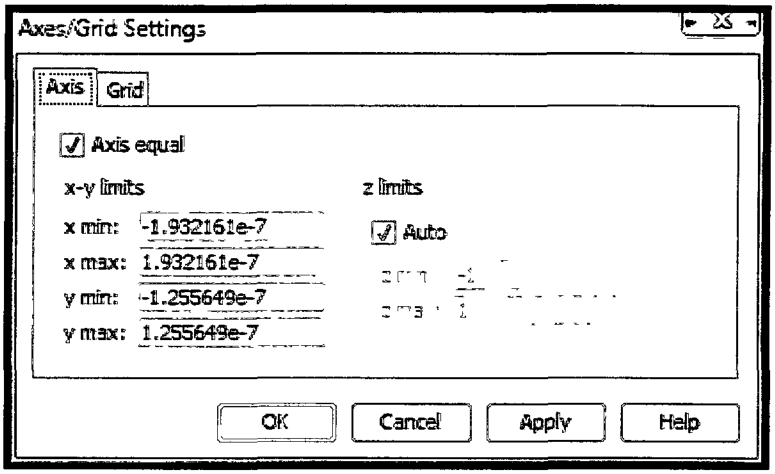

☑ Axis equal

x-y limits

x min: -1.932161e-7
x max: 1.932161e-7
y min: -1.255649e-7
y max: 1.255649e-7

z limits

☑ Auto

Figure 5. 5 The 2D Axes/Grid Settings Dialog Box

The GUI in Figure 5.6 is a schematic diagram of the geometry of the system being modeled in this work. The circle containing the three regions (subdomains) is the domain of the problem. Each of the regions will be referred to as a subdomain. The circle consists of five points and seven curves. One point is at the origin or center of the domain. Another point defines the radius of the circle. The other three points define the three straight lines. Four of the curves are arcs in the circle that forms the external boundary of the domain. The other three curves are the straight lines that are seen in the interior of the domain.

5.3.1.2 Specifying Mathematical Equations

Defining the chemical and physical phenomena within the geometry and at the boundaries of the domain for the problem is done in this step. It consists of three procedures: Subdomain Setting, Boundary Setting, and Constant Setting. The three procedures will be discussed in the following sections.

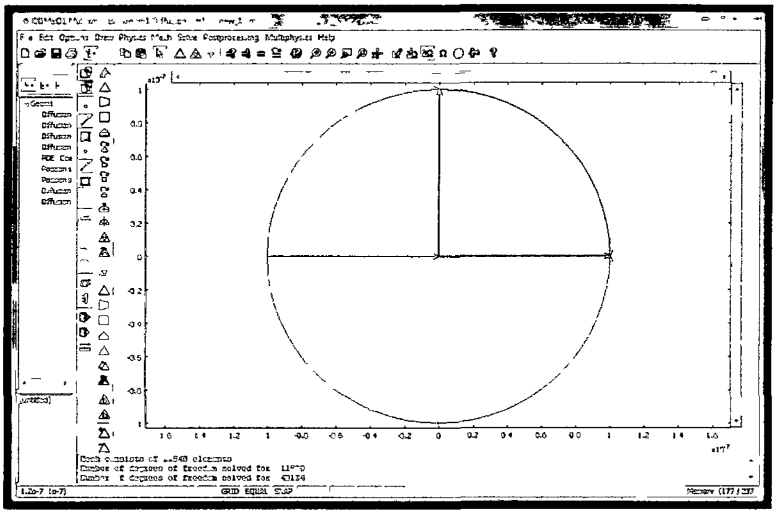

Figure 5. 6 A Schematic Diagram of the COMSOL Workspace and the Geometry of the system in the GUI

5.3.1.2.1 Subdomain Settings and Material Properties

The mathematical equations that describe the phenomena in each subdomain are entered in separate dialog boxes. An appropriate dialog box for each specific type of equation exists. This dialog box is accessible by choosing Subdomain Settings from the Physics menu, or by double-clicking a subdomain in Subdomain Mode. A Subdomain Setting dialog box has been shown in Figure 5.7. In Subdomain Setting dialog boxes, constants, coefficients and expressions of every PDE assigned to the subdomain are entered. In this dialog box the diffusion coefficient was given the symbol DHNi, which is the diffusion coefficient of hydrogen atoms in the Ω_{Ni}. The rate of reaction for this particular case, conversion of hydrogen atoms inside the Ω_{Ni}, was set equal to zero.

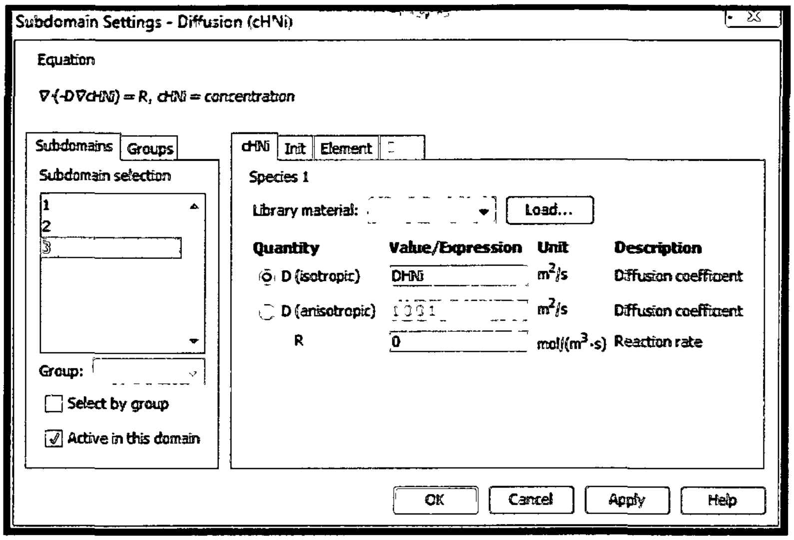

Subdomain Settings - Diffusion (cHNi)

Equation

$\nabla\cdot(-D\nabla cHNi) = R$, cHNi = concentration

Subdomain selection: 1, 2, 3

Species 1

Quantity	Value/Expression	Unit	Description
● D (isotropic)	DHNi	m^2/s	Diffusion coefficient
○ D (anisotropic)	1 0 0 1	m^2/s	Diffusion coefficient
R	0	$mol/(m^3\cdot s)$	Reaction rate

☐ Select by group

☑ Active in this domain

Figure 5. 7 Subdomain Settings Dialog Box in COMSOL

The Diffusion equation, Figure 5.7, has a general form of $\nabla. (D\ \nabla\ C) = R$ in COMSOL, in which C is the concentration, D is the diffusion coefficient, and R is a reaction rate. The PDE Coefficient form has the general formulation of $\nabla.(-D\nabla C + \alpha C - \gamma) + \beta.\nabla C + \alpha u = f$ *in* which $-D\nabla C$ is the diffusion term, αC is the convection term, and γ is the source term for flux. $\beta.\nabla C$ represents convection, αC represents absorption, and f represents a source term. The Poisson's equation has the general form of $-\nabla.(c\nabla u) = f$ in COMSOL.

5.3.1.2.2 Boundary Settings

Boundary conditions define the interface between the model domain and its surroundings. Interface conditions on interior and exterior boundaries in a model are to be specified. An exterior boundary is an outer boundary of the modeling domain, and a interior boundary is a dividing interface between two subdomains in the modeling domain. Neuman and Dirichlet are two basics boundary conditions. A Neuman boundary condition is used to specify the flux conditions (derivatives) on the boundaries while a Dirichlet boundary condition specifies the value of a variable on the boundaries.

Setting up boundary conditions is performed by inserting boundary values in the Boundary Settings dialog box, Figure 5.8. The Boundary Settings dialog box provides the appropriate boundary conditions for each application mode that is chosen. For the Diffusion Application Mode for instance, there are several possibilities: constant concentration $c = c_\circ$, flux boundary condition $-n \cdot (-D\nabla C) = N_\circ + k_b(C_b - C)$, insulation/symmetry condition $-n \cdot (-D\nabla C) = 0$, flux discontinouity $-n \cdot (N_1 - N_2) = N_\circ$ and thin boundary layer $-n_1 \cdot (-D\nabla C)_1 = \frac{D}{d}(C_1 - C_2)$.

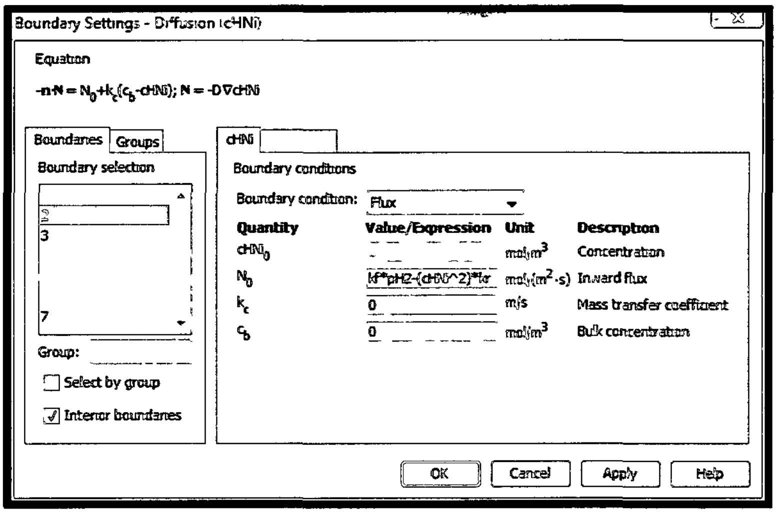
Boundary Settings - Diffusion (cHNi)

Equation

$-n \cdot N = N_0 + k_c(c_b - cHNi);\ N = -D\nabla cHNi$

Boundary condition: Flux

Quantity	Value/Expression	Unit	Description
$cHNi_0$		mol/m^3	Concentration
N_0	kf*pH2-(cHNi^2)*kr	$mol/(m^2 \cdot s)$	Inward flux
k_c	0	m/s	Mass transfer coefficient
c_b	0	mol/m^3	Bulk concentration

☐ Select by group

☑ Interior boundaries

Figure 5. 8 Boundary Settings Dialog Box COMSOL

5.3.1.2.3 Defining Constants

Defining constants and variables is required for model specification and postprocessing. This is done using the appropriate commands on the options menu of main toolbar in the GUI. In the Constant dialog box, the name of the constant, its expression, value and units are specified. The constant may contain any mathematical function or it may have a single value. The function defining the value of the constant is entered in the Expression edit field.

5.3.1.3 Meshing the Geometry

Meshing the domain is performed by using either (a) the built-in COMSOL mesh generator algorithms, or (b) the customized mesh feature. Irregular and arbitrary meshes are generated. In general meshes can be specified by making selections in the mesh menu of the COMSOL user interface.

For a 2D geometry either a Free Mesh generator or a Mapped Mesh generator can be used in order to create the mesh. A Free Mesh consists of triangular elements, while a Mapped Mesh consists of quadrilateral elements. A Mapped Mesh generator can be used for a geometry that is regular in shape and does not contain holes. A Free Mesh generator, on the other hand, can be used on all types of geometrical objects. It creates unstructured meshes that have no restrictions in terms of element distributions.

Either a Free Mesh containing tetrahedral elements or a Swept Mesh containing prism elements can be used for a 3D geometry. A 3D mesh can also be created by extruding or revolving a 2D mesh. An extruded or revolved mesh is structured in the direction of the extrusion or revolution. 3D meshing is outside the scope of this thesis.

5.3.1.3.1 Mesh Element Type

There are three types of elements in COMSOL terminology. The elements, constructed on the boundaries are called boundary elements. The elements constructed on the points of every domain are called vertex elements and there is also a subdomain element that is constructed inside each subdomain.

Based on a different categorization, an element could be either triangular or quadrilateral. Triangular and quadrilateral elements are two element types that are used in 2D meshing. A triangular element is a 2D mesh element with three corners and three edges. A quadrilateral element, on the other hand, is a 2D mesh element with four corners and four edges.

5.3.1.3.2 Refining Mesh

When trying to solve a problem that does not converge, or having solved a problem where the solution does not seem properly resolved, there is often a need for re-solving the problem using a finer mesh. It is only possible to refine free meshes containing triangular elements in 2D, or tetrahedral elements, in 3D, respectively. In 2D and 3D, however, two refinement methods are available: regular and longest. The regular refinement method divides each element into four triangular elements of the same shape in 2D, or eight tetrahedral elements of the same shape in 3D. The longest refinement method bisects the longest edge of each element. Figure 5.9 shows a refined mesh of the initial meshed (Figure 5.3) model geometry.

For the 2D model in this thesis a set of solutions was obtained from repeating the calculation on a series of meshes successively refined from 740 elements to 11840 elements that corresponds to an increase in degrees of freedom from 6225 to 95625. An Adaptive mesh refinement Solver was used in order to achieve the best result. The Adaptive mesh refinement Solver created 82957 elements and 637798 degrees of freedom.

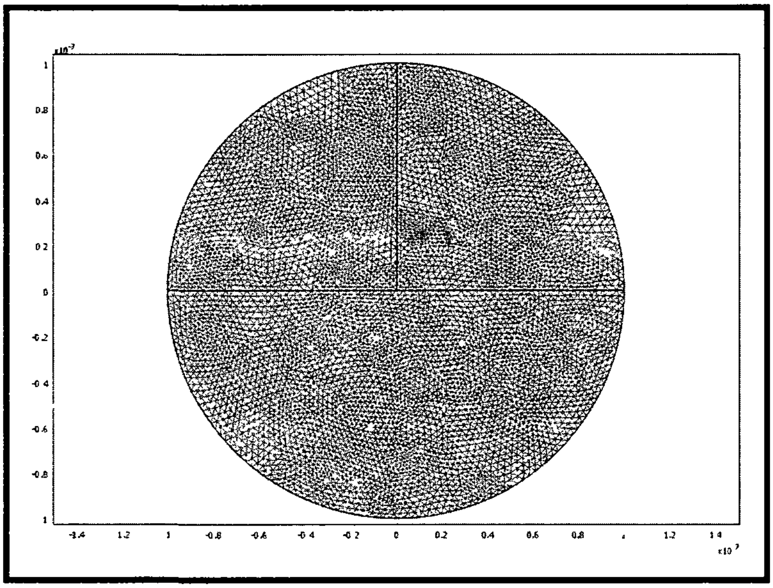

Figure 5. 9 Schematics of A Refined Meshed Domain

5.3.1.3.3 Model Mesh Properties

The mesh parameters for the Free Mesh generator can be specified by using the Mesh menu and choosing Free Mesh Parameters, Figure 5.10. The Free Mesh parameters dialog box will open. The local mesh element sizes, elements distribution, etc. are specified in this dialog box.

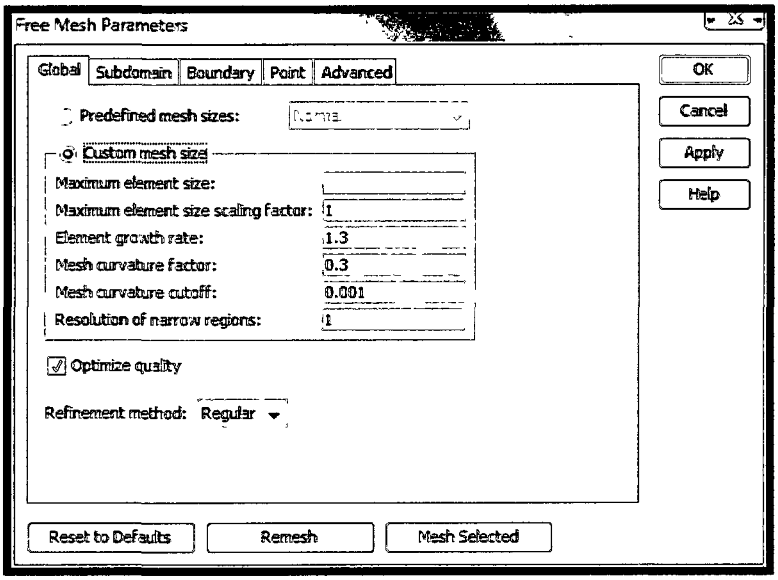

○ Predefined mesh sizes: Normal

● Custom mesh size

Maximum element size:

Maximum element size scaling factor: 1

Element growth rate: 1.3

Mesh curvature factor: 0.3

Mesh curvature cutoff: 0.001

Resolution of narrow regions: 1

☑ Optimize quality

Refinement method: Regular

Figure 5. 10 Free Mesh Parameters Dialog Box

There are several quantities to be specified in Figure 5.10. The value in the “maximum element size” edit field has a default value of 1/10 of the maximum distance in the domain. The “maximum element size scaling factor” is important when an explicit maximum element size is not specified. In that case the mesh generator multiplies the default maximum element size by this factor. Its default value is 1. The “element growth rate” determines the maximum rate at which the element size can grow from a region with small elements to a region with larger elements. The value must be greater or equal to one. The default value is 1.5, meaning that the element size can grow by approximately 50% from one element to another.

The value in the "mesh curvature factor" edit field determines the size of boundary elements compared to the curvature of the geometric boundary. The curvature radius of the boundary multiplied by the curvature factor, which must be a positive scalar, gives the maximum allowed element size along the boundary. A lower value gives a finer mesh along curved boundaries. The number of layers of elements that need to be created in narrow regions is set in "resolution of narrow regions".

The parameter in the "mesh curvature cutoff" edit field prevents the generation of many elements around small curved parts of the geometry. This parameter must be a positive value, and it has a default value of 0.03. The smallest radius of curvature that the mesh generator will use is the product of the mesh curvature cutoff value times the maximum distance in the domain. (eg. the diameter of the circle in our case).

The "optimize quality" check box requires the mesh generator to carry out mesh quality optimization at the end of the meshing process. From the "refinement method" list the regular or longest refinement method is selected for the mesh generator to use when refining the mesh. The model mesh properties will be discussed in more detail in the section on mesh independent solutions.

5.3.1.4 Solving the Model

COMSOL includes a number of different solvers for PDE-based problems. Examples are the stationary and time dependent solvers, Figure 5.11. COMSOL automatically detects nonlinearity, so normally there is no need to decide whether to use a linear or a nonlinear solver. The automatic detection works through analysis of the variables contributing to the Jacobian matrix. If the algorithm finds that both these matrices are complete and do not depend on the solution, the stationary solver and the parametric solver use the linear solver. Otherwise, they use the nonlinear solver.

COMSOL has a default solving selection. The settings in the Solver Parameters dialog box that is accessible through the Solver menu can be changed. As can be seen in Figure 5.11, the Solver Parameters dialog box consists of general, stationary, adaptive, optimized and advanced sections. Whether working on a stationary or a time-dependent model, the major task for the solver is solving one or several systems of linear equations. The type of linear solver is specified in the general section of the model Solver Parameters dialog box. The Linear system solver consists of direct and iterative solvers. The direct solver uses Gaussian elimination to solve a system of linear equations. For example direct (UMFPACK) is a highly efficient direct solver for nonsymmetrical systems that require large amounts of memory. Iterative solvers, however, are suitable for systems with a large number of degrees of freedom. Their solutions are less stable than those obtained from direct solvers.

On the left hand side of the Solver Parameters dialog box the analysis type (stationary, time dependent, etc) can be specified. For example, for stationary analysis, nonlinear solver settings (relative tolerance and maximum number of iterations) can be specified. Checking the adaptive mesh refinement box in Figure 5.11 will cause the Adaptive mesh refinement solver to be used. The Adaptive mesh refinement solver identifies the regions that require a high mesh density and automatically produces an appropriate mesh. It was mentioned in Section 5.3.1.3.2.

For this work a direct (UMFPACK) linear solver and a damped Newton nonlinear solver were chosen. The relative tolerance and maximum number of iterations are 10^{-12}, and 25 respectively. Relative tolerance is the error set by the user. The nonlinear-solver iterations stop when the relative error is less than the relative tolerance. The value of the maximum number of iterations limits the number of nonlinear iterations.

COMSOL uses second-order Lagrange elements as the default element type for most application modes. These and other higher-order elements add additional degrees of freedom on the interior nodes in the mesh elements. These added degrees of freedom provide a more accurate solution but also require more memory due to the reduced sparsity of the discretized system.

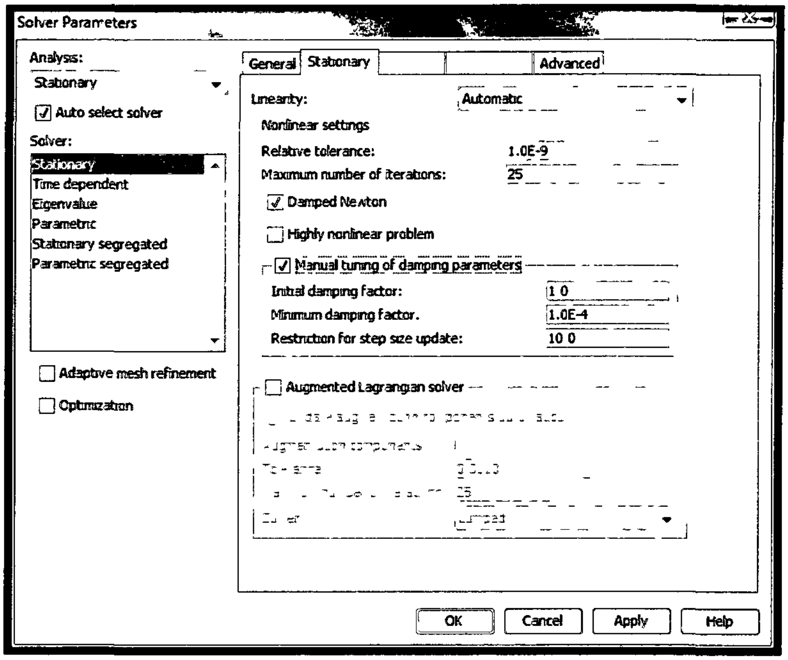

Analysis: Stationary

☑ Auto select solver

Linearity: Automatic

Relative tolerance: 1.0E-9

Maximum number of iterations: 25

☑ Damped Newton

☐ Highly nonlinear problem

☑ Manual tuning of damping parameters

Initial damping factor: 1 0

Minimum damping factor. 1.0E-4

Restriction for step size update: 10 0

☐ Augmented Lagrangian solver

☐ Adaptive mesh refinement

☐ Optimization

Figure 5. 11 Solver Parameter Dialog Box

5.3.1.5 Postprocessing the Solution

Postprocessing the solution refers to visualizing any variable or expression of variables. Selections made from the various plot parameters, that are available in the Cross-section Plot Parameters and Domain Plot Parameters dialog boxes (Figure 5-12) determine the outputs from post-processing. The surface plot is the default and standard plot in 2D. Standard plots in 2D visualize the colored solution as part of the domain. 2D Standard Plots contains Surface, Counter, Boundary, Arrow and Streamline plots.

The window of 2D Domain Plot Parameters, Fig 15.12, shows a quantity on one or several subdomains, boundaries or geometric edges for a constant point in time. A quantity can have a specific value within its permitted parameter range. The 2D line/extrusion cross-section plot visualizes a quantity (eg. a field variable) as a function of location in a 2D subdomain, for a constant point in time.

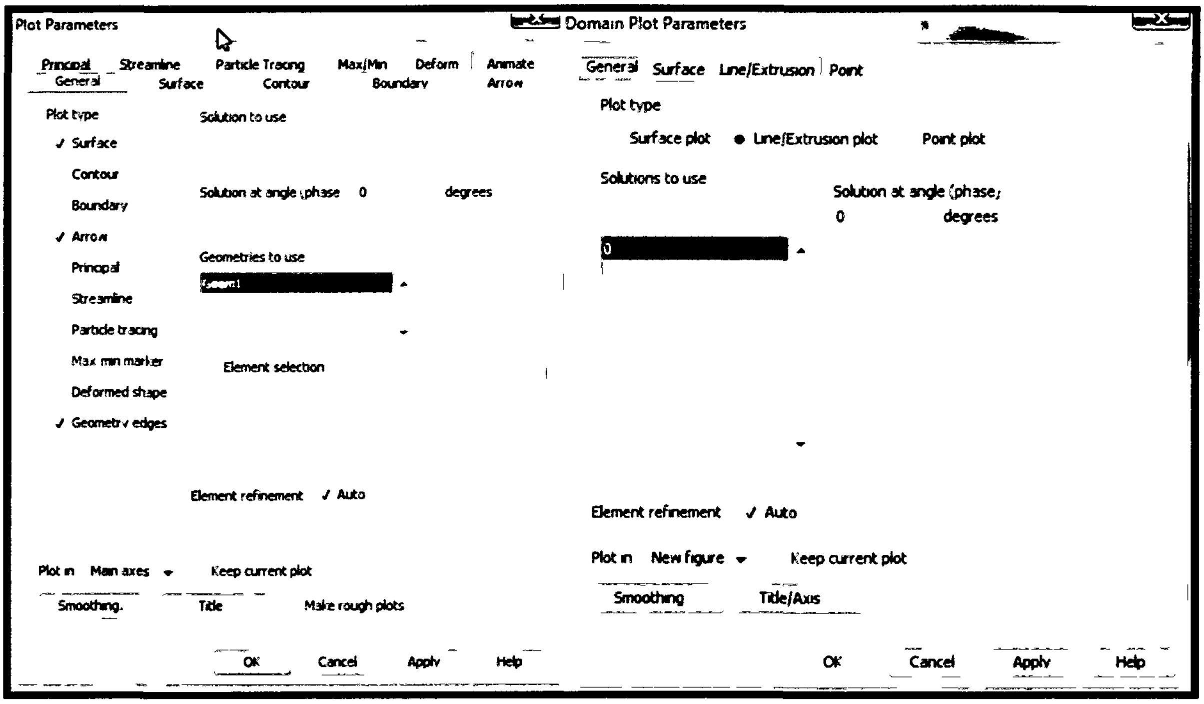

Plot type: ✓ Surface, Contour, Boundary, ✓ Arrow, Principal, Streamline, Particle tracing, Max min marker, Deformed shape, ✓ Geometry edges

Solution at angle (phase) 0 degrees

Geometries to use: Geom1

Element refinement ✓ Auto

Plot in Main axes ▾ Keep current plot

● Line/Extrusion plot

Solution at angle (phase) 0 degrees

Solutions to use: 0

Element refinement ✓ Auto

Plot in New figure ▾ Keep current plot

Figure 5 12 Cross-Section Plot Parameters and Domain Plot Parameters

5.3.2 COMSOL (Script) as a Programming Language

In addition to a graphical user interface, COMSOL also offers an interface to MATLAB for a large variety of programming possibilities through COMSOL Script. COMSOL Script is a numerical computing and programming language using the same syntax as MATLAB. COMSOL Script allows the user to write user defined functions that may be needed for special simulation models. It is also possible to add a computer aided design package (CAD) to COMSOL.

5.4 Finite Element Method as Used in COMSOL

The types of calculations used in the FEM are described below. Constraints on a variable can be stated in either strong form or weak form. The strong form is the partial differential equation system and the appropriate boundary conditions. The following equation with a proper boundary condition is an example of a strong form of the constraints on the variable "u". In solving Equation $(5-3)$ in a domain called Ω for a single variable u

$$\nabla . \mathrm{N}(\mathrm{u}) = \mathrm{F}(\mathrm{u}) \qquad (5-3)$$

A weak form could be used instead. The weak form places a weaker restriction on the functions that could satisfy the constraints. Instead of the partial differential equation, the weak form is stated in integral form.

The first step for the weak formulation is to assume a trial function U and a test function v. The trial function, U, is a solution to the PDE Equation$(5-3)$. v is any arbitrary function defined on the same domain, Ω, where u and U are defined. So by substituting U into Equation$(5-3)$, the residual R is obtained:

$$\mathrm{R} = |\nabla . \mathrm{N}(\mathrm{U}) - \mathrm{F}(\mathrm{U})| \qquad (5-4)$$

The objective is the minimization of this residual. In the next step Equation $(5-4)$ is multiplied by the test function v, and integrated over the domain:

$$\mathrm{R}(\mathrm{x}) = \int_{\Omega} (\nabla . \mathrm{N}(\mathrm{U})\mathrm{v} - \mathrm{F}(\mathrm{U})\mathrm{v})\mathrm{dx} \qquad (5-5)$$

By applying the divergence theorem (Gauss's theorem) on the right hand side of Equation(5 − 5), the equation is simplified:

$$R = \int_{\partial\Omega} vN.\,n dS - \int_{\Omega} \nabla v.\,N(U)dx - \int_{\Omega} vF(U)\ dx \qquad (5-6)$$

Forming the same surface integral on the boundary of two adjacent elements produces the same boundary integral (first term on the right hand side of Equation 5-6) at their interface, except that the direction of integration is opposite in the two finite elements. If the integrals are added together to form the total integral, the shared boundary integrals cancel. When the PDE is constrained by Neumann boundary conditions, the finite element boundary term on $(5-6)$ vanishes. This is one of the reasons that FEM have Neumann natural boundary conditions.

Now U and v are decomposed to a series of interpolation functions. The element interpolation function φ is expressed within the element through the use of its nodal values in the form of

$$\varphi = \sum_i N_i \varphi_i \qquad (5-7)$$

where the sum is taken over all of the nodes, i. N_i is the shape function of node i and φ_i is the nodal value, and i is the element nodal numbering. Shape functions are a subset of element interpolation functions φ. The shape functions are associated with a node and must have a value of unity at one node and a zero value at all other nodes.

$$\sum_i N_i = 1 \qquad (5-8)$$

In Galerkin's method:

$$U = v = \varphi \qquad (5-9)$$

After substituting an appropriate interpolation function φ in equation$(5-6)$, R will be minimized by taking its derivative respect to each of the N_i, and setting each derivative equal to zero. After this step, the N algebraic equations that have to be solved simultaneously have been produced. These equations can be rewritten in matrix form. The result consists of a Jacobian matrix (stiffness matrix). The linear Jacobian equation should find an improved approximate solution U, and this procedure can be iterated until a solution is found to acceptable accuracy.

Usually in addition to the PDE constraint, there are some boundary conditions that need to be satisfied. Since not all the test and trial functions contribute to the boundary conditions, the number of boundary condition equations is less than the original equations. By writing the boundary integrals for each function, an equation for the boundary constraints can be achieved. The appropriate lines of the Jacobian matrix (the stiffness matrix) equation are replaced by direct constraints on the unknowns u so that the order of the stiffness matrix is preserved. COMSOL has a unique way in dealing with boundary condition problems. It usually uses Lagrange multipliers in order to solve the PDE equation and its boundary conditions. The Lagrange multipliers method is a well-known method for dealing with equality constraints in optimization problems. It provides a strategy for finding the maxima and minima of a function subject to constraints.

For the 2D steady-state simulations a stationary nonlinear solver and a direct (UMFPACK) solver, using Gaussian elimination in COMSOL package were employed with a tolerance error of less than10^{-12}. Relative tolerance is the error set by the user. At the end an adaptive mesh refinement solver was used to optimize the solution. The algorithm of these solvers will be discussed in the following section.

5.5 Solution Procedure

As shown in Figure 5.3 the domain was divided into small triangular elements (mesh). The physics of one element was approximately described by degrees of freedom (DOF). Each element was assigned a set of characteristic equations describing physical properties, boundary conditions, with an imposed force function, which were then solved as a set of simultaneous equations to predict the object behavior at that node. In solving Equation $(5-3)$ $U_\circ$ was the initial guess. The solver formed the initial solutions using these guessed values. It solves the discretized form of the linearized model with the following Newton method, using a Newton step δU.

$$J(U_\circ)\delta U + J'(U_\circ)^T\Lambda = -R \qquad (5-10)$$

A Newton step is the difference in the position variable from the previous trial function (guess),U_N to the next trial function,U_{N+1}. $J(U_\circ)$ is the Jacobian matrix, which is the matrix of all first-order partial derivatives of the residual function, and $R\,(U_\circ)$, represents discretized residual equation. $J'(U_\circ)^T$ is the transpose of boundary condition equation Jacobean matrix. Λ is the matrix of Lagrange multipliers. In the next step the software computed the updated iteration with a new set of solutions $U_1 = U_\circ + \lambda\delta U$, where λ is the damping factor and its value is between zero and one. The error, E, was estimated by solving $J(U_\circ)E = -R\,(U_1)$. If the relative error, corresponding to E, were larger than the relative error of the previous step, the solver would reduce the damping factor and recalculate U_1. This procedure was repeated until the relative error reached a value less than the previous iteration. The solver then proceeded to the next Newton iteration.

Newton iteration is iteration within the Newton method. A damped Newton method was used for solving the non-linear equation. In a damped Newton method the software kept recalculating the problem to reach a damping factor value of $\lambda = 1$ for the assigned error.

Therefore even if the calculated error was less than the desired error, the damping factor should be equal to 1 in order to stop the calculation process.

5.5.1 Mesh Density Independent Solution

It is important to select a mesh that minimizes the errors. Adaptive mesh refinement (see Figure 5.11) was used for this model to obtain optimized mesh density and distribution. It identifies the regions requiring a high resolution and then produces an appropriate mesh for those regions

The adaptive mesh refinement solver performs the following steps in an iterative algorithm:

1. Solves the problem on the existing mesh using the stationary solver.
2. Evaluates the residual of the PDE on all mesh elements.
3. Estimates the error in the solution on all mesh elements.
4. Terminates execution if it has made the requested number of refinements or if it has exceeded the maximum number of elements.
5. Refines a subset of the elements based on the sizes of the local error.
6. Repeats the procedure from Step 1 until the appropriate convergence is obtained.

In order to use the Adaptive mesh refinement, an initial mesh distribution was specified. The error was minimized by refining a fraction of those elements with the largest error, in such a way that the total number of elements increased roughly by 70% or 1.7. The model was solved first for a refined mesh and then the adaptive mesh refinement solver was used to achieve the best mesh distribution and density. The result of using adaptive mesh refinement solver is shown in Figure 5.13.

All mesh properties used in this model for both cases are shown in Table.1.

Parameter	(a)Value (Refined Mesh)	(b)Value (Adaptive Mesh)
Number of degrees of freedom	95625	637798
Number of mesh points	6017	41720
Number of mesh elements	11840	82957
Number of Triangular elements	11840	82957
Number of quadrilateral	0	0
Number of boundary elements	288	1124
Number of vertex elements	5	5
Minimum element quality	0.7104	0.6091
Element area ratio	0.1649	2.71e-6

Table 5. 1 The Mesh Properties for a) Refined Mesh and b) Adaptive Mesh

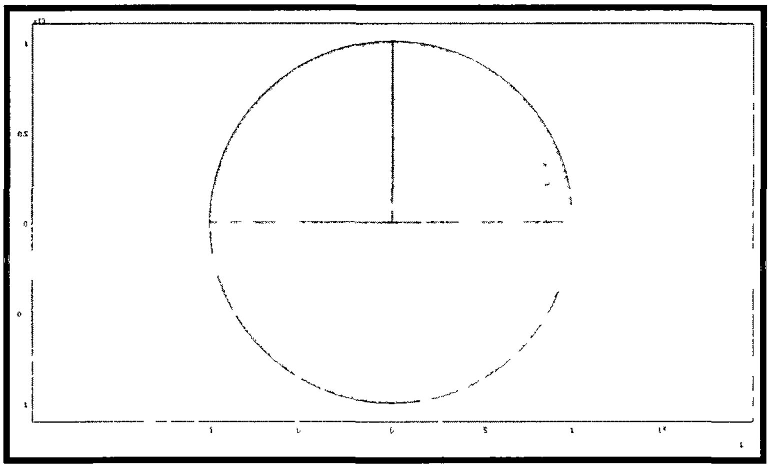

Figure 5. 13 Adaptive Mesh

One property of the mesh is the minimum element quality. For triangular elements, COMSOL computes the mesh quality q as:

$$q = {}^{6.8\,A}\!\Big/\!\left(h_1{}^2 + h_2{}^2 + h_3{}^2\right) \qquad (5-11)$$

where A is the area, and h_1, h_2, and h_3 are the side lengths of the triangle. The value of q is a number between 0 and 1. If $q > 0.3$, the mesh quality should not affect the solution's quality. So the minimum value of q is one of the mesh properties and it is shown in the Table 5.1. The other measure of quality, reported by COMSOL, is the element area ratio. The Element area ratio is defined as the minimal element area divided by the maximal element area.

Refining the mesh density stopped when a further increase in the mesh density had a minor effect on the final results. For instance the calculated value for the integral of flux only changed by 0.01% when the mesh density increased from 11840 to 82957. Therefore the last calculation performed had a mesh density of 82957.

5.6 Validation

5.6.1 Computational Validation: Verifying Model Convergence and Accuracy

It is important that the solution obtained by the finite element method accurately captures local variations in the phenomena. In some cases the results can be compared to values from handbooks, analytical solutions, literature values, or other similar modeling results. If a model has not been verified by other means, a convergence test is useful for determining if the mesh density is appropriate. The mesh can be refined and the analysis can be run again. If the solution is converging to a stable value, as the mesh is refined, the accuracy of the model is satisfied. Otherwise the solution is mesh dependent, and the model requires a finer mesh. In this case an adaptive mesh refinement can be used, as described in the previous section.

One goal in numerical modeling is to eliminate or minimize the error over the whole domain. For this work a direct (UMFPACK) linear solver and a damped Newton nonlinear solver were chosen. The relative tolerance and maximum number of iterations are 10^{-12}, and 25 respectively. The nonlinear-solver iterations stop when the relative error is less than the relative tolerance. The value of the maximum number of iterations limits the number of nonlinear iterations. In the nonlinear solver the nonlinear iterations stop when the relative tolerance exceeds the relative error computed as the weighted Euclidean norm:

$$\mathrm{err} = \left(\frac{1}{N}\sum_i (|E_i|/W_i)^2\right)^{0.5} \qquad (5-12)$$

here N is the number of degrees of freedom and E_i is the estimated error of the current approximation to the true solution vector. W_i is the weight factor, and is defined as:

$$W_i = \max(|U_i|, S_i) \qquad (5-13)$$

in which S_i is the scale factor that the solver determines on the basis of the type of scaling option selected. For Automatic Scaling that was chosen for this study, S_i was the average of $|U_j|$ for all DOFs j having the same name as DOF i times 0.1.

When modeling, it is important to select a mesh that minimizes the errors in the quantities of interest. COMSOL provides several ways to set the mesh size manually. However, it is not easy to minimize the error in a desired quantity by manually specifying a mesh. In many applications, the algorithm must resolve the solution in great detail only on small portions of the domain (such as boundary layers, shocks, small geometrical details, or localized loads). For such situations, adaptive mesh generation could be used. It identifies the regions that require a high resolution and produces an appropriate mesh. Adaptive mesh adds mesh elements based on an error criterion to resolve those areas where the error is large.

5.6.2 Physical Validation: The Mass Transport-Only Case

The main phenomenon that occurs in a fuel cell is the electrochemical reaction that is the combination of individual reaction mechanisms. If all reaction phenomena were eliminated from the model, diffusion and migration (mass transport) would be the only phenomena remaining. In this situation, the concentration of a species would be expected to be constant throughout a subdomain. This possibility was investigated by setting all the rate constants to a zero value. The values of concentrations obtained are discussed below.

The results of the mass transport-only case are presented in six different figures and Table 5.2. The field variables are the partial pressure of H_2 in the Ω_G, the concentration of hydrogen molecules in both the $\Omega_{Ni,}$ and Ω_{YSZ}, the concentration of O^{2-} ions in the $\Omega_{Ni,}$ and Ω_{YSZ}, and the electrical potential profile.

Species	Value
$H_2(g)$	$1.013 * 10^5$ (Pa)
H_2 (Ni)	$3.183 * 10^{-4}$(mol.m^{-3})
H_2 (YSZ)	0.101(mol.m^{-3})
O^{2-}(Ni)	0.044(mol.m^{-3})
O^{2-}(YSZ)	$5.311 * 10^4$(mol.m^{-3})
φ (Ni)	0 (V)
φ(YSZ)	0.4(V)

Table 5. 2 Values of Different Species in Different Bulk Phases

Some species that are formed when reactions occur do not exist when mass transfer is the only phenomena occurring. The partial pressure of hydrogen gas in the $\Omega_{G,}$ is constant. Atomic hydrogen would be the dominant hydrogen species in the $\Omega_{Ni,}$ if molecular hydrogen dissociation reaction to form atomic hydrogen radicals could occur. When no reactions occur, hydrogen molecules are the only hydrogen species in the system. Since no reaction is occurring, no protons (hydrogen ions) are formed. The dominant hydrogen containing species in the Ω_{YSZ}, is water. Since no reaction was allowed in the mass transfer-only case, no water was formed.

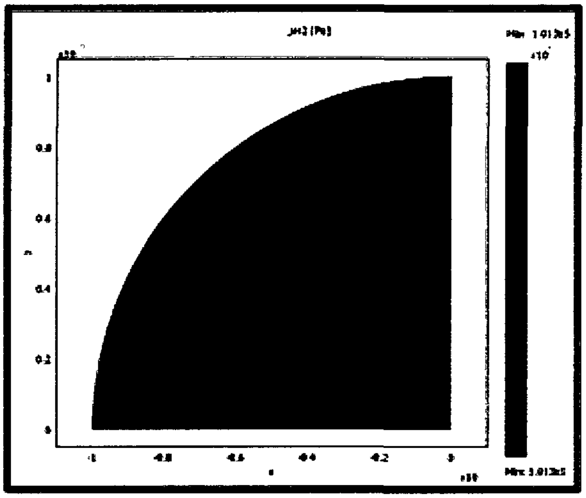

Figure 5. 14 Pressure Distribution of H_2 Molecules in the Ω_G for Diffusion Case

Diffusion of H_2 through the gas, Ni, and YSZ phases will occur in the mass transfer-only case. Therefore the hydrogen supplied from the gas channel will keep diffusing through the Ω_G, until the H_2 pressure is constant throughout the whole Ω_G domain. The H_2 partial pressure specified as a boundary condition on the external boundary of the Ω_G is the process variable that sets the steady-state H_2 pressure throughout the Ω_G. The uniform pressure of H_2 in the Ω_G, as can be seen in Figure 5.14, is due to the diffusion process being the only phenomenon assumed to occur in this case. The initial pressure of H_2 was set at 1.013×10^5 (Pa) at the outer arch of the Ω_G and it remained constant from the external domain boundary of the Ω_G to the origin, to the $\Gamma_{G/Ni}$, and to the $\Gamma_{YSZ/G}$.

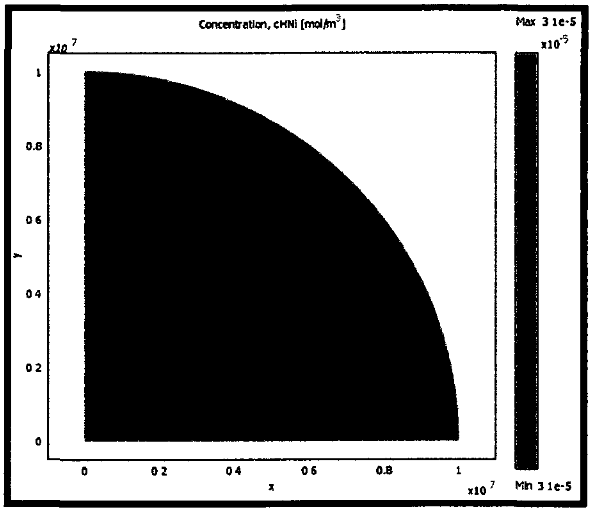

Figure5. 15 Concentration Profile of H_2 in Ω_{Ni} for Diffusion Case

If the model is functioning correctly, the H_2 concentration throughout the Ω_{Ni} should also be uniform. At the $\Gamma_{G/Ni}$, the hydrogen molecules on the gas side of the interface will be in equilibrium with the hydrogen molecules on the Ni side of the interface. The solubility was assumed to be proportional to the square root of hydrogen pressure (Sievert's law):

$$C_{H_2} = k_H \sqrt{P_{H_2}} \qquad (5-14)$$

The solubility of hydrogen in pure nickel and nickel-vanadium alloy was investigated by Ebisuzaki et al. in 1966. They obtained an empirical equation for calculating the solubility of hydrogen in pure nickel for a temperature range of 400°K -1000 °K:

$$S = (3.26 \pm 0.17) \times 10^{-3} \exp\,[-(3.60 \pm 0.06)\,\mathrm{kcal/RT}] \qquad (5-15)$$

in which S is a solubility of hydrogen in pure nickel in atoms/atom, fitted to an Arrhenius type expression. R and T are ideal gas constant and temperature respectively. Nickel –Vanadium alloy, however have a different solubility expression:

$$S = (1.11 \pm 0.05) \times 10^{-3} \exp\left[-(2.90 \pm 0.05)\,\mathrm{kcal/RT}\right] \qquad (5-16)$$

Our results are in reasonably good agreement with these equations. The hydrogen molecules on the Ni side of the interface will diffuse throughout the Ω_{Ni} until a uniform concentration of hydrogen molecules is achieved as shown in Figure 5.15. The value of the hydrogen concentration in the Ω_{Ni} was $3.1 * 10^{-5}$ (mol.m^{-3}).

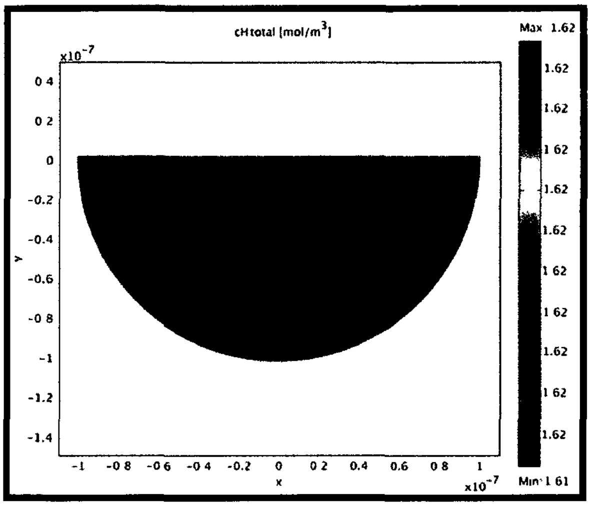

Figure5.16 Concentration Profile for H_2 molecules in the Ω_{YSZ} for Diffusion Case

It was reported in the literature that the hydrogen molecules are able to diffuse through Ω_{YSZ} (Nigara 2004, Wagner 1968). The pressure of gaseous hydrogen molecules on the gas phase side of the $\Gamma_{YSZ/G}$ will be in equilibrium with the concentration of hydrogen molecules on the YSZ side. In addition diffusion of molecular hydrogen from the $\Gamma_{YSZ/G}$ will continue until the molecular hydrogen concentration in the bulk Ω_{YSZ} is equivalent to that on the $\Gamma_{YSZ/G}$.

Therefore at a constant temperature of 1273 (K) the concentration of H_2 gas dissolved in the Ω_{YSZ} will be proportional to the pressure of the H_2 in the Ω_G. Its concentration will be constant through the whole domain, as shown in Figure 5.16. The maximum value of the H_2 in the Ω_{YSZ} was 1.62(mol.m^{-3}).

There are very few experimentally determined hydrogen solubility data in oxide ceramics. Wagner et al. have reported the hydrogen solubility of YSZ (Wagner 1962). (Sakai et al. 1999) also evaluated the hydrogen solubility in oxide ceramic and particularly in Ω_{YSZ}. They obtained the following equation for determination of hydrogen solubility in the Ω_{YSZ}.

$$\log C_H(\mathrm{atm/cm^{-3}}) = \log\left(I_D/I_H\right) + 20.66 \qquad (5-17)$$

In which $\log(I_D/I_H)$ is a secondary intensity ratio and is -2.66 for YSZ. Our value 1.1 (mol/m^{-3}), is approximately within order of magnitude agreement with their results. The comparison between COMSOL obtained value and literature values are shown in Table 5.3.

	Ni	YSZ
H_2 Solubility (Literature)	3.15×10^{-5} (mol.m^{-3})	1.66 (mol.m^{-3})
COMSOL Values	3.1×10^{-5} (mol.m^{-3})	1.62 (mol.m^{-3})

Table 5. 1 Comparison between the given data and COMSOL's Value

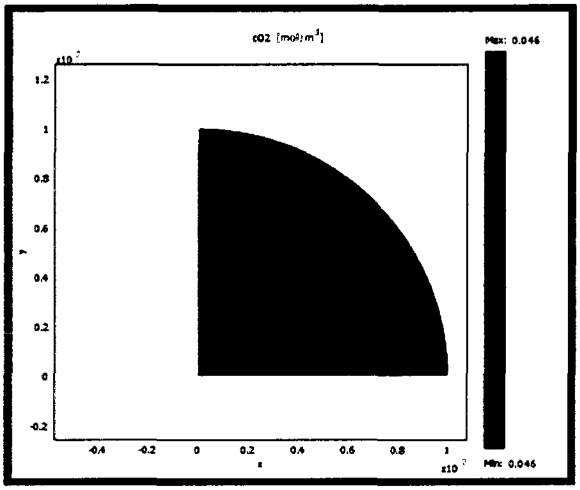

Figure 5. 17 O^{2-} Anions Distribution in the Ω_{Ni} for Diffusion Case

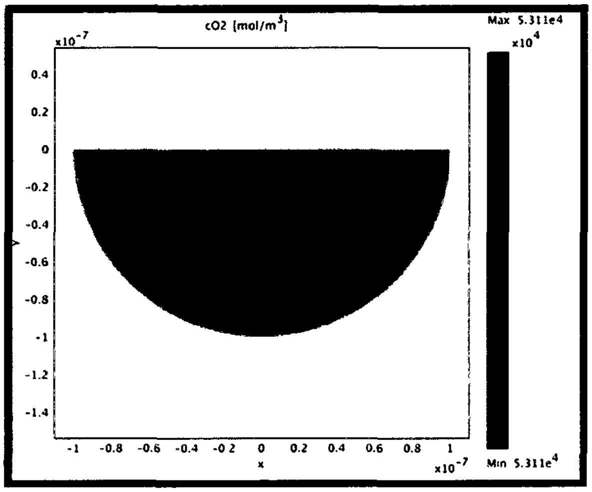

Figure 5. 18 O^{2-} Anions Distribution through the Ω_{YSZ} for Diffusion Case

The amount of O^{2-} anions presented in the Ω_{Ni} is highly dependent on the solubility constant value, for the O^{2-} inside the Ω_{Ni}. Solubility of oxygen in the Ω_{Ni} has been determined (Park 2007, Jackson 2008) at 1073 (K) at atmospheric pressure. The model allows oxygen anions to diffuse through the $\Gamma_{Ni/YSZ}$ to establish equilibrium in the absence of any reaction that consumes the anions. The large O^{2-} anions can diffuse through the Ω_{Ni} by converting Ni to NiO. In this case the distribution of O^{2-} anions is shown in Figure 5.17. The O^{2-} concentration in the Ω_{Ni} is 0.046 (mol.m^{-3}).

The O^{2-} concentration throughout the Ω_{YSZ} can be seen in Figure 5.18. The O^{2-} concentration at the external boundary of the Ω_{YSZ} was assigned a constant value of 5.311×10^4 (mol. m^{-3}). As with other species in other domains, the O^{2-} species will diffuse from the external boundary throughout the Ω_{YSZ} until equilibrium is attained. As can be seen in the figure the concentration is become constant throughout the Ω_{YSZ}. It is apparent that the concentration of O^{2-} in the Ω_{YSZ} is orders of magnitude greater than that in the Ω_{Ni}.

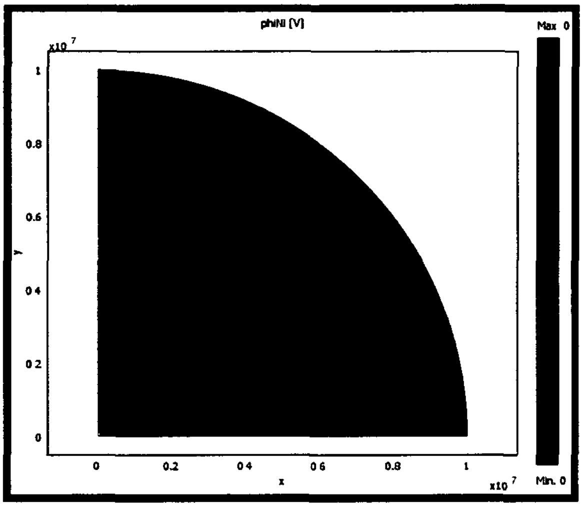

Figure 5. 19 Potential in Ω_{Ni}

The standard relationship between electrical potential and the reaction rate, that generates current, is used to find the potential distribution. Since there is no reaction in the Ω_{Ni} the current generation by reaction is zero and the Poisson type equation is reduced to:

$$\nabla.(\sigma_{Ni}\nabla\varphi) = R \quad R = 0 \qquad (5-18)$$

The electrical potential value is equal to its boundary condition value which was 0 (V). This value is equal to the equilibrium electrical potential throughout the Ω_{Ni}.

Similarly the electrical potential in the Ω_{YSZ} has a constant value of 0.4(V) throughout the domain. In the Ω_{YSZ} the Poisson type equation is reduced to

$$\nabla.(\sigma_{YSZ}\nabla\varphi) = 0 \qquad (5-19)$$

The electrical potential in the Ω_{YSZ} has the same value as the boundary condition throughout, and it is equal to 0.4 (V).

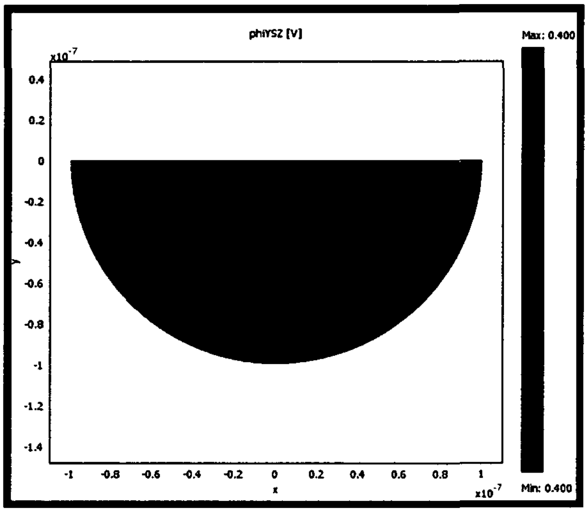

Figure 5. 20 Potential in the Ω_{YSZ}

5.7 Summary

A direct (UMFPACK) linear solver and a damped Newton nonlinear solver were chosen for solving the PDE equations and related boundary conditions of different species present in the vicinity of the anode TPB in a SOFC. The relative tolerance and maximum number of iterations were chosen to be 10^{-12}, and 25 respectively. The methodology and solution procedure used by the COMSOL package, as well as the applied FEM strategy behind COMSOL computation have been discussed.

The model was first solved by eliminating the impact of having any reaction between species. This provided a prediction from the mass transfer equations and their diffusion coefficients. The results show that, for the mass transfer-only case, with the system at steady state, the concentration of each species is uniform in each subdomain. The solution is stable throughout the whole domain. The concentration of different species remains constant throughout each of the subdomains. Since the effect of overpotential on the Ni and YSZ potential distribution was eliminated by setting the reaction term equal to zero, the electrical potential value is also constant in each subdomain.

In the mass-transport only case, no reaction occurs so that the equations do not contain any source or sink terms. At steady-state mass transport would be expected to continue to occur until all of the concentration gradients had been eliminated, and each variable had attained a constant value in each of the subdomains. The above computations show constant concentrations in each subdomain, exactly as was expected. Therefore the results from the model are consistent with the expectations for the mass-transport only case. The conclusion is that the mass-transfer only results have validated the model.

Bibliography

COMSOL Multiphysics. http://www.comsol.com/ (accessed Jun 2010).

Ebisuzaki, Y., WJ Kass, and M. Publication O'Keeffe. "Diffusion and Solubility of Hydrogen in Single Crystals of Nickel and Nickel—Vanadium Alloy." J. Chem. Phys. 46, 1967: 1378-1341.

Madenci, E., I, Guven. The Finite Element Method and Applications in Engineering Using Ansys®. New York: Springer.

Sakai, N , K. Yamaji , T. Horita , H. Yokokawa. "Determination of Hydrogen Solubility in Oxide Ceramics by Using SIMS Analyses." Journal of Power Sources 174 , 2007: 246-254.

Wagner, C. Berichite der Bunsen gesellschaft. "Die Löslichkeit von Wasserdampf in ZrO2-Y2O3-Mischkristallen." Berichte der Bunsengesellschaft für physikalische Chemie72 (7), 1962: 778 - 781.

Zimmerman, W. Process Modelling and Simulation with Finite Element Methods. World Scientific Publishing Company, 2004.

Chapter 6 Results and Discussion

In this thesis, it has been argued that accurate characterization of the TPB is important in understanding the various physical and electrochemical processes in fuel cells. In support of this argument and on the basis of the two dimensional, isothermal model of an anode TPB in a SOFC, using hydrogen as a fuel, a numerical solution based on both mass and charge transfer was developed in Chapter 4. As it is mentioned in Chapter 4 several elementary charge transfer reactions can be assumed to take place at the $\Gamma_{Ni/YSZ}$. Only one charge transfer reaction, the rate limiting step, has been investigated in this study. The only other chemical reaction included was the dissociative chemisorption of hydrogen at the gas-nickel interface. In those computations that include mass transport plus reaction at the TPB the charge transfer reaction was assumed to take place at $\Gamma_{Ni/YSZ}$.

The results of the computations are presented in this chapter. The simulation results for two different domain radii are illustrated in several figures in Section 6.1. The various processes causing the species distribution and the potential profile are explained in the discussion section of this chapter. A comparison between the model results and literature values is presented in Section 6.2.

6.1 Computational Results

6.1.1 Domain Radius = 0.1 (μm)

Results of mass transport plus surface reaction with a domain radius of 10^{-7} (m) are presented in this section. Initially H_2 molecules are in the gaseous phase. They dissociate to form hydrogen radicals at the gas-nickel surface. Then the hydrogen radicals diffuse through the Ω_{Ni} to arrive at the $\Gamma_{Ni/YSZ}$. There the hydrogen radicals react with O^{2-} ions that had migrated through the Ω_{YSZ} to form water molecules and electrons. The water molecules diffuse through the Ω_{YSZ}. Electrons are conducted through the Ω_{Ni}. Finally the water molecules exit the TPB domain through the gaseous phase.

Figure 6.1 shows that the movement of various hydrogen species through the entire domain would follow a circular path: H_2 molecules in the Ω_G, H radicals in the Ω_{Ni}, and H_2O molecules in the Ω_{YSZ}. In this figure the direction of movement of hydrogen containing species for the mass transport plus reaction case is clearly seen. The hydrogen molecules diffuse though the binary water vapour- hydrogen mixture in the Ω_G, and are dissociated to hydrogen radicals at the surface of the Ni catalyst. The hydrogen radicals then diffuse through the Ω_{Ni}. At the $\Gamma_{Ni/YSZ}$ they react with O^{2-} anions coming from Ω_{YSZ} to form water molecules. These water molecules then diffuse through the Ω_{YSZ} to reach the $\Gamma_{YSZ/G}$. At the $\Gamma_{YSZ/G}$ surface they enter the Ω_G, diffuse, and eventually leave the TPB domain at the external boundary of the Ω_G.

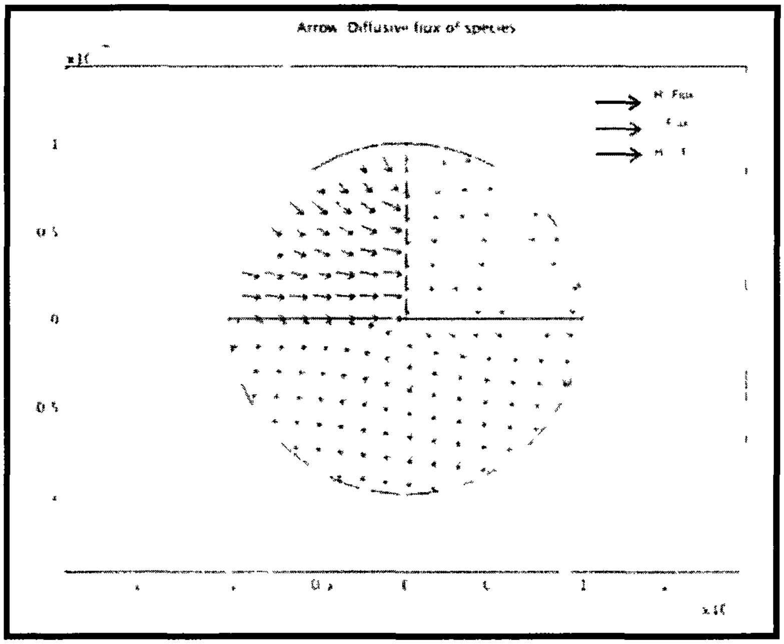

Figure6 1 Diffusive Flux Path of H_2, H Radicals and H_2O in the Entire Domain for a Domain Radius of 0 1 (μm)

The pressure distribution of H_2 in the gaseous phase for a domain radius of 0.1 (μm) is shown in Fig 6.2. Hydrogen diffuses through the binary mixture of H_2 and H_2O molecules in the Ω_G. It diffuses towards the Ni surface where it is consumed at the $\Gamma_{G/Ni}$. The vertical bar on the left hand side of Figure 6-2 represents the calculated pressure of H_2 in the gas phase. The horizontal axis shows the radial distance from the origin of the domain. The radius of the gas portion is 10^{-7} (m) in this case. The total pressure of the gas is 101.3 (kPa) at the $\Gamma_{Bulk/G}$. This includes hydrogen and water. Here the initial pressure of H_2 at bulk gas boundary is 99 (kPa). The water vapour partial pressure accounts for the remainder of the pressure. There is a small H_2 pressure gradient in the Ω_G because the reaction at the $\Gamma_{G/Ni}$ is consuming H_2 molecules. The maximum value of H_2 in the Ω_G is 9.9×10^4 (Pa) at $\Gamma_{G/Ni}$ and the minimum value, 98999.36 (Pa) is located at the origin. On the basis of rapid kinetics at 1000°C nearly all H_2 molecules that collide with the $\Gamma_{G/Ni}$ might be expected to dissociate into two chemisorbed H atoms. The pressure gradient of H_2 in the Ω_G shows that the vast majority of H atoms recombine to H_2. Only a few net H atoms result from the dissociation process.

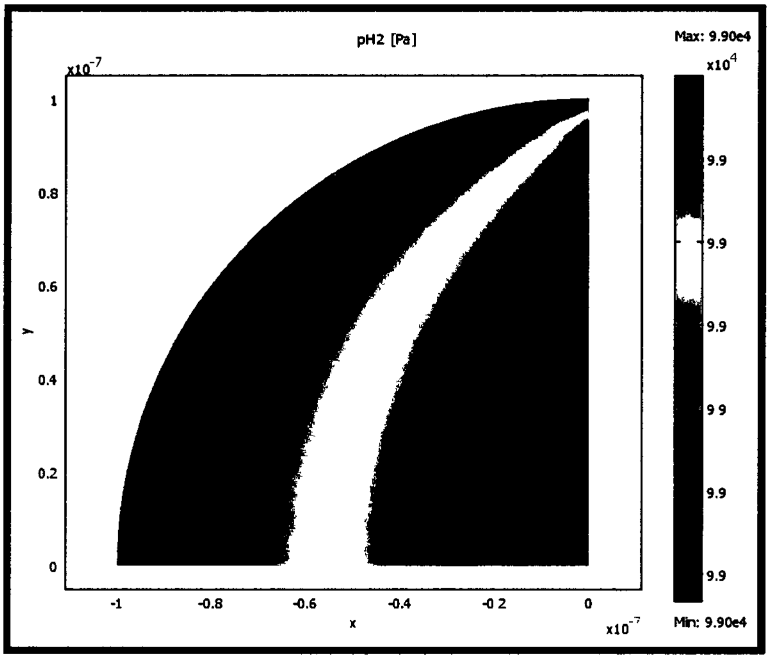

Figure6. 2 Calculated Distribution of the H_2 Pressure in the Gaseous Domain for a Binary Gas Mixture H_2-H_2O for a 0.1 µm Domain Radius

Figure 6.3 shows the calculated H radical concentration in the Ω_{Ni}. The gradient of the dissociated H_2 molecules is higher in the Ω_{Ni}, compared to Ω_G. The larger gradient might be partially explained by the difference in diffusivity of the H within the Ω_{Ni} compared to H_2 in Ω_G. The minimum concentrations of H radicals,2.77×10^{-6}, is on the $\Gamma_{Ni/YSZ}$ line, since the electrochemical reaction consumes H radicals at this interface. The maximum concentration of

H radicals is on the $\Gamma_{G/Ni}$at the intersection of $\Gamma_{G/Ni}$ and $\Gamma_{Ni/Bulk}$ in Fig 6-3 is 1.15×10^{-4} (mol.m^{-3}).

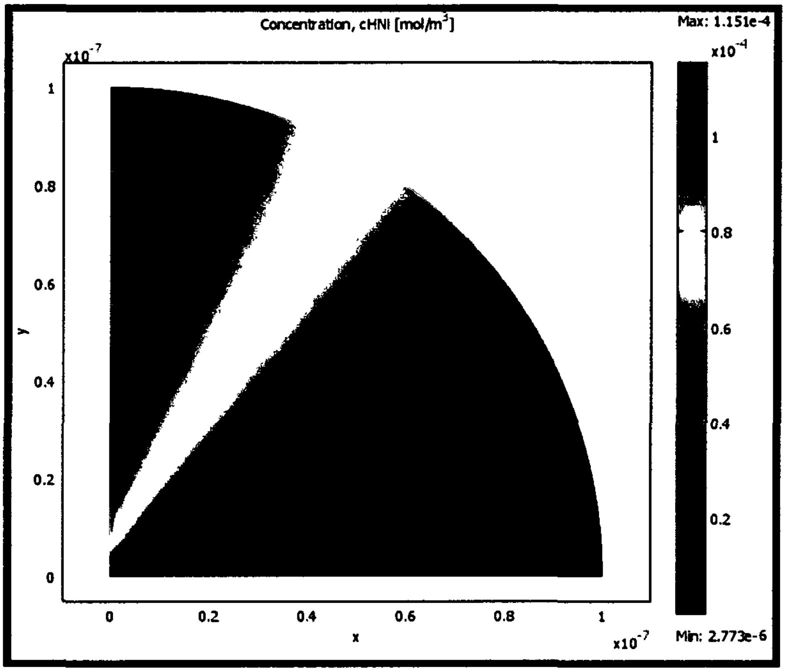

Figure6. 3 Calculated Hydrogen Radical Concentration Distribution in the Ω_{Ni} for a 0.1 μm Domain Radius

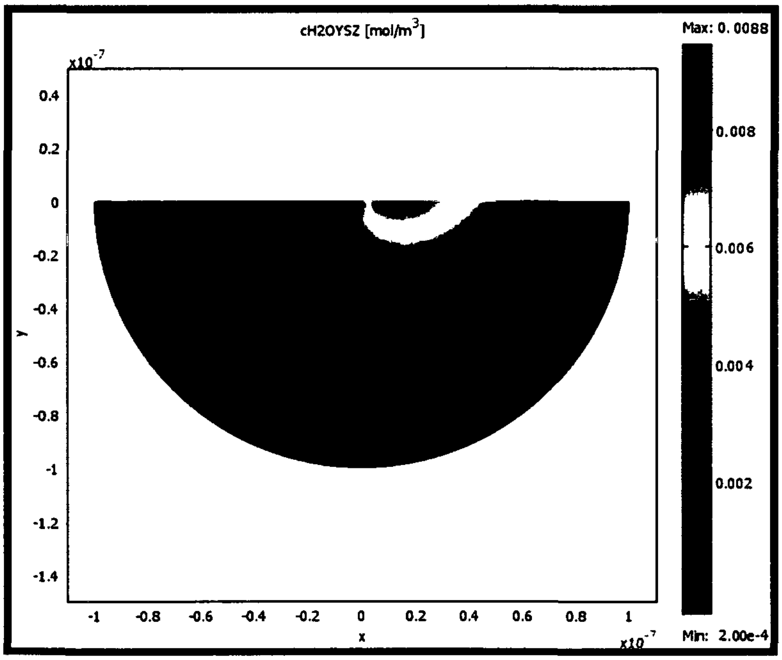

Figure6. 4 Calculated Distribution of the H_2O Concentration in the Ω_{YSZ} for a 0.1 (μm) Domain Radius

Figure 6.4 shows the water distribution in the Ω_{YSZ}. H_2O is produced at the $\Gamma_{Ni/YSZ}$. It is the major product of the electrochemical reaction that takes place at the $\Gamma_{Ni/YSZ}$. The maximum value of H_2O, 0.0088 ($mol.m^{-3}$), is at a location that is slightly displaced from the origin of the domain (the triple phase point) and along the $\Gamma_{Ni/YSZ}$. Molecular desorption of water takes place at the surface of the $\Gamma_{YSZ/G}$. The adsorption/desorption equilibrium of water at the surface was represented by a Henry's law type equation which relates the solute concentration of H_2O in the Ω_{YSZ} to the H_2O pressure in the Ω_G, so the water concentration on the surface of YSZ on the YSZ side of the interface is proportional to the water pressure at the gas side of the interface.

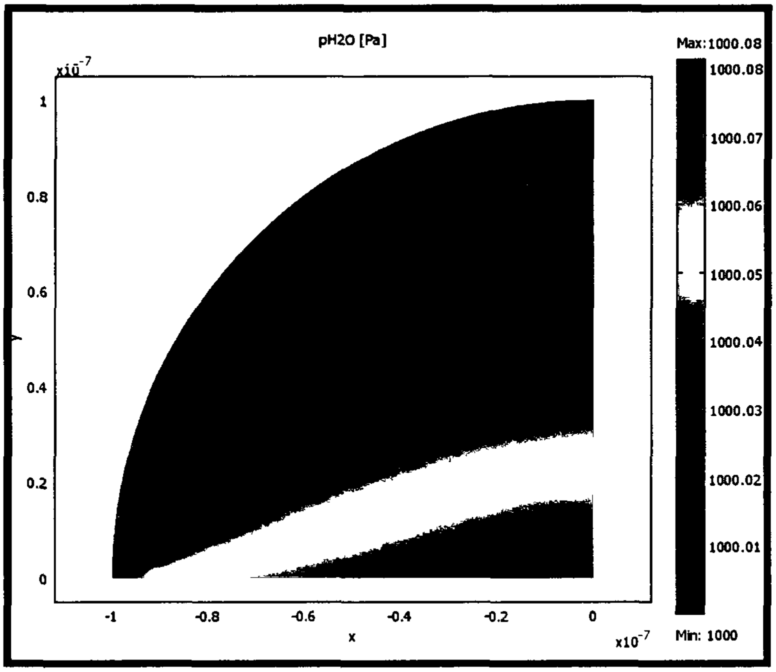

Figure6. 5 Calculated Distribution of the H_2O Pressure in the Gaseous Domain for a Binary Gas Mixture H_2-H_2O for 0.1 μm Domain Radius

Figure 6.5 shows the distribution of H_2O gas molecules (H_2O partial pressure), which were initially produced at the $\Gamma_{Ni/YSZ}$ and are diffusing through the binary H_2/H_2O mixture in the Ω_G. The highest H_2O partial pressure value, 1000.08 (Pa) shown in the figure is at the origin of the domain. The minimum value of H_2O partial pressure is 1 (kPa) on the $\Gamma_{Bulk/G}$. These values indicate that the water partial pressure in the Ω_G was almost uniform.

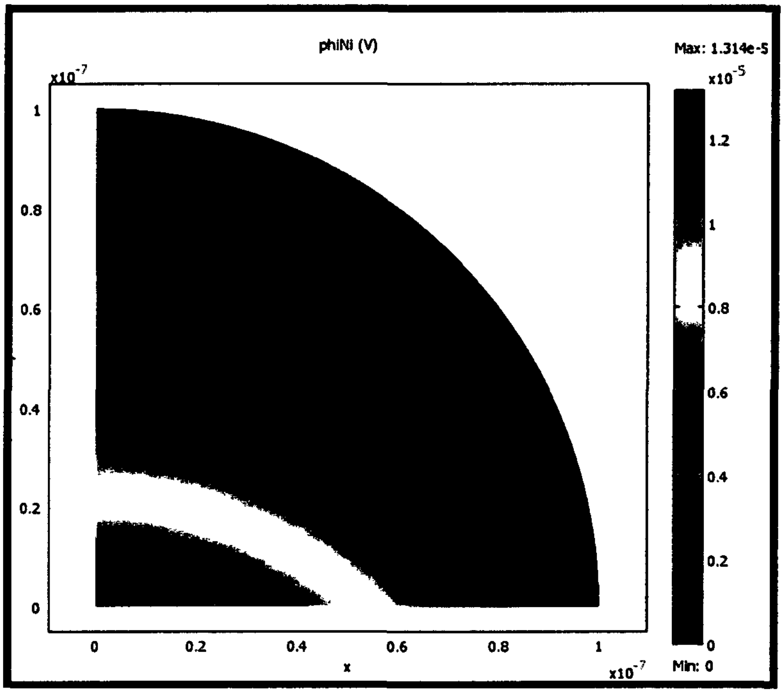

Figure6. 6 Potential Distribution through the Ω_{Ni} for a 0.1 μm Domain Radius

In Figure 6.6 the electrical potential distribution inside the Ω_{Ni} has been shown. It can be seen that the potential at the $\Gamma_{Bulk/Ni}$ is zero. In addition the maximum value, 1.3×10^{-5} (V), at the origin is very close to zero. In this model the only charged species are the O^{2-} anions and the electrons. Ni metal conducts electrons with very little resistance. The O^{2-} anions are in the YSZ part of the domain. Therefore the charge transfer equation has almost no effect on the potential in the Ω_{Ni}. As a result the potential profile in Ni is essentially uniform. Having the Butler Volmer equation as a boundary condition at $\Gamma_{Ni/YSZ}$ causes only a small gradient in the value of potential at the $\Gamma_{Ni/YSZ}$. The maximum value of potential at the $\Gamma_{Ni/YSZ}$, 1.3×10^{-5} (V), is slightly different than zero. This difference is due to the charge transfer reaction at the $\Gamma_{Ni/YSZ}$.

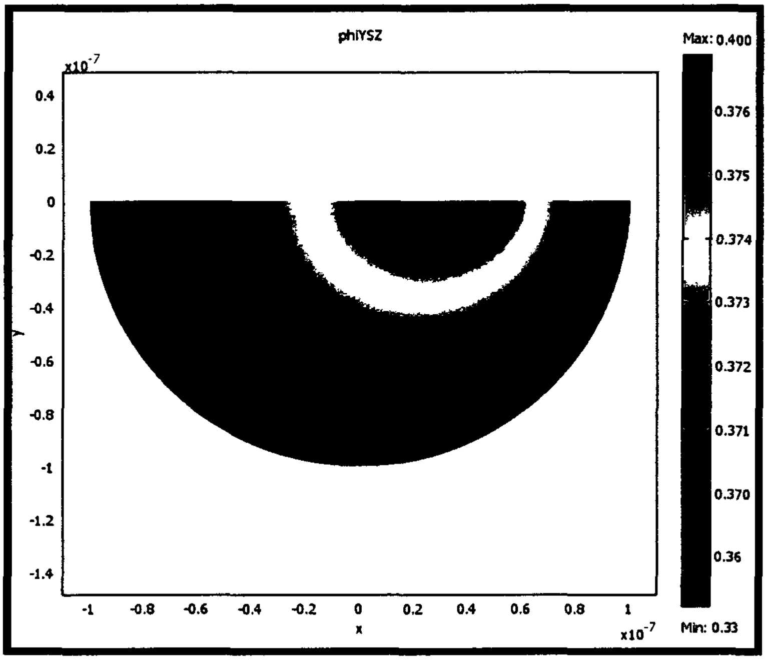

Figure6. 7 Potential Distribution through the Ω_{YSZ} for a 0.1 (μm) Domain Radius

The potential gradient in the electrical potential profile of the Ω_{YSZ} is shown in Figure 6-7. The electrochemical reaction was assumed to take place at the boundary between the Ni and the YSZ phase. A potential gradient very close to the $\Gamma_{Ni/YSZ}$ was expected. The electrochemical reaction affects the potential profile via the Butler-Volmer equation and the Ohm's law equation. As the $\Gamma_{Ni/YSZ}$ is approached from the Ω_{YSZ} the potential changes from the 0.4 (V) boundary condition at the Ω_{YSZ} exterior to 0.33 (V) at the minimum potential position on the the $\Gamma_{Ni/YSZ}$.

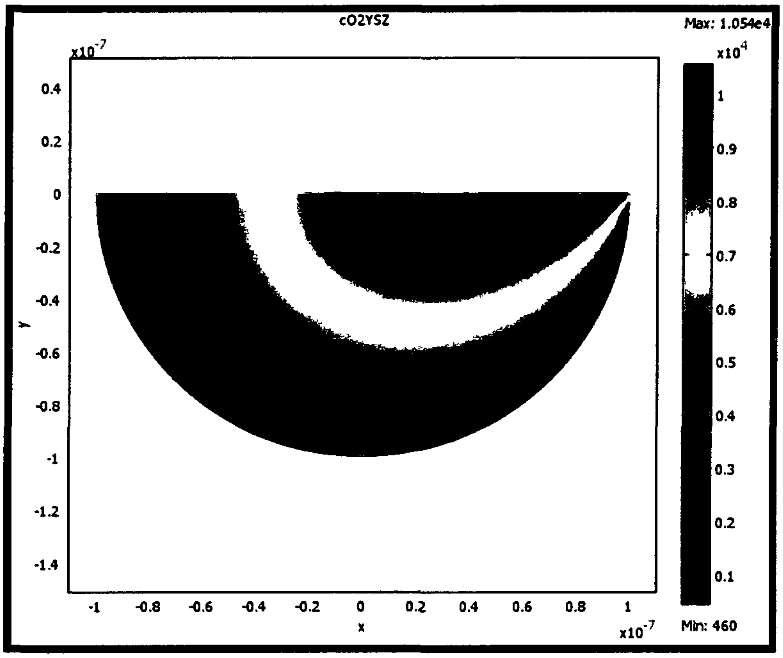

Figure6. 8 Calculated Distribution of the O^{2-} Anions Concentration in the Ω_{YSZ} for a 0.1 (μm) Domain Radius

The distribution of O^{2-} anions inside the Ω_{YSZ} is shown in Figure 6.8. The oxygen anions migrate via a solid state vacancy transport mechanism through the electrolyte and the Ω_{YSZ} in the TPB domain of the anode. Since the concentration of oxygen anions at the $\Gamma_{Bulk/YSZ}$ is large and the concentration of O^{2-} vacancies and the diffusion coefficient of O^{2-} in Ω_{YSZ} are small, a relatively sharp O^{2-} concentration gradient was expected through the whole Ω_{YSZ}. The Butler-Volmer charge transfer equation describes the depletion of O^{2-} by the reaction that takes place at the $\Gamma_{Ni/YSZ}$. The blue part of the graph represents O^{2-} concentrations that are smaller than the value of O^{2-} at the bulk $\Gamma_{Bulk/YSZ}$. The maximum and minimum values in Fig 6-8 are 5.31×10^4 and 460 ($mol.m^{-3}$) respectively.

6.1.2 Domain Radius = 0.01 (μm)

Results for mass transport plus surface reaction for a domain radius of 10^{-8} (m), 0.01 (μm), are shown in Figures 6.09 to 6.15. As mentioned earlier in this chapter the mass transport plus reaction case has been examined with different domain radii to see the extent to which the various phenomena occur as the distance from the TPB origin changes. All of the parameters, equations, boundary conditions were essentially the same for the 0.1 (μm) and 0.01 (μm) computations. As for the model with a domain radius of 10^{-8} (m), 0.01 (μm), here we also show the results of H_2 and H_2O pressure distributions in the Ω_G, H radicals in Ω_{Ni} and the distributions of O^{2-} and H_2O in Ω_{YSZ}. The smallest mesh size for which the model of the 0.1 (μm) domain converged, with 6017 mesh points (corresponding to a relative tolerance [Eq. 5-12] of 10^{-12}) was larger than the mesh size (corresponding to a relative tolerance of 10^{-20}) at which the model for the 0.01 (μm) domain converged, with 23873 points (The maximum mesh element size used by default by the software is 1/15th (in 2D) of the maximum distance in the geometry). This means that computations for the 0.01 (μm) domain size had a smaller numerical error than those for the 0.1 (μm) domain size. The values of the variables calculated for the 0.01 (μm) domain size are different from those for the 0.1 (μm) domain size.

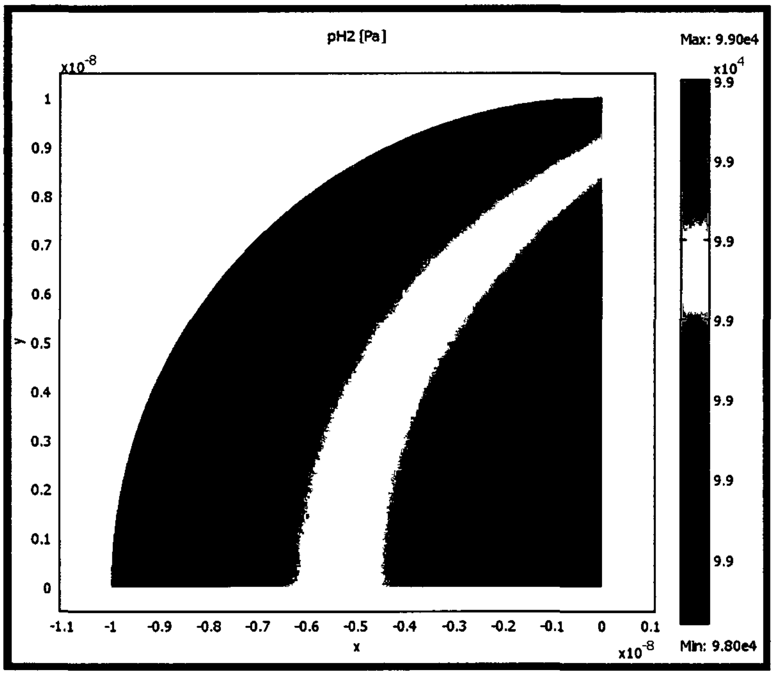

Figure6. 9 Calculated Distribution of the H_2 Pressure in the ΩG for a Binary Gas Mixture H_2-H_2O for 0.01 (μm) Domain Radius

The hydrogen partial pressure distribution through the Ω_G, in Figure 6-9 for a domain radius of 0.01 (μm), appears to be essentially the same as that in Figure 6-2 for a 0.1 (μm) domain radius. The maximum value for the H_2 partial pressure at the external surface of the Ω_G is 99 (kPa) in both cases. The minimum value of H_2 pressure is 98 (kPa) for the 0.01 (μm) domain size, in Figure 6-9 versus 98.999 for the 0.1 μm domain size in Figure 6-2. For both cases the absolute value of the pressure difference between the external boundary of the Ω_G and the origin of the TPB domain appear to be qualitatively somewhat similar.

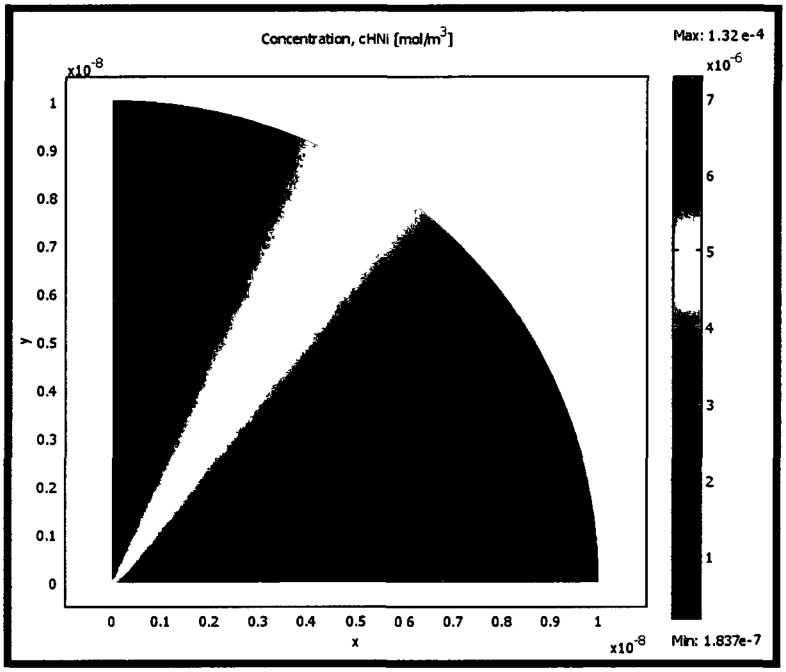

Figure6. 10 Calculated Hydrogen Radical Concentration Distribution in the Ω_{Ni} for a 0.01 (μm) Subdomain Radius

The distribution of H through the Ni catalyst section is shown in Figure 6.10 for a Ω_{Ni} with the radius of 0.01 (μm). The maximum value for H is 1.32×10^{-4} (mol.m^{-3}) and the minimum value at $\Gamma_{Ni/YSZ}$ is 1.837×10^{-7}(mol.m^{-3}). In contrast for a domain radius of 0.1 (μm), in Figure 6.3, the maximum and minimum values are 1.151×10^{-4} (mol.m^{-3}) and 2.773×10^{-6} (mol.m^{-3}). In the 0.1 (μm) Ω_{Ni} the hydrogen radical concentration difference is similar to the 0.01 (μm) Ω_{Ni}. However, the hydrogen radical concentration gradient in the 0.1 (μm) Ω_{Ni} is an order of magnitude smaller than in the 0.01 (μm) Ω_{Ni} – because there is a greater radius over which the similar concentration drop occurs.

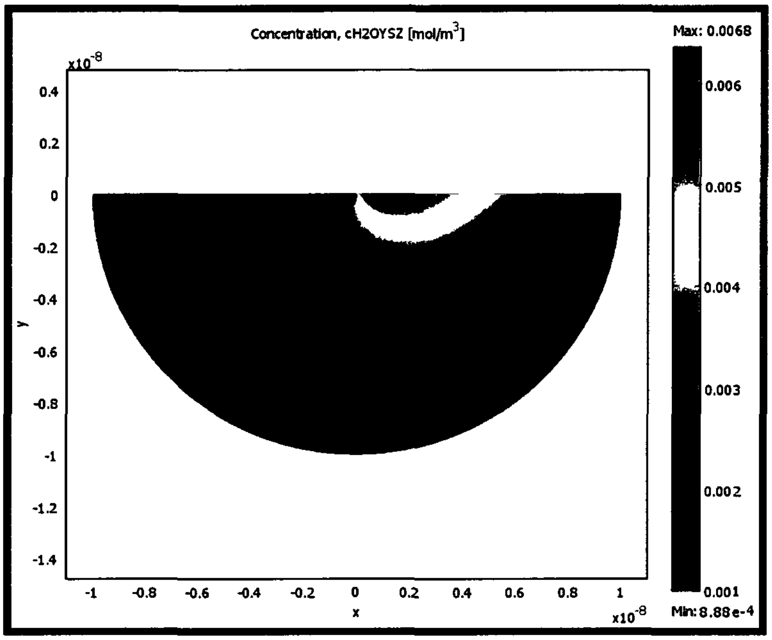

Figure6. 11 Calculated H_2O Concentration Distribution in the Ω_{YSZ} for a 0.01 (μm) Domain Radius

Figure 6.11 shows the concentration profile of the water product of the fuel cell in the Ω_{YSZ}. As has been discussed previously the concentration of H_2O at the $\Gamma_{Ni/YSZ}$ has its maximum value at the $\Gamma_{Ni/YSZ}$ due to the fact that the only reaction that produces H_2O takes place at this boundary. Then it diffuses through the Ω_{YSZ} and reaches the $\Gamma_{YSZ/G}$. The boundary condition that was used for H_2O at the $\Gamma_{Bulk/YSZ}$ is the water flux = 0. Therefore all of the water produced at the $\Gamma_{Ni/YSZ}$, must exit through the $\Gamma_{YSZ/G}$. This explains the distribution profile of H_2O in this domain. The maximum value, 0.0068 ($mol.m^{-3}$) occurs close to the origin at the position (x,y):($1.349679 \times 10^{-9}, -1.532786 \times 10^{-16}$). In the case of 0.1(μm) the maximum value occurs at the position (x,y):(8.432128×10^{-9}, $-3.266815 \times 10^{-12}$).

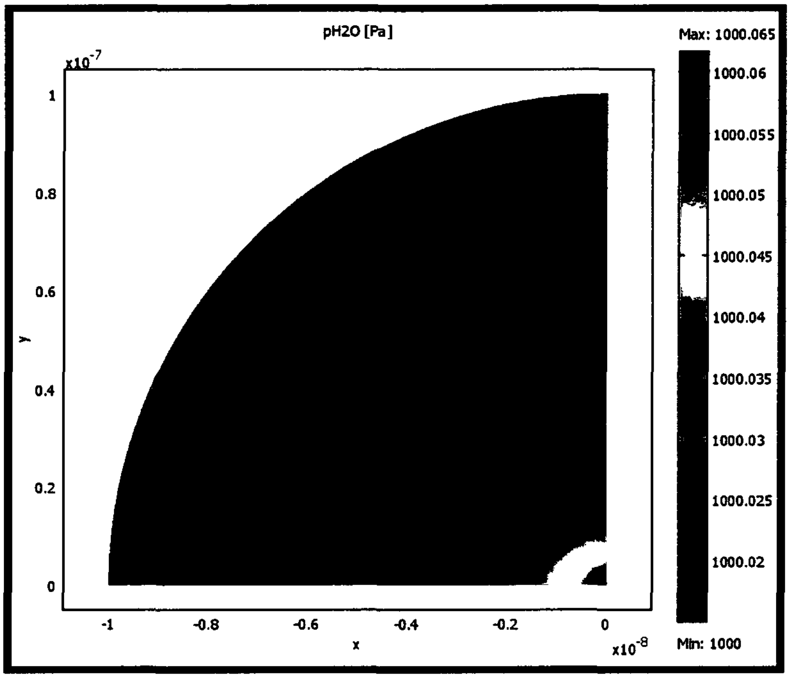

Figure6. 12 Calculated Distribution of the H_2O Pressure in the Gaseous Domain for Binary Gas Mixture H_2-H_2O for a 0.01 (μm) Domain Radius

The partial pressure of H_2O in the 0.01 (μm) domain, Figure 6-12, is almost uniform. The same was observed for the 0.1 (μm) domain, Figure 6-5. The maximum – minimum pressure differences 0.065 (Pa) for the 0.01 (μm) domain and 0.08 for the 0.1 (μm) domain are similar. However, because the 0.01 (μm) domain radius is an order of magnitude smaller, its pressure gradient is an order of magnitude larger. The pressure of water molecules is slightly higher at the origin; exist close to the origin in Fig 6.12. This profile was expected because the origin is the closest point to the reaction sites. And there are more spaces for large H_2O molecule to diffuse from Ω_{YSZ} to Ω_G along the $\Gamma_{G/Ni}$.

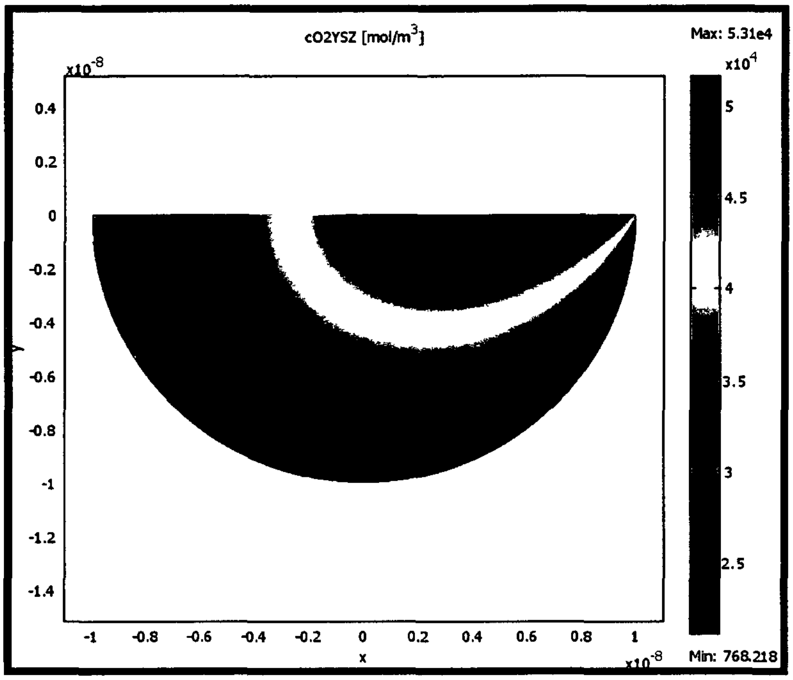

Figure6. 13 Calculated Distribution of the O^{2-} Anions Concentration in the Ω_{YSZ} for a 0.01 (μm) Domain Radius

The minimum oxygen anion concentration in Fig 6.13, 768 ($mol.m^{-3}$) is similar to the minimum value in Fig 6.8, 460 ($mol.m^{-3}$). As in the case of the 0.1 (μm) domain radius, the oxygen anions move to the reaction sites at $\Gamma_{Ni/YSZ}$ where they will be consumed by reaction with H radicals that are on the Ni side of the interface. There are two driving forces for oxygen anions: One driving force is the O^{2-} anion concentration gradient (diffusion) and the other driving force is the local potential gradient (migration) that exists in the Ω_{YSZ}. Migration and concentration gradient drives O^{2-} in the opposite direction. The latter push the oxygen anions towards the $\Gamma_{Ni/YSZ}$, while the migration pushes O^{2-} away from the $\Gamma_{Ni/YSZ}$. Since there is a large concentration gradient of O^{2-} in the Ω_{YSZ} and a low diffusion coefficient, 1.4×10^{-14} ($m^2.s^{-1}$), as will be explained below diffusion is only mechanism that drives O^{2-} anions in the direction towards the $\Gamma_{Ni/YSZ}$.

Based on Nernst-Plank equation the diffusive flux of O^{2-} is equal to $-(D_{O2-}\nabla C_{O2-})$. Since the concentration gradient is negative, the diffusive flux become positive and point toward the $\Gamma_{Ni/YSZ}$. The migration part on the other hand is equal to $-(D_{O2-}C_{O2-})\frac{FZ}{RT}\nabla\varphi$, in which

$z = -2$ for oxygen anions and $\nabla\varphi$ is negative. So the migration flux is negative and pointing towards $\Gamma_{YSZ/G}$.

The concentration gradient, for the 0.01 (μm) Ω_{YSZ} is higher than for the 0.1 (μm) Ω_{YSZ}, because the concentration difference in the 0.1 (μm) Ω_{YSZ} is divided by a distance that is 10 times greater than in the 0.01 (μm) Ω_{YSZ}. Even though the lowest concentration for the 0.01 (μm) radius size Ω_{YSZ}, 768.218 (mol.m^{-3}), is greater than the minimum concentration for 0.1 (μm) Ω_{YSZ}, 460 (mol.m^{-3}), the concentration difference has less effect on the O^{2-} concentration gradient than dimension of the subdomain.

For the same reaction rate, the smaller area at the $\Gamma_{Ni/YSZ}$ interface for the 0.01(μm) radius size Ω_{YSZ}, compared to the 0.1 (μm) radius size Ω_{YSZ}, will require that the flux of oxygen anions to the reaction sites be larger than for the 0.1 (μm) Ω_{YSZ}. The greater flux will require a larger concentration gradient. That is consistent with the concentration O^{2-} gradient being larger for the 0.01 (μm) Ω_{YSZ}.

An alternative computation can be performed for the 0.01 (μm) domain size. It can be seen in Figure 6.8, for the 0.1 (μm) domain size, that the oxygen anion concentration at a distance of 0.01 (μm) from the origin of the triple phase boundary has the average value of approximately 0.1×10^4(mol.m^{-3}). Then a computation can be performed for the 0.01 (μm) domain size with an oxygen anion concentration boundary condition of 0.1×10^4(mol.m^{-3}) at the external boundary of the gas domain. In this case the minimum value of the oxygen anion concentration, in the vicinity of the triple phase point, is 486.94 (mol.m^{-3}). This value is almost the same as the 3.9×10^4 460 (mol.m^{-3}) value in Figure 6-8, in contrast to the 768.218 (mol.m^{-3}) value in Figure 6.13. Therefore this alternative computation for the 0.01 (μm) domain size is consistent with the computations shown in Fig. 6.8.

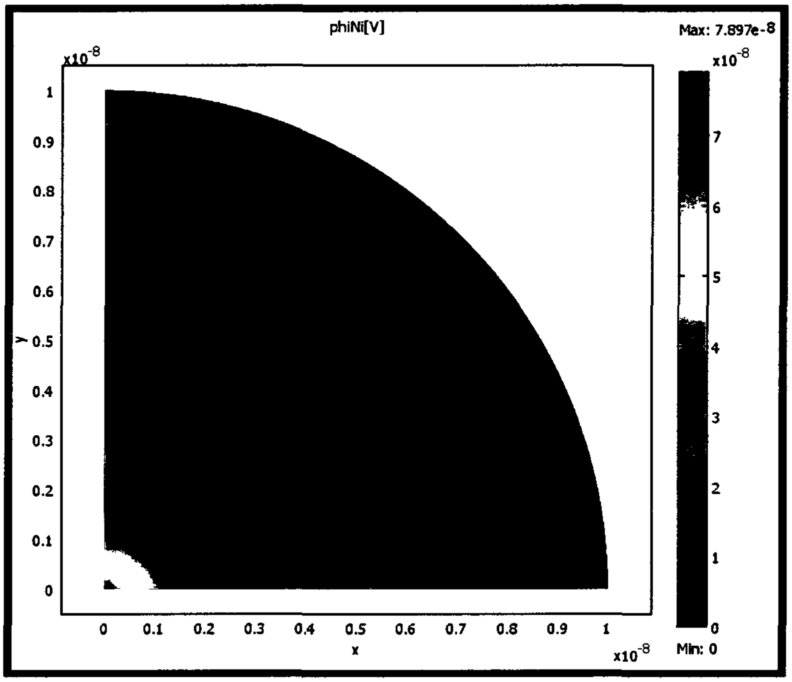

Figure6. 14 Potential Distribution through the Ω_{Ni} for a 0.01 (μm) Domain Radius

The potentials in both Ω_{YSZ} and Ω_{Ni} for the 0.01 (μm) Ω_{YSZ} radius are shown in Figure 6.14 and 6.15 respectively. The values of the potentials in the 0.01 (μm) Ω_{YSZ} (Figs 6.14 and 6.15) are almost the same as in the 0.1 (μm) Ω_{YSZ} (Figures 6.6 and 6.7). However, because there is an order of magnitude difference in the radius, the potential gradient is very different in the two cases. The potential profile in Ω_{YSZ} for the case of 0.1 (μm) Fig 6.7 shows that the minimum potential occurs at the position (x,y): $(4.275695 \times 10^{-8},-9.671361 \times 10^{-10})$ and is equal to 0.33(V). The minimum value of the potential for the 0.01 (μm) is 0.35 (V). The results and profile of potential distribution in Ω_{YSZ} in case of 0.01 (μm) are reasonable considering that the minimum value in the 0.1 (μm) Ω_{YSZ} is at closer to the origin than the 0.01(μm) location in the 0.1 (μm) Ω_{YSZ}.

Negative charges flow from small potentials to large potentials. An example would be electrons that flow from a smaller potential at the anode to a larger potential at the cathode. In the Ω_{YSZ}, the O^{2-} anions are negatively charged so the migration phenomena would cause them to flow from the smaller potential (0.33 or 0.35 (V)) at the $\Gamma_{Ni/YSZ}$ interface to the larger potential of 0.4 (V) at the $\Gamma_{YSZ/Bulk}$. In other words the migration phenomena will push the O^{2-} anions away from the reaction sites at the $\Gamma_{Ni/YSZ}$ interface. The diffusion phenomena, mentioned above, will have to dominate the migration phenomena so that the O^{2-} anions ultimately arrive at the reaction sites.

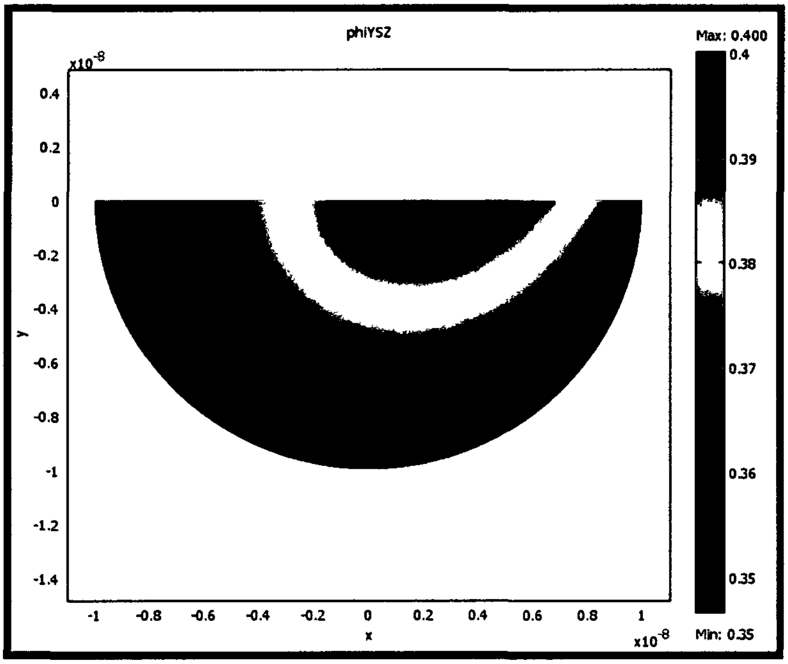

Figure6. 15 Potential Distribution through the Ω_{YSZ} for a 0.01 (μm) Domain Radius

A comparison of the results of 0.01(μm) with 0.1(μm) shows that when the region around the classical TPB point is expanded from 0.01(μm) to 0.1(μm), phenomena occur in the expanded region. Other significant differences are the larger concentration gradients (and therefore larger fluxes) and the smaller length of the Ni/YSZ interface (and therefore smaller number of reaction sites) for the 0.01 (μm) domain radius. Therefore the model developed here indicates that there are differences in the reaction phenomena as a function of position away from the classical TPB and that not all reactions are located at the classical single line TPB.

In the next section the mass conservation equations are examined through the calculation of the flux of hydrogen containing species at four major interfaces: $\Gamma_{Bulk/G}$, $\Gamma_{G/Ni}$, $\Gamma_{Ni/YSZ}$, $\Gamma_{YSZ/G}$. The results are shown in Figures 6.16- 6.19.

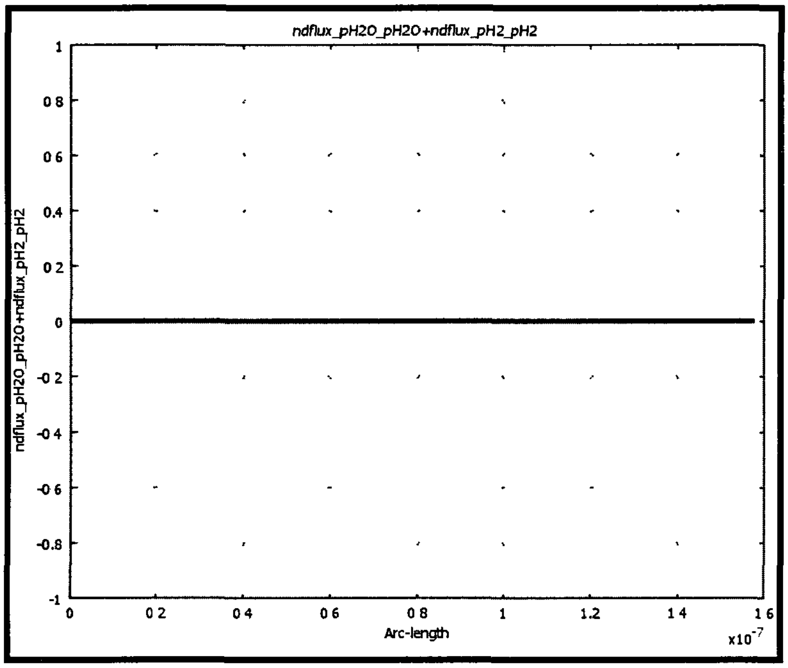

Figure6. 16 The Summation of Diffusive Flux of H_2O and Diffusive Flux H_2at the $\Gamma_{Bulk/G}$ for a 0.1 (μm) Domain Radius

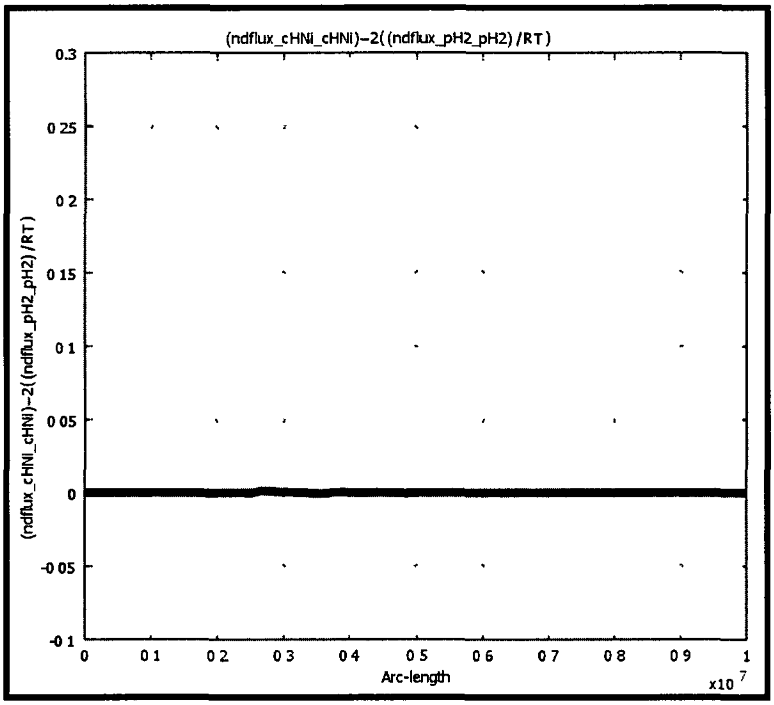

Figure6. 17 The Summation of Diffusive Flux of two times $H_2$and H_{Ni} the $\Gamma_{G/Ni}$ for a 0 1 (μm) Domain Radius

During the overall process at the anode one H_2 molecule is oxidized causing the production of one H_2O molecule. The overall molar flow at $\Gamma_{Bulk/G}$ is therefore should be equal to zero:

$$N_{H_2O_{gas}} + N_{H_{2gas}} = 0 \qquad (6-1)$$

As it can be seen in Figure 6.16 the flux of hydrogen molecules entering the Ω_G (negative values) is equal in magnitude to the water diffusive flux exiting across the boundary (positive values), so the absolute value of the total summation of the two fluxes at the boundary is constant.

The H_2 molecules leaving the Ω_G, convert to two H atoms at the $\Gamma_{G/Ni}$. The flux of H_2 to the $\Gamma_{G/Ni}$ should be equal to the flux of H atoms leaving the interface to the reaction site. At the $\Gamma_{G/Ni}$:

$$N_{H_{Ni}} - 2N_{H_{2gas}} = 0 \qquad (6-2)$$

The summation of two times diffusive fluxes of H_{2gas} and H_{Ni}at the $\Gamma_{G/Ni}$ for a 0. 1 (μm) domain radius are shown in Figure 6.17

At $\Gamma_{Ni/YSZ}$ the incoming H radicals react with O^{2-} to produce H_2O and electrons. The rate at which H radicals are consumed must be twice the rate of H_2O production. Their fluxes should have the same sign:

$$N_{H_{Ni}} - 2N_{H_2O_{YSZ}} = 0 \qquad (6-3)$$

The summation of the diffusive flux of H_2O_{YSZ} minus half of the diffusive flux of H_{Ni} at the $\Gamma_{Ni/YSZ}$ is shown in Figure 6. 18 for a 0.1 (μm) domain radius

The H_2O molecules produced at the $\Gamma_{Ni/YSZ}$ will diffuse through the Ω_{YSZ} and reach the $\Gamma_{YSZ/G}$. The flux of water molecule leaving the $\Gamma_{YSZ/G}$ interface should be equal to the flux of water arriving at the $\Gamma_{YSZ/G}$ interface from Ω_G:

$$N_{H_2O_{YSZ}} - N_{H_2O_{gas}} = 0 \qquad (6-4)$$

The summation of the diffusive flux of H_2O_{gas} and minus the diffusive flux of H_2O_{YSZ} at the $\Gamma_{YSZ/G}$ is shown in Figure 6.19 for a 0. 1 (μm) domain radius.

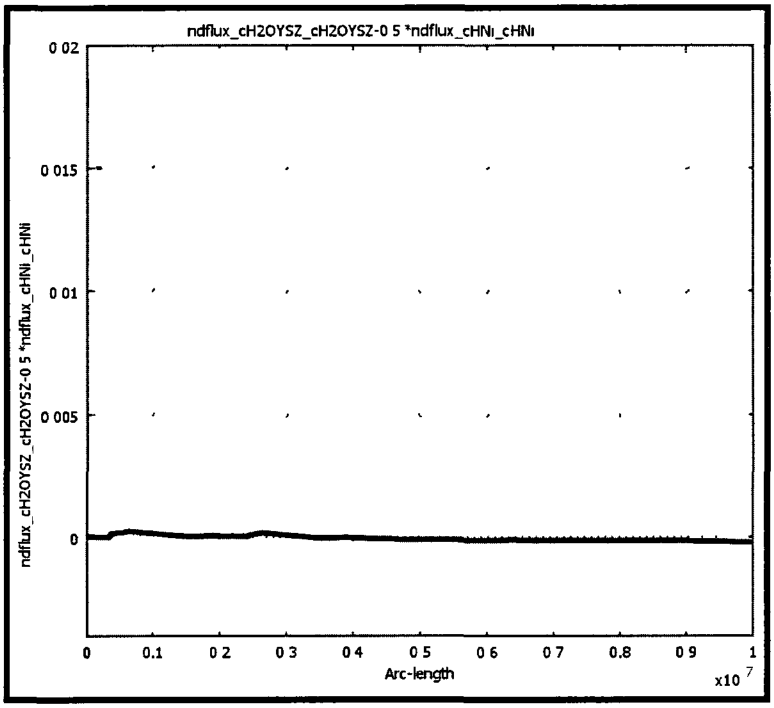

Figure6. 18 The Summation of Diffusive Flux of H_2O and Minus Half of Diffusive Flux of H_{Ni} and at the $\Gamma_{Ni/YSZ}$ for a 0.1 (μm) Domain Radius

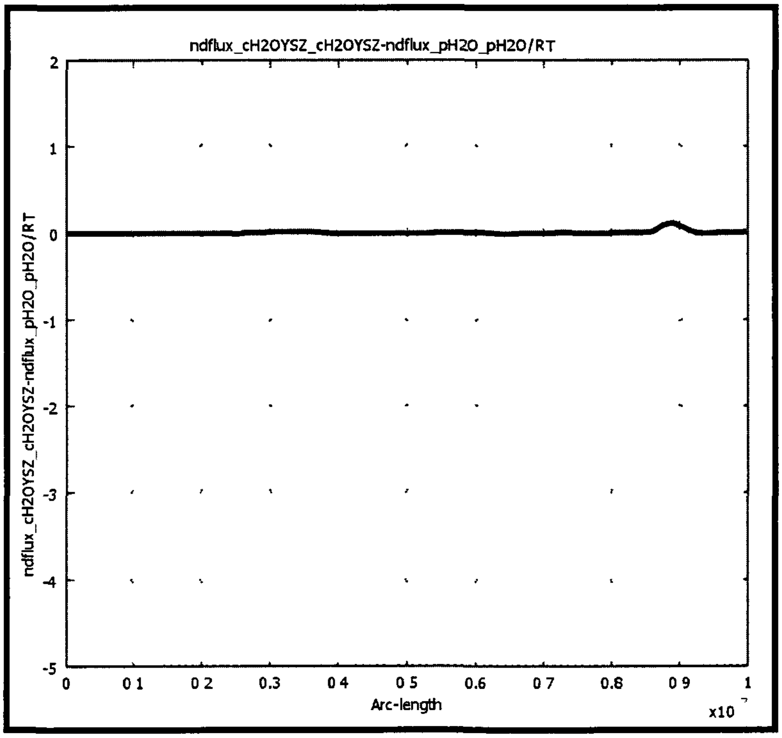

Figure6. 19 The Summation of Diffusive Flux of H_2O and Minus Diffusive Flux of H_2 O_{YSZ} at the $\Gamma_{YSZ/G}$ for a 0. 1 (μm) Domain Radius

The values of subdomain integration of flux and boundary integration of normal diffusive fluxes at certain important boundaries of the geometry are shown in Table 6.1.

Table 6.1 lists the normal diffusive fluxes integrated over the appropriate boundaries. Depending on whether the direction of the unit normal flux, perpendicular to the surface area of the circle, points outwards or inwards, the signs of the fluxes will be either positive or negative.

Domain Radius	0.1μm	0.01 μm
$\Gamma_{Bulk/G}$		
H_2 in	-3.0	-12
H2O out	3.0	12
$\Gamma_{G/Ni}$		
H_2 in	3.0	12
H out	5.9	24
$\Gamma_{Ni/YSZ}$		
H in	6	24
H_2O out	3	12
H_2O in	3.0	12.0
H_2O out	3.0	12.0

Table 6. 1 Summary of Fluxes integrated over sub-domain interfaces (mol.m-1.s-1)

Arc Length integration for 0.1 μm is 7.85×10^{-8}m at $\Gamma_{Bulk/G}$, $\Gamma_{Bulk/Ni}$, and $=1.57 \times 10^{-7}$m at $\Gamma_{Bulk/YSZ}$ and 5×10^{-8} m for the rest.

Arc Length integration for 0.01 μm = 7.85×10^{-9}m at $\Gamma_{Bulk/G}$, $\Gamma_{Bulk/Ni}$, and $=1.57 \times 10^{-8}$m at $\Gamma_{Bulk/YSZ}$ and 5×10^{-9} m for the rest.

Table 6.1 Subdomain integration of Flux and Boundary Integration of Normal Flux of TPB Species

6.2 Comparison between the Model Results and the Results in the Literature

There are several theoretical and experimental methods that have been used to describe the TPB at the anode of a SOFC. The reports of experimental work describe both TPB length estimation and reaction mechanisms. These experiments have indicated that both structure and composition of the anode material have a major effect on the TPB length (Sun 2007). They have also suggested that the classical concept of a TPB being a single line having the thickness of one reaction site was suspect. The experiments performed by Kleitz, Siebert and co-workers (Kleitz and Siebert 1989; Hammouche et al. 1991) were interpreted in terms of reaction occurring in the vicinity of the TPB with an extension to a surface where diffusion occurred. Later experimental work (Bieberle et al. 2001) led to a suggestion that at some conditions the TPB has a width that extends from the "TPB line" along one of the interfaces.

The kinetics of the reaction process and the mechanism of the reaction at the TPB were also studied experimentally. The electrochemical information about the system is usually obtained from electrochemical impedance spectroscopy (EIS) measurements and by fitting this data to equivalent circuits (Kakac 2007). It is found that in addition to charge transfer, spillover of H, H_2O, and O^{2-} is also possible. For example, spillover occurs when a molecule adsorbs or reacts on one of the constituent's surface of a composite electrode (cermet) before diffusing onto a second constituent surface where it might react with a different adsorbed species and subsequently desorbs (Bieberle 2001). In general experimental results reported in different studies on the anode TPB have not been performed at the same experimental conditions. As a result it is extremely difficult to compare the results of different investigations.

Mathematical models of SOFCs are also used in order to understand and examine the TPB. Although there are numerous studies on the mechanism of the oxygen reduction reaction (Steele 1997, Adler 2004) and the TPB at the cathode (Mitterdorf and Gauckler 1999, Flieg 2002, Flieg 2004, Chan 2004, Karan 2007, Lynch et al. 2008, Fehribach 2009), the hydrogen oxidation reaction has attracted little attention in the literature. Because the most common catalyst at a SOFC cathode is lanthanum strontium manganite, LSM, a mixed ionic electronic conductor, the phenomena at the cathode is different than that at the anode which has a Ni/YSZ cermet. In contrast to the relatively simple oxygen reduction and oxygen evolution mechanism at the cathode, the reaction mechanism at the anode consists of several complex elementary steps that are not understood yet.

O'Hayra et al. proposed a simple analytical TPB mathematical model to describe the nature, property and scaling for a Pt/Nafion PEM fuel cell. It was claimed that it is also applicable to SOFC with only minor changes in the original model. The simplifying assumption of the model is that the reaction is limited to the electrolyte/electrode interface. The attractiveness of the model is its dimensionless parameter, the effective TPB width, which describes the ratio between the rates of reaction and diffusion in the system. Berg, Novruzi, Volkov (2008) applied numerical techniques, FEM, to solve the problem numerically. Their finite element implementation of this model produced numerical values of the electric potential and the concentrations of species in the vicinity of the TPB. When compared to the simple oxygen-only analytical solution, in O'Hayra's work, it shows the importance of taking into account the rate of migration of ions to the TPB.

(Williford and Chick 2003) challenged the common assumption for SOFCs that the oxidation reaction is strictly localized at TPB by considering oxygen spillover onto the Ni surface. Their results indicate that the reactive area simply spreads over an increasing portion of the Ni surface as the current density increases. The spillover of oxygen is one of the mechanisms that have been well-studied in the literature (Mizusaki 1994). In contrast the approach we took in this thesis has received less study. Our mechanism describes the well known diffusion of H radicals (Oriani 1994) inside the metal phase

(Williford 2006) proposed a reaction mechanism for the hydrogen oxidation in his paper. To the best of our knowledge, his paper is the only one on modeling the TPB at the anode. Although there are a few papers that addressed TPB cathode modeling explicitly, other the papers on TPB anode couldn't be found at the time of writing this thesis. In Williford's proposed mechanism H_2 dissociatively chemisorbs on the Pt anode of a SOFC and diffuses on the Pt surface to the TPB. O^{2-} from the YSZ spills over onto the Pt metal. He concludes reactions can occur at locations that are a finite distance away from the TPB. As the current density increases the electrochemical reaction occurs on a progressively larger Pt surface area near the TPB.

In our model, the dissociation of the H_2 molecules into two separated adsorbed atoms on the surface of Ni is assumed to be fast when compared to the electrochemical charge transfer reaction at the $\Gamma_{Ni/YSZ}$. This means that the dissociation of H_2 molecules to H radicals is at equilibrium. That is equivalent to surface diffusion being infinitely fast. Another assumption in our model is that H atoms can diffuse through bulk Ni at 1000°C. It has been reported that there is a relatively high mobility of the H radicals in Ω_{Ni} (Oriani 1994).

O^{2-} anions diffuse to the $\Gamma_{Ni/YSZ}$ to participate in the electrochemical reaction. O^{2-} transport in electrolyte is usually described by considering the ion transport from Ohm's Law, migration, and the conservation of charge. That is an oversimplification. Here both migration and diffusion were considered. No spill over of O^{2-} into the $\Gamma_{G/Ni}$ was considered. O^{2-} could diffuse into Ni and form NiO in the vicinity of the classical TPB. But it is a large species in contrast to H radicals and so it will not diffuse very far before encountering the H radicals that diffuse faster. As a result only a small fraction of the $\Gamma_{G/Ni}$ would be covered with O^{2-} anions. In contrast all of the $\Gamma_{Ni/YSZ}$ will have O^{2-} anions on the YSZ side of the interface. Therefore the majority of the reaction sites will be at the $\Gamma_{Ni/YSZ}$ and comparatively few at the $\Gamma_{G/Ni}$. Therefore in our model an active role for YSZ in the kinetics of the oxidation process has been suggested. The H_2O molecules produced at the $\Gamma_{Ni/YSZ}$ diffuse through the Ω_{YSZ} to the $\Gamma_{YSZ/G}$. Finally in our model the H_2O molecules transfer to the Ω_G from the Ω_{YSZ} at the $\Gamma_{YSZ/G}$. In summary, our model is consistent with known experimental phenomena and is different from the only other model, (Williford 2006) that has been reported to date.

Bibliography

Adler, B.S., “Factors Governing Oxygen Reduction in Solid Oxide Fuel Cell Cathodes”, Journal of the Electrochemical Society, 155, 937-B952.

Barczak, W.M., J.Stawowska. European federation of catalysis societies school on catalysis. 2004.

Berg, P., A. Novruzi, O. Volkov "Reaction Kinetics at the Triple-phase Boundary in PEM Fuel Cells" J. Fuel Cell Sci. Technol. 2008:021007.

Bhatia, B., D.S. Sholl,. Journal of Chem, Phys, 122, 2005: 204707.

Bieberle, A., L. P. Meier, L. J. Gauckler” The Electrochemistry of Ni Pattern Anodes Used as Solid Oxide Fuel Cell Model Electrodes” Journal of The Electrochemical Society, 148, 6, A646-A656, 2001.

Cao, G.X., Nabighian, E., Zhu, X.D. Journal of Phys:Rev.Lett, 79, 1997: 3696.

Carter, T.J. , L.A. Cornish. "Hydrogen in Metals." Engineering Failure Analysis 8, 2001: 113-121.

Chan X.J, S.H. Chen, K.A Khor, "Simulation of a Composite Cathode in Solid Oxide Fuel Cells", Electrochimica Acta 49 (2004) 1851–1861.

Ebisuzaki, Y., W.J.Kass,M.O'keefe. "Diffusion and Solubility of Hydrogen in Single Crystalline of Nickel and Nickel Vanadium Alloy." Journal of Chem. Phys. 46, 1967: 1378.

Ebisuzaki, Y., WJ.Kass, M. O'Keeffe,. "Diffusion and Solubility of Hydrogen in Single Crystals of Nickel and Nickel—Vanadium Alloy." J. Chem. Phys. 46, 1967: 1378.

Eguchi, K., J. Nishiyama, K. Sekizawa, K. Sasaki. "Analysis of Gas Transport in Porous Ni-YSZ Anodes by Transient Response Method." solid oxide fuel cell VII. Japan: The electrochemical society, 2001. 719.

Etsell, T.H., S.N. Flengas. "The Electrical Properties of Solid Oxide Electrolyte." Chemical Reviews,70,3, 1970: 339-376.

Fehribach, J. D.,R. O'Hayre. "Triple Phase Boundaries in Solid-Oxide Cathodes." SIAM J. Appl. Math,70,2, 2009: 510-530.

Fleig, J., "On The Width of the Electrochemically Active Zone in a Mixed Conducting Solid Oxide Fuel Cell (SOFC) Cathode”J.Power Sources 105 (2002) 228-238.

Galdikas, A.,C. Descorme,D. Duprez. Solid state ionics,166, 2004: 147.

Gordon, R.S. "Ion Conducting Ceramic Electrolytes:A Century of Progress." Solid Oxide Fuel Cell VIII. usa: The electrochemical society, INC, 2003-2007. 141.

Hanneken, John W[. "Hydrogen in metals and other materials] a comprehensive reference to books\ bibliographies\ workshops and conferences ." International Journal of Hydrogen Energy 24, 1999: 1005-1026.

Hammouche, A., E. Siebert, A. Hammou, M. Kleitz, J. Electrochem. Soc. 138 (1991) 1212-1216.

Hwang, S , H. Lee, H. Shin. "Crystalline Structure of YSZ Thin Films Deposited on Si(111) Substrate by Chemical Vapor Deposition ." Korean Journal of Chemical Engineering,15,3, 1998: 243-245.

Inderwildi, O.R, D.Lebiedz, O. Deutschmann, J.Warnatz. Journal of Chem. Phys 122,, 2005: 034710.

Jackson, R.W.,F.S. Pettit, G.H. Meier. "Environment, The Behavior of Nickel and Silver in a Simulated Solid Oxide Fuel Cell." Journal of Power Sources,185,2, 2008.

Jones, F. G.,Pehlke,R. D. "Solubility of Hydrogen in Solid Ni–Co and Ni–Cu Alloys." Metallurgical and Materials Transactions B, 1971: 2655-2663.

Keneshea, F. J.,D. L. Douglass. "The Diffusion of Oxygen in Zirconia as a Function of Oxygen Pressure." Oxidation of Metals,3,1, 1971: 1-14.

Klietz, M.,E. Siebert, in Chemical Sensor Technology, vol. 2, T. Seiyama, Ed., Kodansha, Japan, 1989:151

Karan, K., B. Kenney, Engineering of microstructure and design of a planar porous composite SOFC cathode: A numerical analysis, Solid State Ionics 177 (2006) 2013–2021.

Lide, D.R. CRC Handbook Chemistry and Physics. CRC; 85 edition, 2004.

Lynch, M.E., D.S. Mebane, Y. Liu, M. Liu, "Triple-Phase Boundary and Surface Transport in Mixed Conducting Patterned Electrodes" J. Electrochem. Soc. 155 (2008) B635-B643

Martin, D.,D.Duprez,. Journal of phys Chem,100, 1996: 9429.

Millini, R.,M. F. Gagliardi. "Physico-chemical Characterization of NiO/YSZ Powders Prepared by the Citrate Route ." Journal of Materials Science,29, 1994: 4629-4632.

Mitterdorf, A., L.J. Gauckler"Identification of the Reaction Mechanism of the Pt, O(g)yttria Stabilized Zirconia System" Solid State Ionics 120 (1999b) 211-225

Mizusaki, J., H. Takagawa, T. Saito, K. Kamitani, T. Yamamura, K. Hirano, S. Ehara, T. Takagi, T. Hikita, M. Ippommatsu, S. Hakagawa, K. Hashimoto, "Kinetics of the Electrode Reaction at the H2-H20 Porous Pt/Stabilized Zirconia Interface" J. Electrochem. Soc. 141 (8) (1994) 2129.

Nigara, Y.,K.Yashiro,J. -O. Hong,T. Kawada, J. Mizusaki. "Hydrogen Permeability of YSZ Single Crystals at High Temperatures." Solid State Ionics,171,1-2, 2004: 61-67.

Oriani, R.A, "A brief survey of useful informaiton about hydrogen in metals" in Int. Symp. Cold Fusion and Adv. Energy Sources. 1994, Minsk, Belarus (250)

Park, J.W,C.J. Altstetter. "The Diffusion and Solubility of Oxygen in Solid Nickel." Metallurgical and Materials Transactions A,18,1, 2007: 43-50.

Poling, A.,J. Prausnitz, J. O'connell. "Diffusion coefficients." In The Properties of Gases and Liquids, 11-10. New York: McGraw-Hill, 2004.

Raz, S., K. Sasaki, J. Maier,I.Riess. Solid state ionic,143, 2001: 181.

Rossmeisl, J.,W.G.,Bessler. Solid State Ionics, 178, 2008: 1694.

Steele, B.C.H, "Behavior of Porous Cathodes in High Temperature Fuel Cells" Solid State Ionics 94 (1997) 239-248

Treybal, R.E. Mass Transfer Operations. McGraw-Hill Education; 2nd edition, 1968.

Vogler, M.,A.Bieberle-Hütter,L.Gauckler,J.Warnatz,W. G. Bessler. "Modelling Study of Surface Reactions, Diffusion, and Spillover at a Ni/YSZ Patterned Anode." Journal of The Electrochemical Society,156, 2009: B663-B672.

Vtilkl, J.,G. Alefeld. "Hydrogen in Metals I-Application-oriented Properties." Topics in applied physics,28, 1978.

Wagner, C., Ber. Bunsenges. Phys. Chem. 72, 1968: 778.

Wahlstrom, E.,E.K Vestergaard, R.Schaub, A. Ronnau, M.Vestergaard,E.Laegsgaard, I. Stensgaard, E.Besenbacher. Sience,303, 2004: 511.

Watson, G.W, R.P.K.Wells,D.J.Willock,G. J. Hutchings. Journal of phys.Chem.B, 105, 2001: 4889.

Williford, R.E., L.A. Chick, "Surface Diffusion and Concentration Polarization on Oxide-supported Metal", Electrocatalyst Particles Surf. Sci. 547 (2003) 421-437.

Williford R.E., "Modeling of Environmentally Significant Interfaces: Two Case Studies", J. Electron Spectroscopy Related Phenomena 150 (2006) 171-184

Yashara, P.C., Barnett,S.A,Hultma,L.,Sproul,W.D. "Deposition and Mechanical Properties of Polycrystalline Y2O3/ZrO2 Superlattices." Journal of material research, 1999: 3614-3622.

Zoltowski, P. "Analysis of electrochemical techniques for studying the diffusion of hydrogen in metals." Journal of Electroanalytical Chemistry 600, 2007: 54-62.

Chapter 7 Conclusion

7.1 Summary

An accepted convention has been that the basic reactions of SOFC anode occur at the intersection of the gas, Ni, and YSZ phases (TPB). In this thesis a 2D mathematical model of the TPB for the Ni/YSZ cermet anode of a SOFC was developed which provided concentration profiles for different reactant and product species: H_2, H, O^{2-}, and H_2O, in the vicinity of the TPB. Transport phenomena occurring over length scales ranging from 0.01 (μm) to 0.1 (μm) were described by fundamental conservation principles of mass and charge.

The global electrochemical anode reaction involves the oxidation of hydrogen with oxide ions to form water and two electrons.

$$H_2 + O^{2-}_{YSZ} \leftrightarrow H_2O_{YSZ} + 2e^- \qquad (7-1)$$

Various mechanisms of elementary steps are proposed in the literature for the reactions in the TPB region. In Chapter 3 and Chapter 4 a detailed listing of almost all possible elementary charge-transfer reactions, their rate expressions, and related transport processes were assembled.

For the modeling part of this work, two reactions were considered: (a) the dissociative chemisorption of gas phase hydrogen to form hydrogen radicals on the surface of the nickel, Equation $(7-2)$, and (b) the charge transfer reaction between hydrogen radicals from the nickel electrode and oxygen anions from the electrolyte that occurs at the $\Gamma_{Ni/YSZ}$, Equation $(7-3)$.

$$H_{2gas} \leftrightarrow 2\ H_{Ni} \qquad (7-2)$$

$$2\ H_{Ni} + O^{2-}_{YSZ} \leftrightarrow H_2O_{YSZ} + 2e^- \qquad (7-3)$$

In addition the model considered the water content of the Ω_{YSZ} to be in phase equilibrium with the water content of the Ω_G, Equation $(7-4)$.

$$H_2O_{YSZ} \leftrightarrow H_2O_{gas} \qquad (7-4)$$

In the proposed reaction/transport sequence hydrogen molecules from the gas phase were first adsorbed on the Ni surface where they dissociated into two hydrogen radicals$(7-2)$. The hydrogen radicals diffused through the Ω_{Ni} to reach the $\Gamma_{Ni/YSZ}$. Similarly oxygen anions were transported through the Ω_{YSZ} to reach the $\Gamma_{Ni/YSZ}$ through a combination of diffusion (concentration gradient) and migration (electrical potential gradient). Water formed by the charge transfer reaction at $\Gamma_{Ni/YSZ}$ diffuses through the $\Omega_{YSZ}(7-3)$. Water molecules are similar in size to oxygen anions, so presumably they could use the same vacancies in the Ω_{YSZ} that are used for oxygen anion transport. At the $\Gamma_{YSZ/g}$ water desorption from the Ω_{YSZ} to the gas phase occurred$(7-4)$.

The computational results from the simple model, described in Chapter 4, were presented in chapter 6. They showed the relative effects of the diffusion and reaction processes on the distribution of different species at the anode TPB in a SOFC. This is the first model of an anode TPB for a SOFC that has reported concentration gradients of reactants and products.

7.2 Contribution to Knowledge

The principal goal of this research was to have a better understanding of the distribution of the different species that exist in the vicinity of an anode TPB in a SOFC. This thesis has presented the numerical results from that work.

In general the results of simulation showed that conventional concept of a TPB that limits reaction sites to a line (triple phase boundary) or a single surface ($\Gamma_{G/Ni}$, $\Gamma_{Ni/YSZ}$ or $\Gamma_{YSZ/G}$) is an oversimplification. The TPB is not only a line. The locations in which transport phenomena occur can extend inside the Ω_{Ni} and Ω_{YSZ}. Reaction phenomena can occur at two surfaces $\Gamma_{G/Ni}$, and $\Gamma_{Ni/YSZ}$.

There is general agreement that the performance of SOFCs is determined by the mass and charge transfer at the O_2/YSZ and electrode/YSZ interfaces at the cathode of a SOFC. Nevertheless, these results showed that, phenomena at the anode side of the SOFC also has an effect on the potential distribution, and therefore has at least a minor influence on the performance of the fuel cell.

There are several papers in the literature describing cathode TPB models. Some of those papers show the distribution of oxygen anions in the vicinity of the TPB. In contrast the number of papers describing SOFC anode TPB models is small. This thesis is the only work to date that describes the distribution of different species in the vicinity of a SOFC anode TPB.

7.3 Future work

The calculations performed in this work could be extended. In general more reaction mechanisms could be considered. For example, oxygen spillover to the Ω_{Ni}, or hydroxyl spillover to the Ω_{YSZ}, or bulk reaction, as described in Chapter 4, could be examined. In future work, a more complete model (anode plus cathode) with all possible interface and bulk reactions could be developed. For the case of the Ni/YSZ system, further experimental validation of the model parameters (diffusion coefficients on surfaces, thermodynamic properties of surface species, and rate constant values of different elementary reactions) would be useful. Experiments could be designed in order to provide data that could be compared to the predictions and modeling results. Hydrocarbon fuels could also be considered instead of just pure hydrogen.

Appendix A List of Symbol

Abbreviations:

Abbreviation	Abbreviation Full Term
AFC	Alkaline fuel cell
CAD	Computer aided design
DGM	Dusty-gas model
DMFC	Direct methanol fuel cell
FDM	Finite difference method
FEM	Finite element method
FM	Fick's model
FVM	Finite volume method
HPD	High power density
MCFC	Molten carbonate fuel cell
MOLB	Mono-block layer built
PAFC	Phosphoric acid fuel cell
PDE	Partial differential equation
PEMFC	Protons exchange membrane fuel cell
SMM	Stefan–Maxwell model
SOFC	Solid oxide fuel cell
TPB	Triple phase boundary

YSZ	Yttrium stabilized zirconia
EIS	Electrochemical impedance spectroscopy

Letter Symbols:

Letter	Unit	Meaning
ΔG°	kJ.mol–1	Changes in Gibbs free energy of a reaction in Standard conditions
ΔG	kJ.mol–1	Change in Gibbs free energy of a reaction
ΔH	kJ.mol–1	Change of enthalpy of a reaction
ΔS	JK–1.mol–1	Change of entropy of a reaction
C_i	mol.m-3	Concentration of species i
C_{dl}	F.m–2	Double-layer capacitance per unit total volume
D_{im}^{e}	m2.s-1	Effective molecular diffusion
D_{ik}^{e}	m2.s-1	Knudsen diffusion coefficient
$\mathrm{D}_{\mathrm{ij}}^{\mathrm{e}}$	m2.s-1	Effective binary diffusion

D_{ij}	m2.s-1	Ordinary binary diffusion
D_i^e	m2.s-1	Effective diffusion
D°	m2.s-1	Pre-exponential factor
d_m	m	Diameter of the molecule
E°	V	Standard potential of the cell
E	V	Equilibrium (reversible) potential of the cell
E_a	J.mol–1	Activation energy
F	C.gmole-1 electron-1	Faraday's constant
H_i°		Interstitial hydrogen atom in the bulk
H_2O_{YSZad}		Adsorbed H_2O on YSZ surface
H_{Niad}		Adsorbed H on Ni surface
H_{Niad}^{+}		Adsorbed H^+ on Ni surface

H_2O_{Niad}		Adsorbed H_2O on Ni surface
i_{el}	A.m-3	Electronic current density
i_{io}	A.m-3	Ionic current density
j_{far}	A.m-2	Faradaic current
k_{fwd}		Forward charge transfer reaction rate constant
k_{bwd}		Backward charge transfer reaction rate constant
k_i	mol. m-n .s-1	Thermal component of the rate expression
l^e	m	Pore effective length
l	m	Distance between two pores
L_{TPB}	m.m-2	TPB length
N_i	mol.m-2s-1	Flux of species i
N_A	mol-1	Avogadro number

OH_i°		Interstitial hydroxyl atom in the bulk
OH^-_{YSZad}		Adsorbed OH^- on YSZ surface
O^{2-}_{Niad}		Adsorbed O^{2-} on Ni surface
OH^-_{Niad}		Adsorbed OH^- on Ni surface
O_0^x		Lattice oxygen
P_i	atm	Pressure of species i
q	C	Elementary charge
R_i		Rate of reaction of species i
R	J.K−1. mol−1	Ideal gas constant
S_{Ni}		Vacant sites on nickel electrode
S_{YSZ}		Vacant sites on YSZ surface
T	K	Temperature

T_H	K	Absolute temperature of the hot reservoir in the Carnot-process
T_C	K	Absolute temperature of the cold reservoir in the Carnot-process
V_V	m3	Volume of void-space of material
V_{Total}	m3	Bulk volume of material
$V_0^{''}$		Oxygen vacancy
X_i	kJ.mol–1	Mole fraction of specie i

Greek Letter

Greek Letter	Unit	Meaning
α_{fwd}		Forward symmetry parameter
α_{bwd}		Backward symmetry parameters
$\beta_\circ$	m2	Permeability of the porous electrode

$\Gamma_{G/YSZ}$		Gas/YSZ interface
$\Gamma_{Bulk/G}$		Bulk gas /G interface
$\Gamma_{\mathrm{Bulk/YSZ}}$		Bulk YSZ/YSZ interface
$\Gamma_{Bulk,Ni}$		Bulk Ni/Ni interface
$\Gamma_{G/Ni}$		Gas/Nickel interface
$\Gamma_{Ni,YSZ}$		Ni/YSZ interface
ε		Porosity of the porous medium
η	V	Overpotential
η_{th}		Theoretical efficiency of a fuel cell
$\eta_{th,Carno}$		Theoretical efficiency of a fuel cell
λ	m	Mean-free path

μ_{mix}	kg.m-1s-1	Mixture-average viscosity
v	m.s	Convection velocity
σ_{el}	Ω-1.m-1	Electronic conductivity
σ_{io}	Ω-1m-1	Ionic conductivity
τ		Tortuosity of porous medium
φ	V	Potential
φ_{el}	V	Electronic potential
φ_{io}	V	Ionic potential
Ω_G		Gas subdomain
Ω_{Ni}		Nickel subdomain
Ω_{YSZ}		YSZ subdomain